LARS Information Note 091974

OPTIMUM CONSTRAINED IMAGE RESTORATION FILTERS

T. E. RIEMER

C. D. MCGILLEM

The Laboratory for Applications of Remote Sensing

Purdue University, West Lafayette, Indiana

1974

LARS Information Note 091974

NASA CR-
141852

OPTIMUM CONSTRAINED IMAGE RESTORATION FILTERS

T. E. RIEMER

C. D. MCGILLEM

The Laboratory for Applications of Remote Sensing

Purdue University, West Lafayette, Indiana

1974

LARS Information Note 091974

OPTIMUM CONSTRAINED IMAGE RESTORATION FILTERS

T. E. Riemer
C. D. McGillem
September 1974

Published by the
Laboratory for Applications of Remote Sensing (LARS)
and the
School of Electrical Engineering
Purdue University
Lafayette, Indiana 47907

This work was sponsored by the National Aeronautics and Space Administration under Grant No. NGL-15-005-112 and Contract No. NAS9-14016. T-1039/4

TABLE OF CONTENTS

LIST OF TABLES

LIST OF FIGURES

ABSTRACT

Riemer, Terry Edmund, Ph.D., Purdue University, December, 1974. Optimum Constrained Image Restoration Filters. Major Professor: C.D. McGillem

An optimum image restoration filter is developed in Hilbert space by minimizing the radius of gyration of the overall or composite system point-spread function subject to constraints on the radius of gyration of the restoration filter point-spread function, the total noise power in the restored image, and the shape of the composite system frequency spectrum.

By satisfying a constraint on the radius of gyration of the restoration filter point-spread function, truncation errors arising from attempted restoration of incomplete segments of blurred data are almost completely suppressed.

An iterative technique is introduced which alters the shape of the optimum composite system point-spread function, producing a suboptimal restoration filter which suppresses undesirable secondary oscillations which may otherwise appear in the composite system point-spread function and introduce "ghosts" in the restored data.

An extensive study of the restoration filter performance as a function of its parameter variations is made. Numerous

examples are provided to demonstrate the fundamental properties of the restoration filter.

Finally this technique is applied to multispectral scanner data obtained from the Earth Resources Technology Satellite to provide resolution enhancement. An experimental approach to the problems involving estimation of the effective scanner aperture and "matching" the ERTS data to available restoration functions is presented.

CHAPTER 1

INTRODUCTION

1.1 General Discussion

The general problem of image processing has been the subject of intense investigation within the last decade. This interest is the result of the need for the highest possible image quality in the increasing application of imagery to the solution of various related problems in many fields of science and engineering. These applications range from x-rays in medicine to satellite-based multispectral scanner data collection systems for monitoring earth resources and to a large degree are made feasible by recent improvements in digital computer hardware.

Since no image collecting or imaging system will produce a perfect replica of the original image, some further processing is usually required. The area of image restoration deals primarily with the problem of processing the output of an imaging system in such a way that the significant parameters or features of the original image are, in some sense, enhanced or restored. This processing may be linear or non-linear, shift-variant or shift-invariant depending upon the type of degradation produced by the imaging system.

The primary purpose of this research is the development of a technique to reduce the effective aperture radius of the multispectral scanner system used for remote sensing of earth resources. Because of the finite point-spread function

of the scanner and the response limitations of the image sensors and signal conditioning electronics, a two-dimensional spatial smearing or blurring of the original image is produced. This type of imaging degradation essentially maps many points from the original image into a single resolution element. In other words, a single resolution element of the imaging system output represents a two-dimensional weighted sum of many points adjacent to the correspondingly located sample of the original image. Thus, depending upon the density and shape of the effective aperture and the spatial and multispectral characteristics of the original image, this type of imaging degradation may not only introduce significant error in the visual presentation of this data, but also introduce serious errors when classification of this data is attempted.

1.2 Previous Investigations

Historically much of the initial work directly related to linear shift or time-invariant restoration filters was performed in the areas of seismographic data analysis and radio astronomy. Basically this work considered the problems associated with defining the restoration filter transfer function as the inverse of the Fourier transform of a linear shift or time-invariant blurring process, which is often referred to as a classical "inverse" filter. The principle problem associated with such a restoration filter occurs when the Fourier transform of the blurring process

becomes very small or perhaps equals zero. Since the spectrum of the restoration filter becomes unbounded at such points, some means of assigning a finite value to the spectrum at these points is necessary.

Typical of this early work, Harris [9] attempted to eliminate this difficulty by arbitrarily modifying the spectrum of the inverse filter to provide a restoration filter having a transfer function that was continuous and finite in those regions where the blurring function spectrum is zero. Bracewell offers an alternative to the problem by employing finite differences [4] and a technique of successive substitutions [5] to define the restoration filter in the temporal or spatial domain. In a more recent study, Kinzly [13] circumvents the problem of infinite gain in the restoration filter by choosing a diffraction-limited system as the correction goal rather than attempting an ideal correction. More sophisticated spectral studies by Bercherer [2] and Horner [10] are based upon minimizing the mean-square error between the original and restored image data, leading to a two-dimensional Wiener filter. Although this type of restoration filter does eliminate the previous problem of spectral infinities, "Apriori" knowledge of the image power spectral density is required. Using a novel approach, Robinson [18] defines the restoration filter in tne temporal or spatial domain in terms of a series derived from the z-transform of the blurring function. Rice [17] provides an

extension to Robinson's work by defining a restoration filter based upon minimizing the mean-square error between the original and restored images. In both of these procedures knowledge of signal characteristics is required. Extensive literature surveys on restoration filter design and related areas of image processing are provided by Huang, et.al. [11] and Sondhi [20]. The previous references represent the earlier studies most closely related to this investigation.

Although several of the previous studies did attempt to optimize the restoration filter, resulting in a Wiener filter, Smith [19] appears to be the first to consider specifying an optimum restoration filter based upon minimizing the radius of gyration of the corrected impulse response or point-spread function subject to a noise constraint. Because no constraint is placed upon the radius of gyration of the restoration filter impulse or point-spread function, serious numerical problems arise. Stuller [1,21] uses basically the same constraints as Smith, but formulates the problem in the spatial domain. By defining the restoration filter using matrix notation, a restoration filter containing an arbitrary number of points may be determined. This appears to be the first attempt to control the duration of the restoration filter impulse or point-spread function. Although the duration of the restoration filter impulse response or point-spread function can be controlled, no control is possible over the shape of this function.

The previously cited investigations have in common one or more of the following deficiencies: no general control over the shape or duration of the restoration filter impulse response or point-spread function, no general control over the shape or duration of the corrected impulse response or point-spread function, no control of the spurious responses resulting from secondary lobes in the restoration filter impulse response or point-spread function, and no way to make tradeoffs among the various conflicting performance requirements of the filter. The significance of these controls will be examined in the next chapter.

1.3 Outline of Investigation

An optimum shift-invariant restoration filter is formulated in Chapter 2 based upon minimizing the radius of gyration of the overall or composite system point-spread function subject primarily to constraints on the radius of gyration of the restoration filter point-spread function and on the total noise in the restored image. In addition, an iterative technique is developed which suppresses secondary oscillations in the composite system point-spread function. For numerical solution convenience, the problem is transformed into the spatial frequency domain and a system of linear differential equations which specify the spectrum of the restoration filter is developed. Finally a comparison is made between the optimum restoration filter and the classical "inverse" filter.

Chapter 3 discusses the application of well known digital computer algorithms to the solution of the previously developed system of linear differential equations specifying the spectrum of the restoration filter.

Chapter 4 presents an investigation of the fundamental properties of the restoration filter. A study of the filter performance as a function of its parameter variations is made. In addition, examples are presented to demonstrate the capability of the restoration filter to suppress truncation error. These examples also provide a qualitative measure of the restoration capabilities of the filter.

Chapter 5 discusses the application of this restoration technique to ERTS multispectral scanner data. The problems of estimating the shape of the scanner aperture and "matching" the ERTS data to previously computed restoration functions are considered. Finally, examples are presented to demonstrate the effectiveness of this technique in the ERTS data.

Chapter 6 presents conclusions made in this study and suggests related work for further investigation.

CHAPTER 2

OPTIMUM IMAGE RESTORATION FILTER

2.1 Introduction

In this chapter the fundamental equations underlying the general image restoration filter are defined. From these equations, a system of equations which specifies the general two-dimensional restoration filter is formulated in the two-dimensional spatial frequency domain. To simplify the analysis of the general problem, two specific types of aperture functions are considered, separable and radially symmetric. A system of equations which specifies the spectrum of the restoration filter for each aperture class is developed. In order to provide additional control over the shape of the point-spread function of the composite imaging system, an iterative technique is defined. The resulting systems of equations which specify the frequency spectrum of the restoration filter for both separable and radially symmetric aperture classes are formulated in terms of the iterative technique. And finally, it is shown that when all defined constraints are removed, the resulting restoration filter is the classical "inverse" filter.

2.2 Formulation of Image Restoration Problem

The basic components of the composite imaging system are defined in Figure 2-1. The fundamental design criterion for determining the optimum image restoration filter is to select the restoration filter point-spread function so that the point-spread function of the composite imaging system is as compact as possible about the spatial origin. Since the classical "inverse" restoration filter, defined by the inverse of the modulation transfer function of the imaging system, would produce an impulse for the composite imaging system point-spread function, representing theoretically the best possible correction, the basis for the fundamental criterion is evident.

One convenient measure of compactness is the square of the radius of gyration, r, defined as

$$r^2 = \frac{\int_{-\infty}^{\infty} |\bar{v}|^2 g^2(\bar{v})\, d\bar{v}}{\int_{-\infty}^{\infty} g^2(\bar{v})\, d\bar{v}} \qquad (2\text{-}1)$$

where $g(\bar{v})$ is the point-spread function for the composite system and $\bar{v}$ is a two-dimensional spatial vector. $g(\bar{v})$ may be expressed as a two-dimensional convolution in terms of the imaging system point-spread function, $h_b(\bar{v})$, and the desired image restoration point-spread function, $h_r(\bar{v})$ as

$$g(\bar{v}) = h_b(\bar{v}) ** h_r(\bar{v}). \qquad (2\text{-}2)$$

An optimum restoration filter based upon minimizing

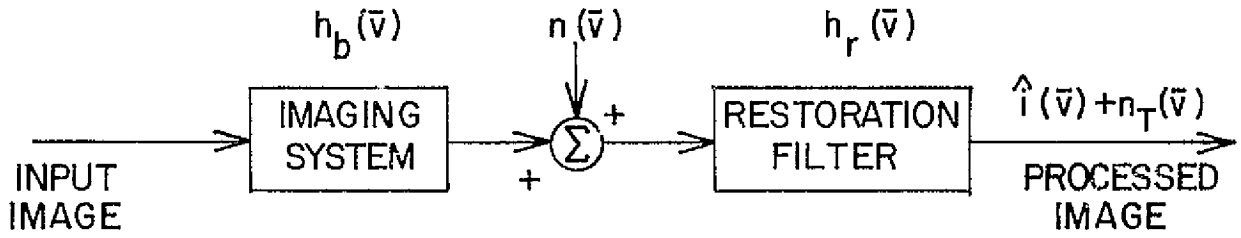

Figure 2.1: Composite Imaging System

Eq. 2-1 would only assure that the composite imaging point-spread function be as compact as possible but would not provide control over oscillations or secondary lobes that might occur and which would lead to ghosts in the restored image. Some additional control over the rate of decay of this function away from its centroid is most desirable. By making a slight change to Eq. 2-1, replacing $|\bar{v}|^2$ by an arbitrary weighting function, $w(\bar{v})$, which will be defined later, control over the rate of decay of the composite imaging system point-spread function becomes possible. Thus the fundamental criterion may be expressed as the ratio of two quadratic functionals

$$F_1 = \frac{\int_{-\infty}^{\infty} w(\bar{v}) g^2(\bar{v})\, d\bar{v}}{\int_{-\infty}^{\infty} g^2(\bar{v})\, d\bar{v}}, \qquad (2\text{-}3)$$

The optimum restoration filter would be determined by choosing a restoration filter that will minimize the numerator of Eq. 2-3 subject to a constraint on the denominator, which corresponds to the energy in the composite filter.

In order to avoid two significant shortcomings encountered with the classical "inverse" filter, two additional constraints must be considered. The first deals with the compactness and rate of decay with respect to the spatial origin of the point-spread function of the optimum restoration filter. Since the point-spread function of the

restoration filter based upon the "inverse" filter is generally much less compact than the point-spread function of the imaging system, and often is of infinite duration as a result of the infinite energy usually associated with such a filter, it is advantageous from a data processing efficiency and cost viewpoint to reduce the duration of this function, thus reducing the amount of data required for image processing. In addition since the image to be restored usually represents only a portion of the original image presented to the imaging system input, significant "edge-effect" errors can result. This error is produced by truncation of the imaging system output, i.e. having only a finite data record available for restoration. It is usually greatest at the boundaries or edges of the restored image and propagates through the restored image[1]. By making the point-spread function of the restoration filter more compact about the spatial origin, both problems concerning data processing efficiency and "edge-effect" errors should be diminished.

Using an analogous development to that of Eq. 2-3,

$$F_2 = \frac{\int_{-\infty}^{\infty} s(\bar{v}) h_r^2(\bar{v})\, d\bar{v}}{\int_{-\infty}^{\infty} h_r^2(\bar{v})\, d\bar{v}} \qquad (2\text{-}4)$$

may be defined, where $s(\bar{v})$ is a weighting function similar in purpose to that of $w(\bar{v})$ in Eq. 2-3, and $h_r(\bar{v})$ is the

---

[1] See Appendix A

restoration filter point-spread function. By using both the numerator and denominator of Eq. 2-4 as additional constraints, arbitrary control with regard to compactness and duration of the optimum restoration filter is possible.

The second additional constraint necessitated by the performance of the "inverse" filter is a constraint on the noise power present in the restored image. Because of the shape of the spectrum of the "inverse" filter, optimum performance is possible only in a noiseless environment. The presence of any noise, however small, would in general be infinitely amplified by such a filter. The additional constraint provides arbitrary control of the signal-to-noise ratio of the restored image. This constraint can be stated as an expectation over $n_T^2(\bar{v})$,

$$F_3 = E\{n_T^2(\bar{v})\} \qquad (2\text{-}5)$$

where $n_T(\bar{v})$, the total noise in the restored image, is defined in Figure 2-1.

A final constraint has been found necessary under certain conditions to control the shape of the modulation transfer function of the composite imaging system to guarantee that this function contains no significant spurious high frequency peaks which could contribute to oscillation near the spatial origin of the composite imaging system point-spread function. This occurs primarily when the first constraint is removed or is near

its unconstrained value. This constraint may be defined in the spatial frequency domain as,

$$F_4 = \int_{-\infty}^{\infty} \left(\frac{\bar{f}}{f_H}\right)^2 |G(\bar{f})|^2 d\bar{f}$$

where $G(\bar{f})$ is the composite imaging system modulation transfer function and f_h is a frequency weighting parameter. Since the previous constraints were defined in the spatial domain, this constraint, as will be shown in the next section, can be written as,

$$F_4 = -\frac{1}{4\pi^2 f_H^2} \int_{-\infty}^{\infty} g''(\bar{v}) g(\bar{v}) \, d\bar{v}. \qquad (2\text{-}6)$$

2.3 Development of Optimum Filter Function

Combining the primary criterion defined in Eq. 2-3 with the constraints of Eq. 2-4 through 2-6, the optimum restoration filter point-spread function $h_r(\bar{v})$ is that function which minimizes the functional

$$F = \int_{-\infty}^{\infty} w(\bar{v}) g^2(\bar{v}) \, d\bar{v} \qquad (2\text{-}7)$$

where $g(\bar{v})$ is defined in Eq. 2-2,
subject to the following constraints,

$$K_1 = \int_{-\infty}^{\infty} s(\bar{v}) h_r^2(\bar{v}) \, d\bar{v} \qquad (2\text{-}8)$$

$$K_2 = E\{n_T^2(v)\} \qquad (2\text{-}9)$$

$$K_3 = -\frac{1}{4\pi^2 f_H} \int_{-\infty}^{\infty} g''(\bar{v}) g(\bar{v}) \, d\bar{v}. \qquad (2\text{-}10)$$

It should be noted that the constraints related to the energy of the composite imaging system, i.e. the denominator of Eq. 2-3, and the energy of the image restoration system, i.e. the denominator of Eq. 2-4, have been dropped since these constraints can always be satisfied by appropriate amplitude scaling of the optimum restoration filter defined by the constraints of Eq. 2-8 through 2-10.

Lagrange multipliers and the methods of functional analysis will be used to solve Eq. 2-7 subject to the constraints of Eq. 2-8 through 2-10 by forming an augmented functional which is the sum of the functional to be minimized, Eq. 2-7, and the constraint functionals each multiplied by a different Lagrange multiplier [7,8].

Thus the augmented functional, I, which must be minimized with regard to $h_r(\bar{v})$ becomes,

$$I = \int_{-\infty}^{\infty} w(\bar{v})g^2(\bar{v})\, d\bar{v} + \lambda_1 \int_{-\infty}^{\infty} s(\bar{v})h_r^2(\bar{v})\, d\bar{v} + \lambda_2 E\{n_T^2(\bar{v})\}$$

$$- \frac{\lambda_3}{4\pi^2 f_H^{\,2}} \int_{-\infty}^{\infty} g''(\bar{v})g(\bar{v})\, d\bar{v}$$

$$= \int_{-\infty}^{\infty} w(\bar{v}) \int_{-\infty}^{\infty} h_r(\bar{z})h_b(\bar{v}-\bar{z})\, d\bar{z} \int_{-\infty}^{\infty} h_r(\bar{u})h_b(\bar{v}-\bar{u})\, d\bar{u}d\bar{v}$$

$$+ \lambda_1 \int_{-\infty}^{\infty}\int s(\bar{u})s(\bar{u}-\bar{v})h_r(\bar{v})h_r(\bar{u})\, d\bar{u}d\bar{v}$$

$$+ \lambda_2 E\{\int_{-\infty}^{\infty} n(\bar{v}-\bar{z})h_r(\bar{z})\, d\bar{z} \int_{-\infty}^{\infty} n(\bar{v}-\bar{u})h_r(\bar{u})\, d\bar{u}\}$$

$$- \frac{\lambda_3}{4\pi^2 f_H^{\,2}} \int_{-\infty}^{\infty}\int \delta''(\bar{\tau}-\bar{v}) \int_{-\infty}^{\infty} h_r(\bar{z})\, h_b(\bar{\tau}-\bar{z})\, d\bar{z} \int_{-\infty}^{\infty} h_r(\bar{u})\, h_b(\bar{v}-\bar{u})\, d\bar{\tau}d\bar{v}d\bar{u}. \tag{2-11}$$

Eq. 2-11 may be written in quadratic functional form as

$$\begin{aligned} I = &\int_{-\infty}^{\infty}\int A_1(\bar{u},\bar{z})\, h_r(\bar{z})\, h_r(\bar{u})\, d\bar{z}d\bar{u} \\ &+ \lambda_1 \int_{-\infty}^{\infty}\int A_2(\bar{u},\bar{z})\, h_r(\bar{z})\, h_r(\bar{u})\, d\bar{z}d\bar{u} \\ &+ \lambda_2 \int_{-\infty}^{\infty}\int A_3(\bar{u},\bar{z})\, h_r(\bar{z})\, h_r(\bar{u})\, d\bar{z}d\bar{u} \\ &+ \lambda_3 \int_{-\infty}^{\infty}\int A_4(\bar{u},\bar{z})\, h_r(\bar{z})\, h_r(\bar{u})\, d\bar{z}d\bar{u} \end{aligned} \tag{2-12}$$

where $A_1(\bar{u},\bar{z})$, $A_2(\bar{u},\bar{z})$, $A_3(\bar{u},\bar{z})$, and $A_4(\bar{u},\bar{z})$ are linear operators defined as [8]

$$A_1(\bar{u},\bar{z}) = \int_{-\infty}^{\infty} w(\bar{v})\, h_b(\bar{v}-\bar{z})\, h_b(\bar{v}-\bar{u})\, d\bar{v} \tag{2-13}$$

$$A_2(\bar{u},\bar{z}) = s(\bar{u})\,\delta(\bar{u}-\bar{z}) \tag{2-14}$$

$$\begin{aligned} A_3(\bar{u},\bar{z}) &= E\{n(\bar{v}-\bar{z})\, n(\bar{v}-\bar{u})\} \\ &= R_{nn}(\bar{z}-\bar{u}), \text{ for } n(\cdot) \text{ a stationary ergodic random process} \end{aligned} \tag{2-15}$$

and

$$\begin{aligned} A_4(\bar{u},\bar{z}) &= -\frac{1}{4\pi^2 f_H^{\,2}} \int_{-\infty}^{\infty}\int \delta''(\bar{\tau}-\bar{v})\, h_b(\bar{\tau}-\bar{z})\, h_b(\bar{v}-\bar{u})\, d\bar{\tau}d\bar{v} \\ &= -\frac{1}{4\pi^2 f_H^{\,2}} \int_{-\infty}^{\infty} h_b''(\bar{v}-\bar{z})\, h_b(\bar{v}-\bar{u})\, d\bar{v}. \end{aligned} \tag{2-16}$$

The stationary points of the augmented functional of Eq. 2-12 will be determined by equating the directional derivative of this functional to zero. It should be noted that for a real functional equating the directional derivative to zero is equivalent to setting the gradient to zero [8]. The gradient of a quadratic functional

$$I_1 = \int_{-\infty}^{\infty} \int A(\bar{u},\bar{z})h(\bar{z})h(\bar{u})\ d\bar{z}d\bar{u}$$

is defined as

$$\nabla I_1 = \int_{-\infty}^{\infty} [A(\bar{u},\bar{z}) + A'(\bar{u},\bar{z})]h(\bar{z})\ d\bar{z}$$

where $A'(\bar{u},\bar{z})$ is the adjoint of the linear operator $A(\bar{u},\bar{z})$.

The adjoint linear operators of Eq. 2-13 through 2-16 are

$$A_1'(\bar{u},\bar{z}) = A_1(\bar{u},\bar{z}) \qquad (2\text{-}17)$$

$$A_2'(\bar{u},\bar{z}) = A_2(\bar{u},\bar{z}) \qquad (2\text{-}18)$$

$$A_3'(\bar{u},\bar{z}) = A_3(\bar{u},\bar{z}) \qquad (2\text{-}19)$$

and

$$A_4'(\bar{u},\bar{z}) = A_4(\bar{u},\bar{z}). \qquad (2\text{-}20)$$

Setting the gradient of Eq. 2-12 with respect to $h_r(\cdot)$ equal to zero, a homogeneous Fredholm integral equation of the second kind, sometimes referred to as a Fredholm integral equation of the third kind, is obtained as

$$\int_{-\infty}^{\infty} [A_1(\bar{v},\bar{z}) + \lambda_2 A_3(\bar{v},\bar{z}) + \lambda_3 A_4(\bar{v},\bar{z})]h_r(\bar{z})\ d\bar{z}$$

$$+ \lambda_1 s(\bar{v}) h_r(\bar{v}) = 0. \qquad (2\text{-}21)^2$$

The solution of this equation coupled with the constraint equations, Eq. 2-8 through 2-10, would give the required point-spread function of the restoration filter, $h_r(\bar{v})$. However because of the numerical difficulties which may arise in the general solution of this type of equation and in order to more conveniently utilize numerical techniques which are readily available, the solution for $h_r(\bar{v})$ will be formulated in the two-dimensional spatial frequency domain .

Eq. 2-12 may be rewritten using inner product notation [8], where the inner product of x(t) and y(t) is defined as

$$(x,y) = \int_{-\infty}^{\infty} x(t) y^*(t)\, dt$$

where the asterisk denotes the complex conjugate. Thus

$$I = (A_1 h_r, h_r) + \lambda_1 (A_2 h_r, h_r) + \lambda_2 (A_3 h_r, h_r) + \lambda_3 (A_4 h_r, h_r). \qquad (2\text{-}22)$$

Eq. 2-22 may also be written as a quadratic functional in

---

[2] For derivation see Appendix B.

the spatial frequency domain as

$$I = (B_1 H_r, H_r) + \lambda_1 (B_2 H_r, H_r) + \lambda_2 (B_3 H_r, H_r) + \lambda_3 (B_4 H_r, H_r), \quad (2\text{-}23)$$

where

$$H_r(\cdot) = \mathcal{F}\{h_r(\cdot)\}$$

$\mathcal{F}(\cdot)$ denotes the Fourier transform and B_1, B_2, B_3, and B_4 are the spatial frequency linear equators which are the Fourier transforms of the spatial domain linear operators, A_1, A_2, A_3, and A_4, respectively. Thus

$$B_1(\bar{f},\bar{v}) = \int_{-\infty}^{\infty} \int A_1(\bar{u},\bar{z}) e^{-j2\pi \bar{f}\bar{u}} e^{j2\pi \bar{v}\bar{z}} \, d\bar{u} \, d\bar{z} \quad (2\text{-}24)$$

which after substituting Eq. 2-13 into Eq. 2-24 may be simplified to

$$B_1(\bar{f},\bar{v}) = H_b^*(\bar{f}) H_b(\bar{v}) W(\bar{f}-\bar{v}) \quad (2\text{-}25)$$

where

$$H_b(\cdot) = \mathcal{F}\{h_b(\cdot)\}$$

$$W(\cdot) = \mathcal{F}\{w(\cdot)\}$$

and $H_b^*(\cdot)$ is the complex conjugate of $H_b(\cdot)$.

The adjoint of $B_1(\bar{f},\bar{v})$, defined as $B_1'(\bar{f},\bar{v})$, may be written as

$$B_1'(\bar{f},\bar{v}) = B_1^*(\bar{v},\bar{f})$$

which from Eq. 2-25 becomes

$$B_1'(\bar{f},\bar{v}) = H_b(\bar{v}) H_b^*(\bar{f}) W^*(\bar{v}-\bar{f}). \quad (2\text{-}26)$$

Similarly

$$B_2(\bar{f},\bar{v}) = S(\bar{f}-\bar{v}) \quad (2\text{-}27)$$

where $$S(\cdot) = \mathcal{F}\{s(\cdot)\},$$

$$B_2'(\bar{f},\bar{\nu}) = S^*(\bar{\nu}-\bar{f}) \tag{2-28}$$

$$B_3(\bar{f},\bar{\nu}) = \Phi_{nn}(\bar{\nu})(\bar{f}-\bar{\nu}) \tag{2-29}$$

where $$\Phi_{nn}(\cdot) = \mathcal{F}\{R_{nn}(\cdot)\}$$

$$B_3'(\bar{f},\bar{\nu}) = \Phi_{nn}(\bar{f})\delta(\bar{\nu}-\bar{f}) \tag{2-30}$$

$$B_4(\bar{f},\bar{\nu}) = \frac{\nu^2}{f_H^2}\,|H_b(\bar{\nu})|^2\delta(\bar{f}-\bar{\nu}) \tag{2-31}$$

and $$B_4'(\bar{f},\bar{\nu}) = \frac{\bar{f}^2}{f_H^2}\,|H_b(\bar{f})|^2\delta(\bar{\nu}-\bar{f}). \tag{2-32}$$[3]

The gradient of the quadratic functional of Eq. 2-23 becomes

$$\nabla I = (B_1+B_1')H_r + \lambda_1(B_2+B_2')H_r + \lambda_2(B_3+B_3')H_r + \lambda_3(B_4+B_4')H_r \tag{2-33}$$

which upon expanding the linear operator notation of Eq. 2-33 becomes

$$\nabla I = \int_{-\infty}^{\infty} [B_1(\bar{f},\bar{\nu}) + B_1'(\bar{f},\bar{\nu}) + \lambda_1\{B_2(\bar{f},\bar{\nu}) + B_2'(\bar{f},\bar{\nu})\} + \lambda_2\{B_3(\bar{f},\bar{\nu}) + B_3'(\bar{f},\bar{\nu})\} + \lambda_3\{B_4(\bar{f},\bar{\nu}) + B_4'(\bar{f},\bar{\nu})\}]H_r(\bar{\nu})\,d\bar{\nu} = 0. \tag{2-34}$$

---

[3] See Appendix C for a derivation of these spatial frequency linear operators.

Substituting Eq. 2-25 through 2-32 into Eq. 2-34,

$$\nabla I = \int_{-\infty}^{\infty} [H_b^*(\bar{f})H_b(\bar{\nu})\{W(\bar{f}-\bar{\nu}) + W^*(\bar{\nu}-\bar{f})\} + \lambda_1\{S(\bar{f}-\bar{\nu}) + S^*(\bar{\nu}-\bar{f})\}]H_r(\bar{\nu})d\bar{\nu} + 2[\lambda_2\Phi_{nn}(\bar{f}) + \lambda_3(\frac{\bar{f}}{f_H})^2|H_b(\bar{f})|^2]H_r(\bar{f}) = 0. \quad (2\text{-}35)$$

Eq. 2-35 represents the general expression for the gradient of Eq. 2-23 with respect to $H_r(\cdot)$, which then combined with the constraint equations, completely specified the spatial frequency spectrum of the restoration filter. The constraint equations, Eq. 2-8 through 2-10, may be rewritten in the spatial frequency domain as

$$K_1 = (B_2H_r, H_r) \quad (2\text{-}36)$$

which after substituting Eq. 2-27 into 2-36 becomes

$$K_1 = \int_{-\infty}^{\infty}\int S(\bar{f}-\bar{\nu})H_r(\bar{\nu})H_r^*(\bar{f})d\bar{\nu}d\bar{f}, \quad (2\text{-}37)$$

$$K_2 = (B_3H_r, H_r) \quad (2\text{-}38)$$

after substituting Eq. 2-29 into 2-38 becomes

$$K_2 = \int_{-\infty}^{\infty} \Phi_{nn}(\bar{f})|H_r(\bar{f})|^2 d\bar{f} \quad (2\text{-}39)$$

and

$$K_2 = (B_4H_r, H_r) \quad (2\text{-}40)$$

after substituting Eq. 2-31 into 2-40 becomes

$$K_3 = \int_{-\infty}^{\infty} (\frac{\bar{f}}{f_H})^2 |H_b(\bar{f})|^2 |H_r(f)|^2 d\bar{f}. \quad (2\text{-}41)$$

Before Eq. 2-35 can be reduced to a form more suitable for the evaluation of the spatial frequency spectrum of the restoration filter, the penalty weighting functions $w(\bar{v})$ and $s(\bar{v})$, introduced in Eq. 2-3 and 2-4 respectively, must be further examined. Since $w(\bar{v})$ is designed to influence the solution of $h_r(\bar{v})$ so that the composite imaging system point-spread function, $g(\bar{v})$, is duration limited, a possible choice for $w(\bar{v})$ would be

$$w(\bar{v}) = 1 \text{ for } \bar{v}_1 \leq \bar{v} \leq \bar{v}_2$$
$$= \infty, \quad \text{otherwise.}$$

However such a choice for $w(\bar{v})$ would lead to analytical difficulties in Eq. 2-35, since the Fourier transform of such a function does not exist. Thus the expression for $w(\bar{v})$ must be chosen in such a manner that it allows enough flexibility to arbitrarily control the duration or radius of gyration as well as the rate of decay of $g(\bar{v})$ and, in addition, to have a Fourier transform [25].

One function for $w(\bar{v})$ which satisfies the previous requirements, written in terms of one variable, is [15]

$$w(v) = \left[\frac{2v - v_1 - v_2}{v_2 - v_1}\right]^{2k} + c \qquad (2\text{-}42)$$

for $0 < c < 1$

and k a positive integer. This function is shown in Figure 2-2. For convenience $s(\bar{v})$ will also be described by the same type of function.

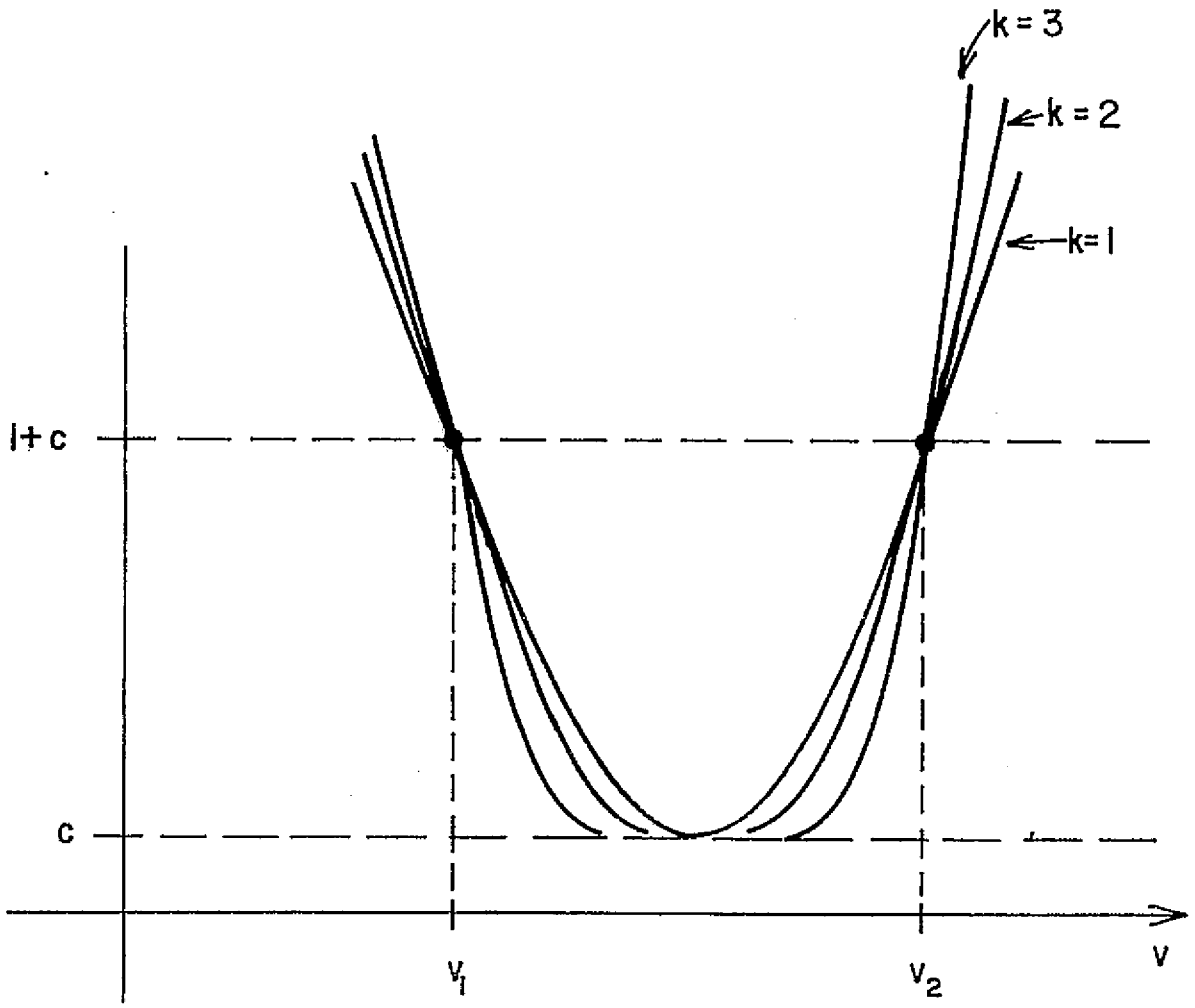

Figure 2-2: One Dimensional Penalty Weighting Function

The following analysis is based upon a rectangular coordinate system. Eq. 2-35 may be rewritten in terms of the x- and y- components of $\bar{f}$ and $\bar{\nu}$,

$$\int_{-\infty}^{\infty}\int [H_b^*(f_x,f_y)H_b(\nu_x,\nu_y)\{W(f_x-\nu_x,f_y-\nu_y) + W^*(\nu_x-f_x,\nu_y-f_y)\}$$

$$+ \lambda_1\{S(f_x-\nu_x,f_y-\nu_y) + S^*(\nu_x-f_x,\nu_y-f_y)\}]H_r(\nu_x,\nu_y)d\nu_x\, d\nu_y$$

$$+ 2[\lambda_2\Phi_{nn}(f_x,f_y) + \lambda_3(\frac{f_x^2+f_y^2}{f_H^2})|H_b(f_x,f_y)|^2]H_r(f_x,f_y) = 0. \qquad (2\text{-}43)$$

For convenience in handling the analysis with respect to a rectangular coordinate system both $w(\bar{\nu})$ and $s(\bar{\nu})$ will be defined as the product of their x- and y- components, from Eq. 2-42,

$$w(\bar{\nu}) = w_x(x)\, w_y(y) \qquad (2\text{-}44a)$$

$$= [\{\frac{2x-x_{w1}-x_{w2}}{x_{w2}-x_{w1}}\}^{2k_{wx}} + c_x]\ [\{\frac{2y-y_{w1}-y_{w2}}{y_{w2}-y_{w1}}\}^{2k_{wy}} + c_y] \qquad (2\text{-}44b)$$

where $0 < c_x < 1$

$0 < c_y < 1$

and for k_{wx} and k_{wy} positive integers.

Similarly

$$s(\bar{\nu}) = s_x(x)\, s_y(y) \qquad (2\text{-}45a)$$

$$= [\{\frac{2x-x_{s1}-x_{s2}}{x_{s2}-x_{s1}}\}^{2k_{sx}} + d_x]\ [\{\frac{2y-y_{s1}-y_{s2}}{y_{s2}-y_{s1}}\}^{2k_{sy}} + d_y] \qquad (2\text{-}45b)$$

where $0 < d_x < 1$

$0 < d_y < 1$

and for k_{sx} and k_{sy} positive integers.

Choosing $k_{wx} = 1 = k_{wy}$, the Fourier transform of Eq. 2-44b becomes

$$W(f_x,f_y) = W_x(f_x)W_y(f_y) \qquad (2\text{-}46)$$

where

$$W_x(f_x) = \frac{1}{(x_{w2}-x_{w1})^2}\left[-\frac{1}{\pi^2}\delta''(f_x) - \frac{j2(x_{w1}+x_{w2})}{\pi}\delta'(f_x)\right.$$

$$\left. + \{(x_{w1}+x_{w2})^2 + (x_{w2}-x_{w1})^2 c_x\}\,\delta(f_x)\right] \qquad (2\text{-}47)$$

and

$$W_y(f_y) = \frac{1}{(y_{w2}-y_{w1})^2}\left[-\frac{1}{\pi^2}\delta''(f_y) - \frac{j2(y_{w1}+y_{w2})}{\pi}\delta'(f_y)\right.$$

$$\left. + \{(y_{w1}+y_{w2})^2 + (y_{w2}-y_{w1})^2 c_y\}\delta(f_y)\right]. \qquad (2\text{-}48)$$

A similar expression results from taking the Fourier transform of Eq. 2-45b,

$$S(f_x,f_y) = S_x(f_x)S_y(f_y) \qquad (2\text{-}49)$$

where

$$S_x(f_x) = \frac{1}{(x_{s2}-x_{s1})^2}\left[-\frac{1}{\pi^2}\delta''(f_x) - \frac{j2(x_{s1}+x_{s2})}{\pi}\delta'(f_x)\right.$$

$$\left. + \{(x_{s1}+x_{s2})^2 + (x_{s2}-x_{s1})^2 d_x\}\delta(f_x)\right] \qquad (2\text{-}50)$$

and

$$S_y(f_y) = \frac{1}{(y_{s2}-y_{s1})^2}\left[-\frac{1}{\pi^2}\delta''(f_y) - \frac{j2(y_{s1}+y_{s2})}{\pi}\delta'(f_y)\right.$$

$$\left. + \{(y_{s1}+y_{s2})^2 + (y_{s2}-y_{s1})^2 d_y\}\delta(f_y)\right]. \qquad (2\text{-}51)$$

If it is assumed, as would usually be the case, that the penalty functions, w(x,y) and s(x,y) are centered about the origin, then

$$x_{w1} = -x_{w2} = x_w$$

$$y_{w1} = -y_{w2} = y_w$$

$$x_{s1} = -x_{s2} = x_s$$

$$y_{s1} = -y_{s2} = y_s. \qquad (2\text{-}52)$$

Substituting Eq. 2-52 into 2-47, 48, 50, and 51,

$$W_x(f_x) = -\frac{1}{4\pi^2 x_w^2}\delta''(f_x) + c_x\delta(f_x) \qquad (2\text{-}53)$$

$$W_y(f_y) = -\frac{1}{4\pi^2 y_w^2}\delta''(f_y) + c_y\delta(f_y) \qquad (2\text{-}54)$$

$$S_x(f_x) = -\frac{1}{4\pi^2 x_s^2}\delta''(f_x) + d_x\delta(f_x) \qquad (2\text{-}55)$$

and

$$S_y(f_y) = -\frac{1}{4\pi^2 y_s^2}\delta''(f_y) + d_y\delta(d_y). \qquad (2\text{-}56)$$

Substituting Eq. 2-53 through 2-56 into Eq. 2-43

$$\frac{H_b^*(f_x,f_y)}{8\pi^4 x_w^2 y_w^2}\left\{\frac{\partial^4}{\partial f_x^2 \partial f_y^2} H_b(f_x,f_y)H_r(f_x,f_y)\right.$$

$$- 4\pi^2 y_w^2 c_y \frac{\partial^2}{\partial f_x^2} H_b(f_x,f_y)H_r(f_x,f_y)$$

$$- 4\pi^2 x_w^2 c_x \frac{\partial^2}{\partial f_y^2} H_b(f_x,f_y)H_r(f_x,f_y)$$

$$\left. + 8\pi^4 x_w^2 y_w^2 c_x c_y H_b(f_x,f_y)H_r(f_x,f_y)\right]$$

$$+ \frac{\lambda_1}{8\pi^4 x_s^2 y_s^2}\left\{\frac{\partial^4}{\partial f_x^2 \partial f_y^2} H_r(f_x,f_y)\right.$$

$$- 4\pi^2 y_s^2 d_y \frac{\partial^2}{\partial f_x^2} H_r(f_x,f_y)$$

$$- 4\pi^2 x_s^2 d_x \frac{\partial^2}{\partial f_y^2} H_r(f_x,f_y)$$

$$\left. + 8\pi^4 x_s^2 y_s^2 d_x d_y H_r(f_x,f_y)\right\} + 2[\lambda_2 \Phi_{nn}(f_x,f_y)$$

$$+ \lambda_3 \frac{(f_x^2+f_y^2)}{f_H^2} |H_b(f_x,f_y)|^2]H_r(f_x,f_y) = 0, \quad (2\text{-}57)$$

which when expanded in terms of $H_r(f_x,f_y)$, becomes

$$[A(f_x,f_y)H_b(f_x,f_y)+B(f_x,f_y)] \frac{\partial^4 H_r(f_x,f_y)}{\partial f_x^2 \partial f_y^2}$$

$$+ 2A(f_x,f_y) \frac{\partial H_b(f_x,f_y)}{\partial f_y} \frac{\partial^3 H_r(f_x,f_y)}{\partial f_x^2 \partial f_y}$$

$$+ 2A(f_x,f_y) \frac{\partial H_b(f_x,f_y)}{\partial f_x} \frac{\partial^3 H_r(f_x,f_y)}{\partial f_x \partial f_y^2}$$

$$+ 4A(f_x,f_y) \frac{\partial^2 H_b(f_x,f_y)}{\partial f_x \partial f_y} \frac{\partial^2 H_r(f_x,f_y)}{\partial f_x \partial f_y}$$

$$+ [A(f_x,f_y) \frac{\partial^2 H_b(f_x,f_y)}{\partial f_x^2} + E(f_x,f_y) H_b(f_x,f_y)$$

$$+ G(f_x,f_y)] \frac{\partial^2 H_r(f_x,f_y)}{\partial f_y^2} + [A(f_x,f_y) \frac{\partial^2 H_b(f_x,f_y)}{\partial f_y^2}$$

$$+ D(f_x,f_y) H_b(f_x,f_y) + F(f_x,f_y)] \frac{\partial^2 H_r(f_x,f_y)}{\partial f_x^2}$$

$$+ [2A(f_x,f_y) \frac{\partial^3 H_b(f_x,f_y)}{\partial f_x^2 \partial f_y}$$

$$+ 2E(f_x,f_y) \frac{\partial H_b(f_x,f_y)}{\partial f_y}] \frac{\partial H_r(f_x,f_y)}{\partial f_y}$$

$$+ [2A(f_x,f_y) \frac{\partial^3 H_b(f_x,f_y)}{\partial f_x \partial f_y^2}$$

$$+ 2D(f_x,f_y) \frac{\partial H_b(f_x,f_y)}{\partial f_x}] \frac{\partial H_r(f_x,f_y)}{\partial f_x}$$

$$+ [C(f_x,f_y) + \frac{\partial^4 H_b(f_x,f_y)}{\partial f_x^2 \partial f_y^2} + D(f_x,f_y) \frac{\partial^2 H_b(f_x,f_y)}{\partial f_x^2}$$

$$+ E(f_x,f_y) \frac{\partial^2 H_b(f_x,f_y)}{\partial f_y^2} + H(f_x,f_y)] H_r(f_x,f_y) = 0, \quad (2\text{-}58)$$

where

$$A(f_x,f_y) = \frac{H_b^*(f_x,f_y)}{8\pi^4 x_w^2 y_w^2} \tag{2-59a}$$

$$B(f_x,f_y) = \frac{\lambda_1 H_b^*(f_x,f_y)}{8\pi^4 x_s^2 y_s^2} \tag{2-59b}$$

$$C(f_x,f_y) = \left[c_x c_y + 2\lambda_3 \frac{(f_x^2+f_y^2)}{f_H^2}\right] |H_b(f_x,f_y)|^2 + \lambda_1 d_x d_y + 2\lambda_2 \Phi_{nn}(f_x,f_y) \tag{2-59c}$$

$$D(f_x,f_y) = \frac{-H_b^*(f_x,f_y) c_y}{2\pi^2 x_w^2} \tag{2-59d}$$

$$E(f_x,f_y) = \frac{-H_b^*(f_x,f_y) c_x}{2\pi^2 y_w^2} \tag{2-59e}$$

$$F(f_x,f_y) = \frac{-\lambda_1 d_y}{2\pi^2 x_s^2} \tag{2-59f}$$

$$G(f_x,f_y) = \frac{-\lambda_1 d_x}{2\pi^2 y_s^2} \tag{2-59g}$$

$$H(f_x,f_y) = c_x c_y |H_b(f_x,f_y)|^2 + \lambda_1 d_x d_y . \tag{2-59h}$$

Similarly in terms of the rectangular spatial frequency coordinate system the constraint equations, Eq. 2-37, 39, and 41 become,

$$K_1 = \int_{-\infty}^{\infty}\int\int\int S(f_x-\nu_x, f_y-\nu_y) H_r(\nu_x,\nu_y) H_r^*(f_x,f_y) df_x df_y d\nu_x d\nu_y \tag{2-60}$$

$$K_2 = \int_{-\infty}^{\infty}\int \Phi_{nn}(f_x,f_y) |H_r(f_x,f_y)|^2 df_x df_y \tag{2-61}$$

$$K_3 = \int_{-\infty}^{\infty}\int \left(\frac{f_x^2+f_y^2}{f_H^2}\right) |H_b(f_x,f_y)|^2 |H_r(f_x,f_y)|^2 df_x df_y. \tag{2-62}$$

Thus Eq. 2-53 and 59 in conjunction with the constraint equations, Eq. 2-60 through 2-62, specify the general form of the optimum restoration filter in terms of the rectangular spatial frequency coordinate system.

2.4 Separable Optimum Restoration Filter

The general system of equations defined by Eq. 2-58 through 2-62 represents a formidable solution problem, which in general would be possible only by a two-dimensional numerical solution technique requiring a computer system having very large data storage capabilities. However for a certain class of aperture functions, which represent a large class of physically realizable apertures, an enormous reduction in the computational complexity of the problem is possible. This class comprises those apertures which may be modelled as separable apertures, where it is assumed that

$$H_b(f_x,f_y) = H_{bx}(f_x) H_{by}(f_y) \tag{2-63}$$

$$\Phi_{nn}(f_x,f_y) = \Phi_{nnx}(f_x)\Phi_{nny}(f_y) \tag{2-64}$$

$$H_r(f_x,f_y) = H_{rx}(f_x) H_{ry}(f_y). \tag{2-65}$$

With the assumptions of Eq. 2-63 through 65, the solution of Eq.2-58 through 62 can be considerably simplified by use of the method of separation of variables. Instead of substituting Eq. 2-63 through 65 into Eq. 2-58 and separating Eq. 2-58 into two differential equations, one a function of f_x and the other a function of f_y, a somewhat more fundamental approach will be used.

Taking the inverse two-dimensional Fourier transform of Eq. 2-63,

$$h_b(x,y) = h_{bx}(x)h_{by}(y) \qquad (2-66)$$

Similarly Eq. 2-64 and 2-65 become respectively

$$R_{nn}(x,y) = R_{nnx}(x)R_{nny}(y) \qquad (2-67)$$

and

$$h_r(x,y) = h_{rx}(x)h_{ry}(y) \cdot \qquad (2-68)$$

Writing Eq. 2-7 in terms of the two spatial dimensions,

$$F = \int_{-\infty}^{\infty}\int w(x,y)\ g^2(x,y)\ dxdy \qquad (2-69)$$

where from Eq. 2-2,

$$g(x,y) = h_r(x,y)**h_b(x,y). \qquad (2-70)$$

Substituting Eq. 2-66 and 2-68 into 2-70,

$$g(x,y) = [h_{rx}(x)h_{ry}(y)]**[h_{bx}(x)h_{by}(y)] = g_x(x)g_y(y) \qquad (2-71)$$

where

$$g_x(x) = h_{rx}(x) * h_{bx}(x) \qquad (2-72)$$

and

$$g_y(y) = h_{ry}(y) * h_{by}(y). \tag{2-73}$$

Substituting Eq. 2-44a and 2-71 into 2-69,

$$F = F_x F_y \tag{2-74a}$$

where

$$F_x = \int_{-\infty}^{\infty} w_x(x) g_x^2(x) dx \tag{2-74b}$$

$$F_y = \int_{-\infty}^{\infty} w_y(y) g_y^2(y) dy. \tag{2-74c}$$

Substituting Eq. 2-45a and 2-68 into 2-8,

$$K_1 = K_{1x} K_{1y} \tag{2-75a}$$

where

$$K_{1x} = \int_{-\infty}^{\infty} s_x(x) h^2_{rx}(x) dx \tag{2-75b}$$

and

$$K_{1y} = \int_{-\infty}^{\infty} s_y(y) h^2_{ry}(y) dy. \tag{2-75c}$$

Substituting Eq. 2-64 and 2-65 into Eq. 2-39,

$$K_2 = K_{2x} K_{2y} \tag{2-76a}$$

where

$$K_{2x} = \int_{-\infty}^{\infty} \Phi_{nnx}(f_x) |H_{rx}(f_x)|^2 df_x \tag{2-76b}$$

and

$$K_{2y} = \int_{-\infty}^{\infty} \Phi_{nny}(f_y) |H_{ry}(f_y)|^2 df_y, \tag{2-76c}$$

and from Eq. 2-15

$$K_{2x} = E\{n^2_{Tx}(x)\} \qquad (2\text{-}76d)$$

and

$$K_{2y} = E\{n^2_{Ty}(y)\} . \qquad (2\text{-}76e)$$

And finally writing Eq. 2-6 in terms of the two spatial dimensions,

$$K_3 = -\frac{1}{4\pi^2 f_H^2} \int_{-\infty}^{\infty}\int g''(x,y)g(x,y)dxdy \qquad (2\text{-}77)$$

and after substituting Eq. 2-71 into 2-77,

$$K_3 = -\frac{1}{4\pi^2 f_H^2} \int_{-\infty}^{\infty} g_x''(x)g_x(x)dx \int_{-\infty}^{\infty} g_y''(y)g_y(y)dy. \qquad (2\text{-}78)$$

Using the results of Eq. 2-72, 73, 16, 20, 31, 32, and 41,

$$K_3 = K_{3x}K_{3y} \qquad (2\text{-}79a)$$

where

$$K_{3x} = \int_{-\infty}^{\infty} \left(\frac{f_x}{f_{Hx}}\right)^2 |H_{bx}(f_x)|^2 |H_{rx}(f_x)|^2 df_x \qquad (2\text{-}79b)$$

and

$$K_{3y} = \int_{-\infty}^{\infty} \left(\frac{f_x}{f_{Hy}}\right)^2 |H_{by}(f_y)|^2 |H_{ry}(f_y)|^2 df_y \qquad (2\text{-}79c)$$

where

$$f_H^2 = -4\pi^2 f_{Hx}^2 f_{Hy}^2 . \qquad (2\text{-}79d)$$

Thus the problem of determining the optimum restoration filter point-spread function, $h_r(x,y)$ reduces to finding the $h_{rx}(x)$ that will minimize Eq. 2-74b subject to the constraints of Eq. 2-75b, 76b, and 79b, and to finding the $h_{ry}(y)$ that will minimize Eq. 2-74c subject to the constraints of Eq. 2-75c, 76e, and 79c. The original two-dimensional restoration problem reduces to two one-dimensional processes which have similar equations. From the preceeding vector notational analysis used in Eq. 2-7 through 2-41, 2-44, and 2-45, the system of equations necessary to solve for $h_{rx}(x)$ and $h_{ry}(y)$ may be formulated.

To solve the $h_{rx}(x)$, the augmented quadratic functional of the form of Eq. 2-11 determined by Eq. 2-74b, 75b, 76b, and 79b becomes,

$$I_x = \int_{-\infty}^{\infty} w_x(x) g_x^2(x)dx + \lambda_{1x} \int_{-\infty}^{\infty} s_x(x) h_{rx}^2(x)dx + \lambda_{2x} E\{n^2_{Tx}(x)\} - \frac{\lambda_{3x}}{4\pi^2 f_{Hx}^2} \int_{-\infty}^{\infty} g_x''(x) g_x(x)dx \qquad (2\text{-}80)$$

which may be written as a quadratic functional in the spatial frequency domain from Eq. 2-23 as

$$I_x = (B_{1x}H_{rx}, H_{rx}) + \lambda_{1x}(B_{2x}H_{rx}, H_{rx}) + \lambda_{2x}(B_{3x}H_{rx}, H_{rx}) + \lambda_{3x}(B_{4x}H_{rx}, H_{rx}) \qquad (2\text{-}81)$$

where

$$B_{1x}(f_x, \nu_x) = H_{bx}^*(f_x) H_{bx}(\nu_x) W_x(f_x - \nu_x) \qquad (2\text{-}82)$$

from Eq. 2-26,

$$B_{1x}'(f_x,\nu_x) = H_{bx}(\nu_x)\ H_{bx}^*(f_x)\ W_x^*(\nu_x-f_x) \qquad (2\text{-}83)$$

from Eq. 2-27,

$$B_{2x}(f_x,\nu_x) = S_x(f_x-\nu_x) \qquad (2\text{-}84)$$

from Eq. 2-28,

$$B_{2x}'(f_x,\nu_x) = S_x^*(\nu_x-f_x) \qquad (2\text{-}85)$$

from Eq. 2-29,

$$B_{3x}(f_x,\nu_x) = \Phi_{nnx}^*(\nu_x)\ \delta(f_x-\nu_x) \qquad (2\text{-}86)$$

from Eq. 2-30,

$$B_{3x}'(f_x,\nu_x) = \Phi_{nnx}(f_x)\ \delta(\nu_x-f_x) \qquad (2\text{-}87)$$

from Eq. 2-31,

$$B_{4x}(f_x,\nu_x) = \left(\frac{\nu_x}{f_{Hx}}\right)^2 |H_{bx}(\nu_x)|^2\ \delta(f_x-\nu_x) \qquad (2\text{-}88)$$

and from Eq. 2-32,

$$B_{4x}'(f_x,\nu_x) = \left(\frac{f_x}{f_{Hx}}\right)^2 |H_{bx}(f_x)|^2 \delta(\nu_x-f_x). \qquad (2\text{-}89)$$

The gradient of Eq. 2-81 may be written in the form of Eq. 2-33,

$$\nabla I_x = (B_{1x}+B_{1x}')H_{rx} + \lambda_{1x}(B_{2x}+B_{2x}')H_{rx}$$

$$+ \lambda_{2x}(B_{3x}+B_{3x}')H_{rx} + \lambda_{3x}(B_{4x}+B_{4x}')H_{rx} \qquad (2\text{-}90)$$

which may be expanded to the form of Eq. 2-35,

$$\nabla I_x = \int_{-\infty}^{\infty} [H^*_{bx}(f_x)H_{bx}(x)\{W_x(f_x-\nu_x) + W^*_x(\nu_x-f_x)\}$$

$$+ \lambda_{1x}\{S_x(f_x-\nu_x) + S^*_x(\nu_x-f_x)\}]H_{rx}(\nu)d\nu_x$$

$$+ 2[\lambda_{2x}\Phi_{nnx}(f_x) + \lambda_{3x}(\frac{f_x}{f_{Hx}})^2|H_{bx}(f_x)|^2]H_{rx}(f_x) = 0. \quad (2\text{-}91)$$

Substituting Eq. 2-53 and 55 into Eq. 2-91, the following differential equation results

$$H''_{rx}(f_x) + \{2H^*_{bx}(f_x)H'_{bx}(f_x)x_s^2/[|H_{bx}(f_x)|^2x_s^2+\lambda_{1x}x_w^2]\}H'_{rx}(f_x)$$

$$+ \{x_s^2[H^*_{bx}(f_x)H''_{bx}(f_x) - 4\pi^2x_w^2\{c_x+\lambda_{3x}(\frac{f_x}{f_{Hx}})^2]|H_{bx}(f_x)|^2$$

$$+ \lambda_{2x}\Phi_{nnx}(f_x)+d_x\}] / [|H_{bx}(f_x)|^2x_s^2+\lambda_{1x}x_w^2]\}H_{rx}(f_x)$$

$$= 0. \quad (2\text{-}92)^4$$

From Eq. 2-36, 2-55, and 2-75b,

$$K_{1x} = -\frac{1}{4\pi^2x_s^2}\int_{-\infty}^{\infty}[H''_{rrx}(f_x)H_{rrx}(f_x) + H''_{rix}(f_x)H_{rix}(f_x)]df_x$$

$$+ d_x\int_{-\infty}^{\infty}|H_{rx}(f_x)|^2df_x \quad (2\text{-}93)$$

---

[4] For derivation, see Appendix D.

where

$$H_{rx}(f_x) = H_{rrx}(f_x) + j\, H_{rix}(f_x) \qquad (2\text{-}94)^5$$

and where $H_{rrx}(f_x)$ is the real part and $H_{rix}(f_x)$ is the imaginary part of $H_{rx}(f_x)$.

Restating Eq. 2-76b,

$$K_{2x} = \int_{-\infty}^{\infty} \Phi_{nnx}(f_x) |H_{rx}(f_x)|^2 df_x \qquad (2\text{-}76b)$$

and Eq. 2-79b,

$$K_{3x} = \int_{-\infty}^{\infty} \left(\frac{f_x}{f_{Hx}}\right)^2 |H_{bx}(f_x)|^2 |H_{rx}(f_x)|^2 df_x . \qquad (2\text{-}79b)$$

Thus the simultaneous solution of the differential equation, Eq. 2-92, and the constraint equations, Eq. 2-93, 2-76b, and 2-79b, specify the form of the x-component of the spatial frequency transform, or equivalently the point-spread function, of the restoration filter.

In a similar manner it is possible to solve for $h_{ry}(y)$ by forming an augmented quadratic functional of the form of Eq. 2-11 determined by Eq. 2-74c, 75c, 76e, and 79c,

$$I_y = \int_{-\infty}^{\infty} w_y(y) g_y^2(y) dy + \lambda_{1y} \int_{-\infty}^{\infty} s_y(y) h_{ry}^2(y) dy$$

$$+ \lambda_{2y}\, E\{n^2_{Ty}(y)\} - \frac{\lambda_{3y}}{4\pi^2 f_{Hy}^2} \int_{-\infty}^{\infty} g_y''(y) g_y(y) dy. \qquad (2\text{-}95)$$

---

[5] For derivation, see Appendix E.

By following an analogous procedure to that used for determining $h_{rx}(x)$ in Eq. 2-81 through 2-94, the equations which specify $h_{ry}(y)$ may be formulated. Only the results will be stated since the derivation of the equations for $h_{ry}(y)$ is identical in procedure to that given for $h_{rx}(x)$ with the appropriate change in variables form x- to y-dependency.

The differential equation specifying the form of $H_{ry}(f_y)$ becomes,

$$H''_{ry}(f_y) + \{2H^*_{by}(f_y)H'_{by}(f_y)y_s^2/[|H_{by}(f_y)|^2 y_s^2+\lambda_{1y}y_w^2]\}H'_{ry}(f_y)$$

$$+ \{y_s^2[H^*_{by}(f_y)H''_{by}(f_y) - 4\pi^2 y_w^2\{[c_y+\lambda_{3y}(\frac{f_y}{f_{Hy}})^2]|H_{by}(f_y)|^2$$

$$+ \lambda_{2y}\Phi_{nny}(f_y)+d_y\}]/[|H_{by}(f_y)|^2 y_s^2+\lambda_{1y}y_w^2]\}H_{ry}(f_y)$$

$$= 0, \qquad (2\text{-}96)$$

while the constraint equations become,

$$K_{1y} = -\frac{1}{4\pi^2 y_s^2}\int_{-\infty}^{\infty}[H''_{rry}(f_y)H_{rry}(f_y)+H''_{riy}(f_y)H_{riy}(f_y)]df_y$$

$$+ d_y\int_{-\infty}^{\infty}|H_{ry}(f_y)^2 df_y \qquad (2\text{-}97)$$

$$K_{2y} = \int_{-\infty}^{\infty}\Phi_{nny}(f_y)|H_{ry}(f_y)|^2 df_y \qquad (2\text{-}76c)$$

and

$$K_{3y} = \int_{-\infty}^{\infty}(\frac{f_y}{f_{Hy}})^2 |H_{by}(f_y)|^2|H_{ry}(f_y)|^2 df_y. \qquad (2\text{-}79c)$$

Thus the simultaneous solution of Eq. 2-96, 2-97, 2-76c, and 2-79c will specify the y- component of the restoration filter.

2.5 Radially Symmetric Restoration Filter

Probably the most common type of aperture, because of physical ease in construction, is the radially symmetric aperture. For this case it is assumed that

$$H_b(f_x,f_y) = H_{br}(f_r) \tag{2-98}$$

$$\Phi_{nn}(f_x,f_y) = \Phi_{nnr}(f_r) \tag{2-99}$$

and

$$H_r(f_x,f_y) = H_{rr}(f_r) \tag{2-100}$$

where

$$f_x^2+f_y^2 = f_r^2 . \tag{2-101}$$

The solution to Eq. 2-58 is analogous to the solution for $h_{rx}(x)$ where all variables dependent upon x are replaced by corresponding r dependent variables. From Eq. 2-44a,

$$w(\bar{v}) = w_r(r) \tag{2-102a}$$

$$= \left[\frac{2r-r_{w1}-r_{w2}}{r_{w2}-r_{w1}}\right]^{2k_{wr}} \tag{2-102b}$$

for k_{wr} a positive integer and

$$r^2 = x^2 + y^2. \tag{2-102c}$$

From Eq. 2-45a,

$$s(\bar{v}) = s_r(r) \tag{2-103a}$$

$$= \left[\frac{2r-r_{s1}-r_{s2}}{r_{s2}-r_{s1}}\right]^{2k_{sr}} \tag{2-103b}$$

for k_{sr} a positive integer.

Choosing

$$k_{wr} = 1 = k_{sr} \text{ and}$$

$$r_{w1} = -r_{w2} = r_w \tag{2-104}$$

$$r_{s1} = -r_{s2} = r_s,$$

the Fourier transforms of Eq. 2-102b and 103b become

$$W_r(f_r) = -\frac{1}{4\pi^2 r_w^2}\,\delta''(f_r) \tag{2-105}$$

$$S_r(f_r) = -\frac{1}{4\pi^2 r_s^2}\,\delta''(f_r). \tag{2-106}$$

To solve for $h_{rr}(r)$, the augmented quadratic functional of the form of Eq. 2-11 which must be minimized with respect to $h_{rr}(r)$ becomes,

$$I_r = \int_{-\infty}^{\infty} w_r(r) g_r^2(r)dr + \lambda_{1r} \int_{-\infty}^{\infty} s_r(r) h_{rr}^2(r)dr$$

$$+ \lambda_{2r}\, E\{n^2_{Tr}(r)\} - \frac{\lambda_{3r}}{4\pi^2 f_{Hr}^2} \int_{-\infty}^{\infty} g_r''(r) g_r(r)dr. \tag{2-107}$$

By following an analogous procedure to that used for determining $h_{rx}(x)$ in Eq. 2-81 through 2-94, the equations

which specify $h_{rr}(r)$ may be formulated. Again only the results will be stated since the derivation of the equations for $h_{rr}(r)$ is identical in procedure to that given for $h_{rx}(x)$ with the appropriate charge in variables.

The differential equation specifying the form of $H_{rr}(f_r)$ becomes,

$$H''_{rr}(f_r) + \{2H^*_{br}(f_r)H'_{br}(f_r)r_s^2/[|H_{br}(f_r)|^2 r_s^2+\lambda_{1r}r_w^2]\}H'_{rr}(f_r)$$

$$+ \{r_s^2[H^*_{br}(f_r)H''_{br}(f_r) - 4\pi^2 r_w^2\{\lambda_{3r}(\frac{f_r}{f_{Hr}})^2 |H_{br}(f_r)|^2$$

$$+ \lambda_{2r}\Phi_{nnr}(f_r)\}] \; / \; [|H_{br}(f_r)|^2 r_s^2+\lambda_{1r}r_w^2]\}H_{rr}(f_r)$$

$$= 0, \qquad (2\text{-}108)$$

while the constraint equations become,

$$K_{1r} = -\frac{1}{4\pi^2 r_s^2}\int_{-\infty}^{\infty}[H''_{rrr}(f_r)H_{rr}(f_r) + H''_{rir}(f_r)H_{rir}(f_r)]df_r \qquad (2\text{-}109)$$

$$K_{2r} = \int_{-\infty}^{\infty}\Phi_{nnr}(f_r)|H_{rr}(f_r)|^2 df_r \qquad (2\text{-}110)$$

and

$$K_{3r} = \int_{-\infty}^{\infty}(\frac{f_r}{f_{Hr}})^2 |H_{br}(f_r)|^2 |H_{rr}(f_r)|^2 df_r . \qquad (2\text{-}111)$$

Thus the simultaneous solution of Eq. 2-108 through 2-111 will give the spatial frequency spectrum of the optimum restoration filter.

2.6 Additional Shape Control of Composite Imaging Function by a Sub-optimal Iterative Technique

The third constraint, originally defined by Eq. 2-10, was chosen to provide control over the composite imaging function in such a way that the magnitude of secondary lobes in the immediate vicinity of the primary lobe could be reduced. These secondary lobes lead to undesirable ghosts in the restored image. Such a constraint is necessary because the weighting function, $w(\bar{v})$ defined by Eq. 2-42, of the fundamental design criterion as expressed by Eq. 2-7 has almost no significant effect on $g(\bar{v})$ in the immediate vicinity of the spatial origin. Thus, without the third constraint, significant secondary lobes in this region of the spatial domain could exist.

In order to provide additional control over the shape of the composite imaging function in the vicinity of the spatial origin, which is not feasible by the third constraint alone, an iterative technique is utilized. To implement the technique, the fundamental design criterion, defined by Eq. 2-7, is modified to be,

$$F = \int_{-\infty}^{\infty} w(\bar{v})[g(\bar{v})-m(\bar{v})]^2 d\bar{v}, \qquad (2\text{-}112)$$

where the criterion function $m(\bar{v})$ will be defined shortly.

The procedure for this technique is as follows. Initially, $m(\bar{v})$ is set equal to zero; Eq. 2-112 thus

reduces to the original fundamental criterion as defined by Eq. 2-7. A solution for the restoration filter based upon minimizing Eq. 2-112 subject to the constraints of Eq. 2-8 through 2-10 is obtained. The existence of a unique solution to this system of equations will be discussed in the next chapter. It should be noted that the resulting composite imaging point-spread function, $g(\bar{v})$, is optimal with regard to having a minimum radius of gyration. However $g(\bar{v})$ may still have some undesirable side lobes in the immediate vicinity of the spatial origin which were not sufficiently suppressed by the third constraint. In such a case, $m(\bar{v})$ is defined to be equal to the optimum $g(\bar{v})$ in the region about the origin containing the primary response lobe but excluding any secondary side lobes, and equal to an appropriately chosen function of the optimum $g(\bar{v})$ outside of this region so as to further constrain against the side lobes.

After choosing an appropriate $m(\bar{v})$, the first iteration is made by minimizing Eq. 2-112, subject to the constraints of Eq. 2-8 through 2-10. The resulting composite imaging function, although no longer optimum with regard to having a minimum radius of gyration, will not deviate significantly from the optimum in this respect because of the way in which $m(\bar{v})$ is chosen and, more importantly, will have significantly lower secondary lobe responses due to the weighting effect introduced by $m(\bar{v})$. If necessary, a second

iteration may be made by choosing an appropriate $m(\bar{v})$ based upon the $g(\bar{v})$ of the first iteration, and so on. There appears to be an almost unlimited number of functions which may be chosen for defining the criterion function including the absolute value, and exponential, Gaussian, and polynomial approximations; however the effect of any of these upon the iterated composite imaging point-spread function should be similar, because of the way in which $m(\bar{v})$ is chosen.

An example of one possible one-dimensional criterion function is shown in Figure 2-3. For this case, $m(\bar{v})$ is equal to the optimum $g(\bar{v})$ in the region of the primary lobe about the origin where $g(\bar{v})$ is positive. Outside of this region, $m(\bar{v})$ is chosen to be the absolute value of the optimum $g(\bar{v})$. A comparison of the $g(\bar{v})$ functions, both before and after iteration, would reveal that the secondary side lobes have been heavily constrained, while the general shape of the primary lobe has remained essentially the same. Thus this technique provides a very powerful means for making minor adjustments to the shape of the composite system point-spread function, $g(\bar{v})$. Although $g(\bar{v})$ could be altered in the same manner as that provided with this iterative technique by the introduction of additional constraint equations, the complexity of the functions necessary to produce the same control over $g(\bar{v})$ makes this alternative less attractive.

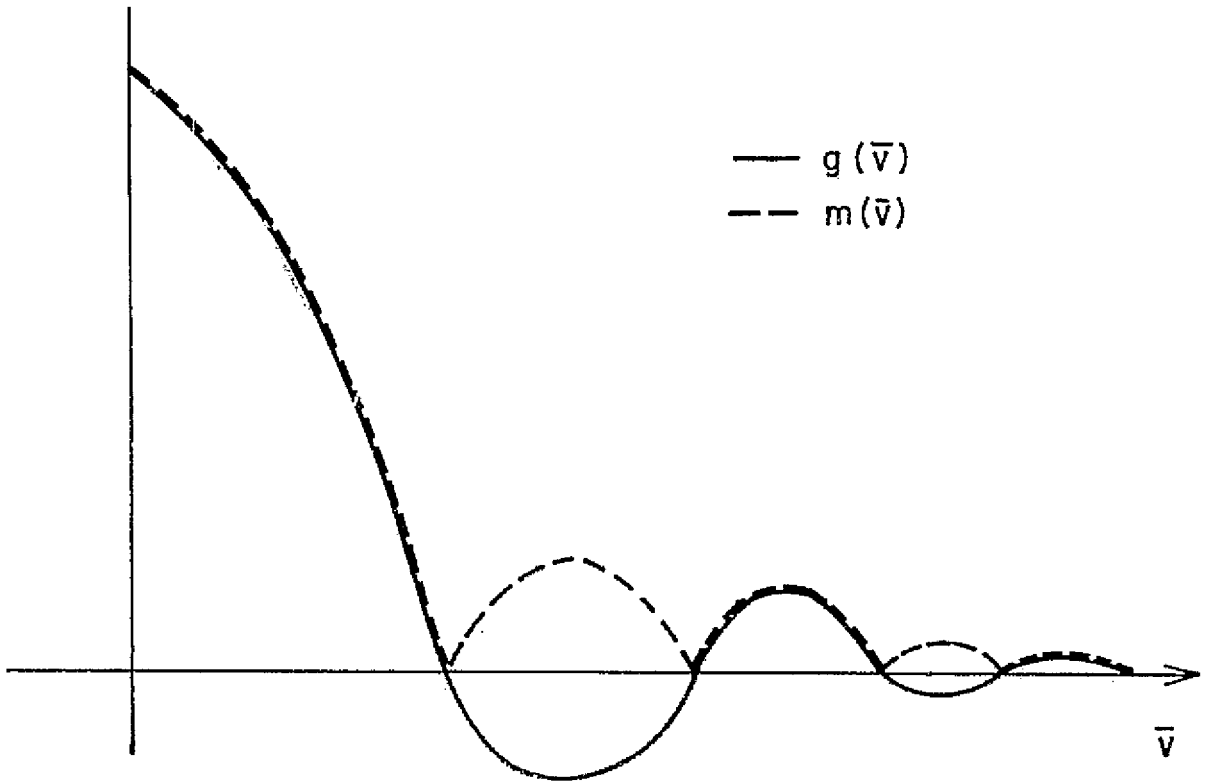

Figure 2-3: One Dimensional Criterion Function Based Upon Absolute Value of Optimum Imaging System Point-Spread Function

The following analysis is based upon the assumption of either a separable or a radically symmetric aperture since these are the most common apertures and are the forms considered in the remainder of this work. The general analysis, based upon a non-separable two-dimensional aperture is straightforward and analogous to that used in the development of Eq. 2-58 through 2-62 except that Eq. 2-58 is non-homogenous.

For a rectangularly separable aperture, Eq. 2-112 will be redefined in an analogous manner to Eq. 2-74 as

$$F = F_x F_y \qquad (2\text{-}113a)$$

where

$$F_x = \int_{-\infty}^{\infty} w_x(x)[g_x(x)-m_x(x)]^2 dx + p_x \qquad (2\text{-}113b)$$

and

$$F_y = \int_{-\infty}^{\infty} w_y(y)[g_y(y)-m_y(y)]^2 dy + p_y \qquad (2\text{-}113c)$$

where

$$0 < p_x, p_y << 1, \qquad (2\text{-}113d)$$

The constraint equations remain as defined by Eq. 2-75, 76, and 79. Thus for a given $m_x(x)$, $h_{rx}(x)$ must be determined by minimizing Eq. 2-113b subject to the constraints of Eq. 2-75b, 76d, and 79b and for a given $m_y(y)$, $h_{ry}(y)$ must be determined by minimizing Eq. 2-113c subject to the constraints of Eq. 2-75c, 76e, and 79c.

To solve for $h_{rx}(x)$, an augmented quadratic functional formed from Eq. 2-113b and Eq. 2-75b, 76d, and 79b can be

written

$$I_x = \int_{-\infty}^{\infty} w_x(x)[g_x(x)-m_x(x)]^2dx + p_x$$

$$+ \lambda_{1x} \int_{-\infty}^{\infty} s_x(x)h_{rx}^2(x)dx$$

$$+ \lambda_{2x} E\{n^2_{Tx}(x)\} - \frac{\lambda_{3x}}{4\pi^2 f_{Hx}^2} \int_{-\infty}^{\infty} g_x''(x)g_x(x)dx. \qquad (2\text{-}114)$$

Expanding the first integral of Eq. 2-114 gives

$$I_x = \int_{-\infty}^{\infty} w_x(x)g_x^2(x)dx - 2\int_{-\infty}^{\infty} w_x(x)g_x(x)m_x(x)dx$$

$$+ \int_{-\infty}^{\infty} w_x(x)m_x^2(x)dx + p_x + \lambda_{1x} \int_{-\infty}^{\infty} s_x(x)h_{rx}^2(x)dx$$

$$+ \lambda_{2x} E\{n^2_{Tx}(x)\} - \frac{\lambda_{3x}}{4\pi^2 f_{Hx}^2} \int_{-\infty}^{\infty} g_x''(x)g_x(x)dx. \qquad (2\text{-}115)$$

Since the functional form of Eq. 2-115 is basically similar to that considered in Eq. 2-80 with the exception of the second, third, and fourth terms, only these terms will now be considered. The second term in Eq. 2-115 may be expanded into operator form as

$$I_m = -2\int_{-\infty}^{\infty} w_x(x)g_x(x)m_x(x)dx$$

$$= -2\int_{-\infty}^{\infty} w_x(x) \int_{-\infty}^{\infty} h_{rx}(\tau)h_{bx}(x-\tau)d\tau\, m_x(x)dx$$

$$= \int_{-\infty}^{\infty} A_{5x}(\tau)h_{rx}(\tau)\, d\tau, \qquad (2\text{-}116)$$

where

$$A_{5x}(\tau) = -2\int_{-\infty}^{\infty} w_x(x)m_x(x)h_{bx}(x-\tau)dx. \qquad (2\text{-}117)$$

Alternately Eq. 2-116 may be written in the frequency domain as

$$I_m = \int_{-\infty}^{\infty} B_{5x}(f_x)H_{rx}(f_x)df_x \qquad (2\text{-}118)$$

where

$$B_{5x}(f_x) = -2H_{bx}(f_x)\int_{-\infty}^{\infty} W_x(\nu_x)M_x^*(f_x+\nu_x)d\nu_x$$

and

$$M_x(\cdot) = \mathcal{F}\{m_x(\cdot)\}. \qquad (2\text{-}119)^6$$

Taking the gradient of the linear functional of Eq. 2-118 with respect to $H_{rx}(f_x)$ gives the conjugate kernel $B_{5x}^*(f_x)$.

$$\nabla I_m = B_{5x}^*(f_x). \qquad (2\text{-}120)$$

Substituting Eq. 2-53 into Eq. 2-119,

$$B_{5x}(f_x) = -2H_{bx}(f_x)\int_{-\infty}^{\infty}\left[-\frac{1}{4\pi^2 x_w^2}\delta''(\nu_x) + c_x\delta(\nu_x)\right] M_x^*(f_x+\nu_x)d\nu_x$$

$$= H_{bx}(f_x)\left[\frac{1}{2\pi^2 x_w^2}\frac{d^2}{df_x^2}M_x^*(f_x) - 2c_x M_x^*(f_x)\right]. \qquad (2\text{-}121)$$

---

6 See Appendix F for derivation

The third and fourth terms of Eq. 2-115 may be neglected since they are not functions of $h_{rx}(\cdot)$, and thus the gradient of these terms with respect to $h_{rx}(\cdot)$is zero. The gradient of Eq. 2-115 may be written in the form of Eq. 2-90 as,

$$\nabla I_x = (B_{1x}+B_{1x}')H_{rx} + \lambda_{1x}(B_{2x}+B_{2x}')H_{rx} + \lambda_{2x}(B_{3x}+B_{3x}')H_{rx} + \lambda_{3x}(B_{4x}+B_{4x}')H_{rx} + B_{5x}^{*} \qquad (2\text{-}122)$$

which, when expanded, is similar in form to Eq. 2-92, except that the resulting differential equation is nonhomogeneous,

$$H_{rx}''(f_x) + 2H_{bx}^{*}(f_x)H_{bx}'(f_x)x_s^2 H_{rx}'(f_x)/[|H_{bx}(f_x)|^2 x_s^2 + \lambda_{1x}x_w^2] + x_s^2[H_{bx}^{*}(f_x)H_{bx}''(f_x) - 4\pi^2 x_w^2\{[c_x+\lambda_{3x}(f_x/f_{Hx})^2]|H_{bx}(f_x)|^2 + \lambda_{2x}\Phi_{nnx}(f_x)+d_x\}]H_{rx}(f_x)/[|H_{bx}(f_x)|^2 x_s^2 + \lambda_{1x}x_w^2] = 2\pi^2 x_s^2 x_w^2 B_{5x}^{*}(f_x) / [|H_{bx}(f_x)|^2 x_s^2+\lambda_{1x}x_w^2]. \qquad (2\text{-}123)$$

Thus Eq. 2-123 in conjunction with constraint Eq. 2-93, 76b, and 79b specify the shape of the x- component of the frequency spectrum of the restoration filter. A similar equation set may be written for the y- axis frequency spectrum component of the restoration by using Eq. 2-97, 76c, and 79c, and replacing the x- variables in Eq. 2-123 with appropriate y- variables.

For a radially symmetric aperture, Eq. 2-112 may be defined as

$$F = \int_{-\infty}^{\infty} w_r(r)[g_r(r)-m_r(r)]^2 dr, \qquad (2\text{-}124)$$

where $w_r(r)$ is as previously defined in Eq. 2-102. The augmented functional to be minimized is similar in form to Eq. 2-107,

$$I_r = \int_{-\infty}^{\infty} w_r(r) g_r^2(r) dr - 2 \int_{-\infty}^{\infty} w_r(r) g_r(r) m_r(r) dr + \int_{-\infty}^{\infty} w_r(r) m_r^2(r) dr + \lambda_{1r} \int_{-\infty}^{\infty} s_r(r) h_{rr}^2(r) dr + \lambda_{2r} E\{n^2_{Tr}(r)\} - \frac{\lambda_{3r}}{4\pi^2 f_{Hr}^2} \int_{-\infty}^{\infty} g_r''(r) g_r(r) dr. \qquad (2\text{-}125)$$

Following a similar development to that for Eq. 2-115, the resulting differential equation in terms of $H_{rr}(f_r)$ becomes,

$$H''_{rr}(f_r) + \{2H^*_{br}(f_r)H'_{br}(f_r)r_s^2/[|H_{br}(f_r)|^2 r_s^2+\lambda_{1r}r_w^2]\}H'_{rr}(f_r)$$

$$+ \{r_s^2[H^*_{br}(f_r)H''_{br}(f_r) - 4\pi^2 r_w^2\{\lambda_{3r}(\frac{f_r}{f_{Hr}})^2|H_{br}(f_r)|^2$$

$$+ \lambda_{2r}\Phi_{nnr}(f_r)\}] \;/\; [|H_{br}(f_r)|^2 r_s^2+\lambda_{1r}r_w^2]\}H_{rr}(f_r)$$

$$= 2\pi^2 r_s^2 r_w^2 B^*_{5r}(f_r) \;/\; [|H_{br}(f_r)|^2 r_s^2+\lambda_{1r}r_w^2] \qquad (2\text{-}126)$$

where

$$B_{5r}(f_r) = \frac{H_{br}(f_r)}{2\pi^2 r_w^2} \frac{d^2}{df_r^2} M^*_r(f_r). \qquad (2\text{-}127)$$

The constraint equations remain as defined by Eq. 2-109 through 2-111.

2.7 Classical "Inverse" Filter

Intuitively one would expect that if the constraints are removed and if the parameters of the weighting function, $w(\bar{v})$, are appropriately chosen so that only the origin is unweighted thus producing an impulse for the composite system point-spread function, then the resulting filter should have the form of the classical "inverse" filter.

For notational convenience, the following analysis will be made in terms of the radially symmetric aperture. From Eq. 2-102 for $k_{wr}=1$ and for a symmetric weighting function as defined by Eq. 2-104,

$$w_r(r) = (\frac{r}{r_w})^2. \qquad (2\text{-}128)$$

It is clear that as r_w approaches zero, only the origin remains unweighted in Eq. 2-107. From Eq. 2-108 which specifies the optimum restoration filter in the frequency domain, if r_w approaches zero and all the constraints are relaxed, the resulting differential equation becomes

$$H''_{rr}(f_r) + \frac{2H'_{br}(f_r)}{H_{br}(f_r)} + \frac{H''_{br}(f_r)H_{rr}(f_r)}{H_{br}(f_r)} = 0$$

or

$$H_{br}(f_r)H''_{rr}(f_r) + 2H'_{br}(f_r)H'_{rr}(f_r) + H''_{br}(f_r)H_{rr}(f_r) = 0. \qquad (2\text{-}129)$$

If it is assumed that

$$H_{rr}(f_r) = k\, H_{br}^{-1}(f_r), \qquad (2\text{-}130)$$

where k is an arbitrary constant, then it can be shown that Eq. 2-129 is satisfied. Since there exists a unique solution for a given differential equation of the form of Eq. 2-129, then Eq. 2-130 represents the only solution to Eq. 2-129 [16,24].

Thus the "inverse" filter represents that $h_r(\cdot)$ function which provides the best restoration possible for any combination of constraints by producing a composite imaging system point-spread function having the smallest radius of gyration.

CHAPTER 3

SYSTEM EQUATION SOLUTION TECHNIQUE FOR OPTIMUM RESTORATION FILTER

3.1 Introduction

The general system of equations defining the restoration filter aperture are examined to establish that a global minimum to the minimization problem exists, thus assuring a unique solution for a given set of constraints. The second-order differential equations of the previous chapter are reduced to a system of first-order differential equations to facilitate numerical solution, a minimization technique based upon the solution of the system of first-order differential equations subject to the constraint equations is described, and the effect of the initial conditions of the system of first-order differential equations upon the restoration filter aperture is examined.

3.2 Existence of Global Minimum to Restoration Filter Equation System

In the following discussion, direct reference will be made to the system of equations which specifies the optimum restoration filter for the x-axis component of a separable aperture, Eq. 2-92,93,76b, and 79b. However, the results are completely general and may also be applied to the systems of equations defining the y-axis component as well as the general restoration filter apertures.

In order to guarantee that the equation system, Eq. 2-92, 93,76b,and 79b, has a unique solution, all the defining functionals, that is the functional to be minimized as well as the constraint functionals, must be convex [14,15]. The property of convexity allows the theory of local extrema for general nonlinear functionals to become a global theory. Since the augmented functional I_x, Eq. 2-80, is a linear combination of the defining functionals, it must also be convex. Thus, there exists only one stationary point of the augmented functional and consequently Eq. 2-92,93,76b,and 79b have a unique solution for a given set of constraints. It can be shown [22] that quadratic functionals which are squares of norms are convex. Since all the defining functionals are of this class, convexity is assured.

3.3 Numerical Solution Technique

As in the previous section, for convenience, specific reference will be made to the equation system defining the x-axis component of a separable restoration filter aperture. However the results of this section are equally applicable to the radially symmetric restoration aperture. To include the results of the iteration technique described in Section 2.6, Eq. 2-92 will be replaced by Eq. 2-123. In order to take advantage of the many numerical techniques available for solving first-order differential equations, it is convenient to convert Eq. 2-123 to the normal form which is done in the following manner. Eq. 2-123 may be written as

$$H'''_{rx}(f_x) + A(f_x)H'_{rx}(f_x) + B(f_x)H_{rx}(f_x) = C(f_x). \qquad (3\text{-}1)$$

where

$$A(f_x) = 2H^*_{bx}(f_x)H'_{bx}(f_x)\, x_s^2/[|H_{bx}(f_x)|^2 x_s^2+\lambda_{1x}x_w^2] \qquad (3\text{-}2)$$

$$B(f_x) = x_s^2[H^*_{bx}(f_x)H'''_{bx}(f_x) - 4\pi^2x_w^2\{[c_x+\lambda_{3x}(f_x/f_{Hx})^2]\cdot$$

$$|H_{bx}(f_x)|^2 + \lambda_{2x}\Phi_{nnx}(f_x) + d_x\}]\, H_{rx}(f_x)/$$

$$[|H_{bx}(f_x)|^2 x_s^2 + \lambda_{1x}x_w^2] \qquad (3\text{-}3)$$

and

$$C(f_x) = \frac{2\pi^2 x_s^2 x_w^2 B^*_{5x}(f_x)}{|H_{bx}(f_x)|^2 x_s^2 + \lambda_{1x} x_w^2} \quad . \tag{3-4}$$

Defining the complex quantities in terms of the corresponding real and imaginary components,

$$H_{rx}(f_x) = H_{rxr}(f_x) + j\, H_{rxi}(f_x) \tag{3-5}$$

$$A(f_x) = A_r(f_x) + j\, A_i(f_x) \tag{3-6}$$

$$B(f_x) = B_r(f_x) + j\, B_i(f_x) \tag{3-7}$$

and

$$C(f_x) = C_r(f_x) + j\, C_i(f_x). \tag{3-8}$$

Eq. 3-1 may be rewritten as

$$\begin{aligned}&[H''_{rxr}(f_x)+j\, H''_{rxi}(f_x)] + [A_r(f_x)+j\, A_i(f_x)] \\ &\cdot [H'_{rxr}(f_x)+j\, H'_{rxi}(f_x)] + [B_r(f_x)+j\, B_i(f_x)] \\ &\cdot [H_{rxr}(f_x)+j\, H_{rxi}(f_x)] = C_r(f_x) + j\, C_i(f_x)\end{aligned} \tag{3-9}$$

or by collecting the real and imaginary components Eq. 3-9 may be written as

$$\begin{aligned}&H''_{rxr}(f_x) + A_r(f_x)H'_{rxr}(f_x) - A_i(f_x)H'_{rxi}(f_x) \\ &+ B_r(f_x)H_{rxr}(f_x) - B_i(f_x)H_{rxi}(f_x) - C_r(f_x) \\ &+ j\,[H''_{rxi}(f_x) + A_i(f_x)H'_{rxr}(f_x) + A_r(f_x)H'_{rxi}(f_x) \\ &+ B_i(f_x)H_{rxr}(f_x) + B_r(f_x)H_{rxi}(f_x) - C_i(f_x)] = 0.\end{aligned} \tag{3-10}$$

Eq. 3-10 may be separated into two differential equations [16] formed by the real and imaginary components of Eq. 3-10

$$H'''_{rxr}(f_x) + A_r(f_x)H'_{rxr}(f_x) - A_i(f_x)H'_{rxi}(f_x) + B_r(f_x)H_{rxr}(f_x) - B_i(f_x)H_{rxi}(f_x) - C_r(f_x) = 0 \quad (3\text{-}11)$$

and

$$H'''_{rxi}(f_x) + A_i(f_x)H'_{rxr}(f_x) + A_r(f_x)H'_{rxi}(f_x) + B_i(f_x)H_{rxr}(f_x) + B_r(f_x)H_{rxi}(f_x) - C_i(f_x) = 0. \quad (3\text{-}12)$$

Eq. 3-11 and 12 may be reduced to a system of first-order differential equations [16] by introducing the variables,

$$H_1(f_x) = H_{rxr}(f_x)$$

$$H_2(f_x) = H'_{rxr}(f_x)$$

$$H_3(f_x) = H_{rxi}(f_x)$$

$$H_4(f_x) = H'_{rxi}(f_x). \quad (3\text{-}13)$$

By substituting Eq. 3-13 into Eq. 3-11 and 12, the following system of first-order differential equations is formed,

$$H'_1(f_x) = H_2(f_x)$$

$$H'_2(f_x) = -B_r(f_x)H_1(f_x) - A_r(f_x)H_2(f_x) + B_i(f_x)H_3(f_x) + A_i(f_x)H_4(f_x) + C_r(f_x)$$

$$H_3'(f_x) = H_4(f_x)$$

$$H_4'(f_x) = - B_i(f_x)H_1(f_x) - A_i(f_x)H_2(f_x)$$

$$- B_r(f_x)H_3(f_x) - A_r(f_x)H_4(f_x) + C_i(f_x), \quad (3\text{-}14)$$

where

$$H_{rx}(f_x) = H_1(f_x) + j\ H_3(f_x). \quad (3\text{-}15)$$

Thus the second-order differential equation represented by Eq. 2-123 has been reduced to a system of first-order differential equations, Eq. 3-14.

The technique for determining a solution to the system of equations defined by Eq. 3-14, 2-93,76b, and 79b is based upon treating the constraint equations, Eq. 2-93,76b, and 79b, as a system of nonlinear equations and using a modified version of the subprogram SECANT [23] which is designed to handle a system of nonlinear equations. From an initial estimate for the Lagrange multipliers, a modified version of the subprogram DHPCG [12] , a subroutine designed to solve a system of first-order linear differential equations, is used to solve Eq. 3-14 for $H_{rx}(f_x)$. The constraint equations, Eq. 2-93,76b, and 79b, are then checked and any resulting error forms the basis for another iteration of SECANT and subsequent choice of Lagrange multipliers. Although SECANT only converges linearly, no derivatives of the functions defining the constraint equations are required.

Since SECANT has control over DHPCG by varying the Lagrange multipliers, it is important to re-examine Eq. 3-14 to determine the conditions for which no solution to this equation exists. It may be shown [16,24] that as long as the coefficients of Eq. 3-14, that is A_r, A_i, B_r, B_i, C_r, and C_i are continuous functions, then for a given set of initial conditions one and only one set of solutions exist. Thus theoretically for any set of finite value Lagrange multipliers, a solution to Eq. 3-14 should exist.

To complete the solution for the optimum x-axis component of the restoration aperture, appropriate initial conditions for Eq. 3-13 must be supplied and are defined as,

$$H_1(0) = H_{rxr}(0)$$

$$H_2(0) = H'_{rxr}(0)$$

$$H_3(0) = H_{rxi}(0)$$

$$H_4(0) = H'_{rxi}(0). \qquad (3\text{-}16)$$

For $h_{rx}(x)$ to be a real function, then

$$H_{rxr}(f_x) = \int_{-\infty}^{\infty} h_{rx}(x) \cos 2\pi f_x x \, dx$$

$$H'_{rxr}(f_x) = 2\pi \int_{-\infty}^{\infty} x \, h_{rx}(x) \sin 2\pi f_x x \, dx$$

$$H_{rxi}(f_x) = \int_{-\infty}^{\infty} h_{rx}(x) \sin 2\pi f_x x \, dx$$

and

$$H'_{rxi}(f_x) = 2\pi \int_{-\infty}^{\infty} x\, h_{rx}(x) \cos 2\pi f_x x \, dx. \qquad (3\text{-}17)$$

From Eq. 3-17,

$$H'_{rxr}(0) = 0 = H_{rxi}(0). \qquad (3\text{-}18)$$

The remaining initial conditions may be used to control the shape of $h_{rx}(x)$. For $h_{rx}(x)$ to be an even function about the x-axis origin, then

$$H_{rxr}(0) \neq 0$$

and

$$H_{rxi}(0) = 0. \qquad (3\text{-}19)$$

To preserve the DC gain, or average value, of the blurring system,

$$H_{rxr}(0) = \frac{1}{\mathrm{Re}[\, H_{bx}(0) \,]}, \qquad (3\text{-}20)$$

where Re[.] denotes the real part of the complex argument.

CHAPTER 4

EXPERIMENTAL VERIFICATION OF FUNDAMENTAL PROPERTIES OF OPTIMUM RESTORATION FILTER

4.1 Introduction

This chapter presents experimental results demonstrating the restoration filter performance as a function of the constraint parameters and from its application to a series of blurred test patterns. These results are based upon the assumption of a Gaussian-shaped blurring aperture. Since the principle application for this restoration technique was the resolution enhancement of the multispectral scanner system used for ERTS data collection, and since no specific information concerning the shape of the multispectral scanner aperture was available, a Gaussian model was chosen. This assumption was based upon two primary considerations. Because of the advantages in correcting a separable aperture as previously described in section 2.4, the first consideration for choosing a Gaussian blurring aperture was that such a model, if chosen to be symmetric about each axis, could also provide a separable blurring function which was also radially symmetric, thus approximating the radial symmetry of the actual scanner aperture. The second consideration for choosing a Gaussian blurring aperture model was for mathematical convenience. Since the frequency spectrum of a Gaussian blurring aperture is also Gaussian, this spectrum may be explicitly computed, thus eliminating

any errors which would have otherwise been introduced into the computation of the blurring aperture spectrum, H_{bx} or H_{by} as defined in Eq. 2-92 or 2-96 respectively, by a subroutine such as FORT.

Based upon a Gaussian blurring aperture model, an investigation of the performance and shape of the restoration filter as a function of its fundamental parameters and constraints is made. Also the composite system performance as a function of blurring aperture error is examined.

In addition, the blurring effects of a specific Gaussian aperture on a series of test patterns are examined to qualitatively demonstrate the degree of resolution enchancement possible for a given set of constraints. Also the truncation error effects for the "classical" inverse and constrained restoration filters are compared.

4.2 Parameter and Constraint Control of Restoration Filter Performance

The following is an investigation of the controlling effect demonstrated by the defined parameters and constraints upon the restoration filter's shape and performance. The constraint variations considered were directed by two primary goals: the first to investigate how parameter variations affect the restoration filter, and the second to apply the restoration filter to a specific enhancement problem which will be discussed in the next chapter. The

restoration filters for three Gaussian blurring apertures having radii of gyration of 1, 3, and 5, respectively, will be examined and compared to the unconstrained or classical "inverse" restoration filter. Since a separable blurring aperture is assumed, the following results may be interpreted as either x-axis solutions to the system of operations defined by Eq. 2-123, 121, 93, 76b, and 79b, or as y-axis solutions defined by a similar equation system where x-dependent parameters are replaced by corresponding y-dependent parameters.

Figure 4.1 shows a Gaussian shaped blurring aperture with a radius of gyration of one. The frequency spectrum of the classical "inverse" restoration filter, is shown in Figure 4.2. It should be noted that this spectral data was obtained not by inverting the spectrum of the blurring aperture of Figure 4.1 but rather by imposing the conditions stated in section 2.7 which define the classical "inverse" filter in terms of the parameters of the constrained restoration filter, Eq. 2-123, 121, 93, 76b, and 79b, and was performed as a test to verify the accuracy of the overall numerical algorithm described in Chapter 3. The corresponding point-spread function of the classical "inverse" restoration filter is shown in Figure 4.3. As a further check on the overall accuracy of the algorithm, the composite system point-spread function, representing the convolution

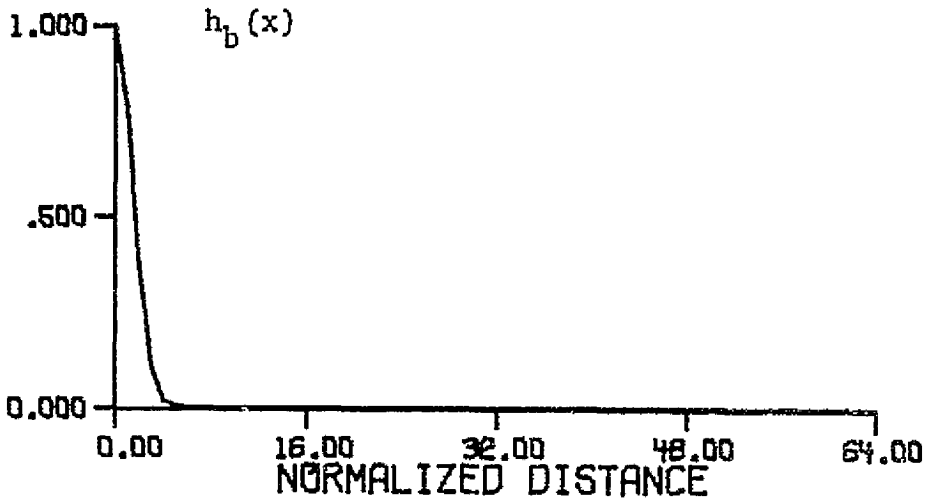

Figure 4.1 Gaussian Blurring Aperture Having a Radius of Gyration of One

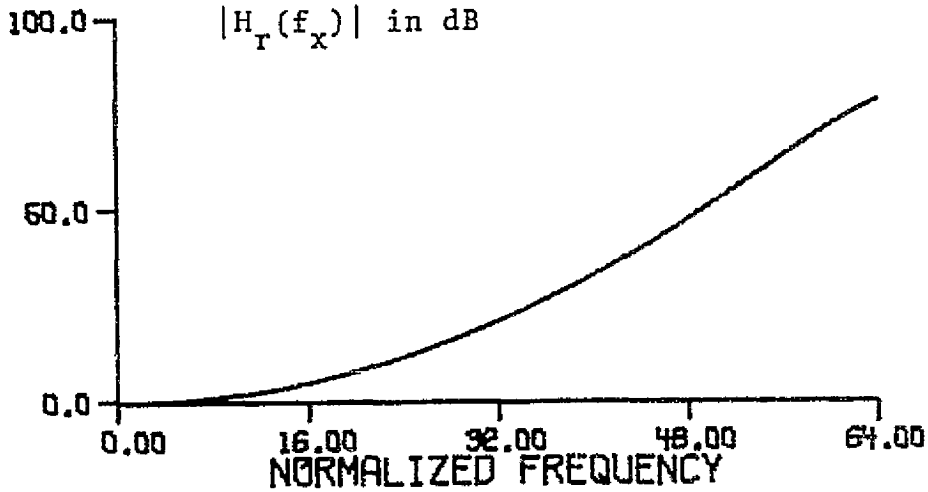

Figure 4.2 Classical "Inverse" Restoration Filter Frequency Spectrum for Blurring Aperture of Figure 4.1

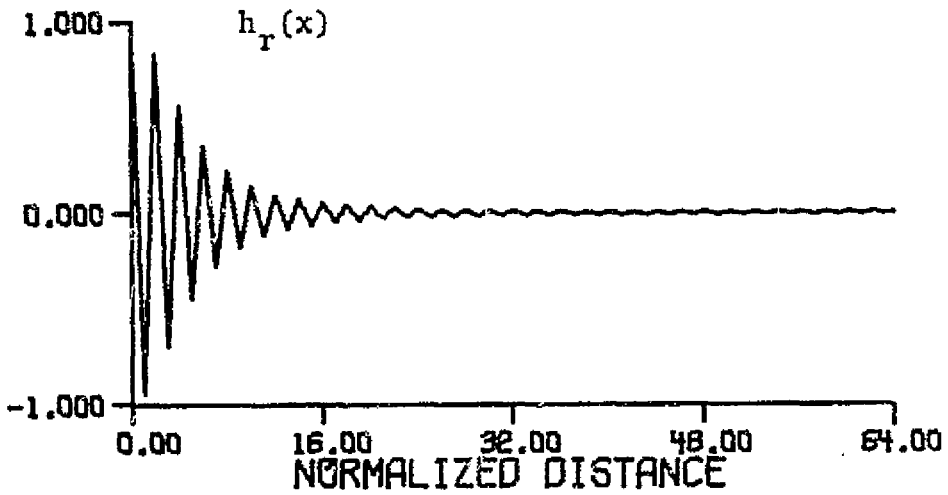

Figure 4.3 Classical "Inverse" Restoration Filter Point-Spread Function for Blurring Aperture of Figure 4.1

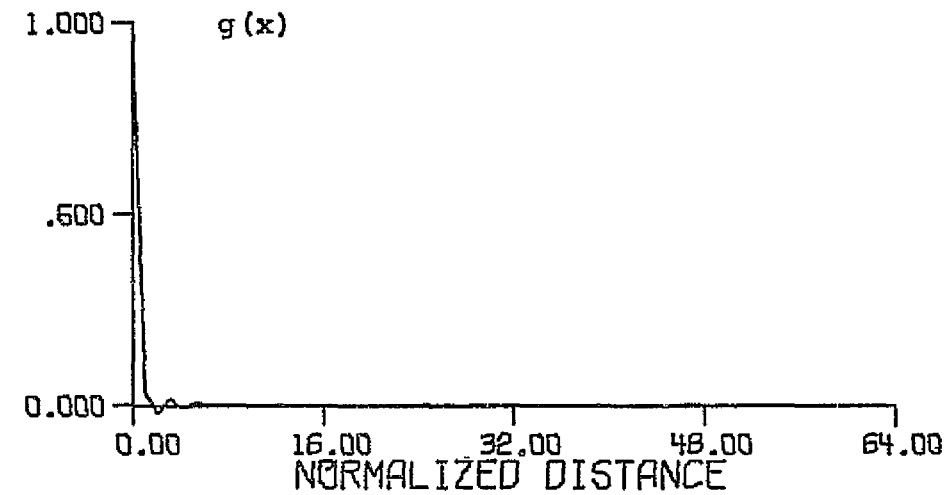

Figure 4.4 Composite System Point-Spread Function Resulting from Correcting the Blurring Aperture of Figure 4.1 with the Restoration Function of Figure 4.3

of the blurring aperture of Figure 4.1 with the "inverse" restoration function of Figure 4.3 is shown in Figure 4.4. As previously stated in section 2.2, the classical "inverse" filter will produce an impulse for the composite system point-spread function. Thus Figure 4.4 should represent a digital approximation to an impulse. Since the base line of the function shown in this figure should be zero, the difference, approximately 7×10^{-6}, represents a measure of the round-off error within the algorithm.

Figure 4.5 represents the restoration filter frequency spectrum for the blurring aperture of Figure 4.1 when the constraint, K_1, is employed to limit the radius of gyration of the resulting restoration filter point-spread function to 0.5 that of the unconstrained or classical "inverse" filter. Figure 4.6 shows the resulting restoration filter point-spread function having a radius of gyration of 0.5 that of the classical "inverse" restoration function shown in Figure 4.3. The resulting composite system point-spread function produced by convolving the blurring aperture of Figure 4.1 with the restoration point-spread function of Figure 4.6, is shown in Figure 4.7. The resulting radius of gyration of the composite system point-spread function is approximately 67% of that of the blurring aperture. Particular attention, however, should be paid to the significant secondary responses which are approximately 10% of

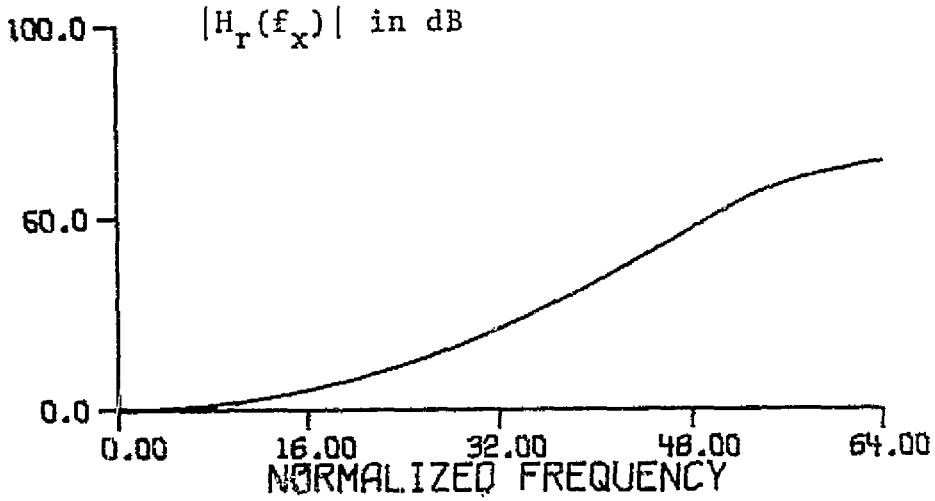

Figure 4.5 Restoration Filter Frequency Spectrum for Blurring Aperture of Figure 4.1 for $K_1 = 0.5$ Unconstrained Value with No Criterion Function Iteration

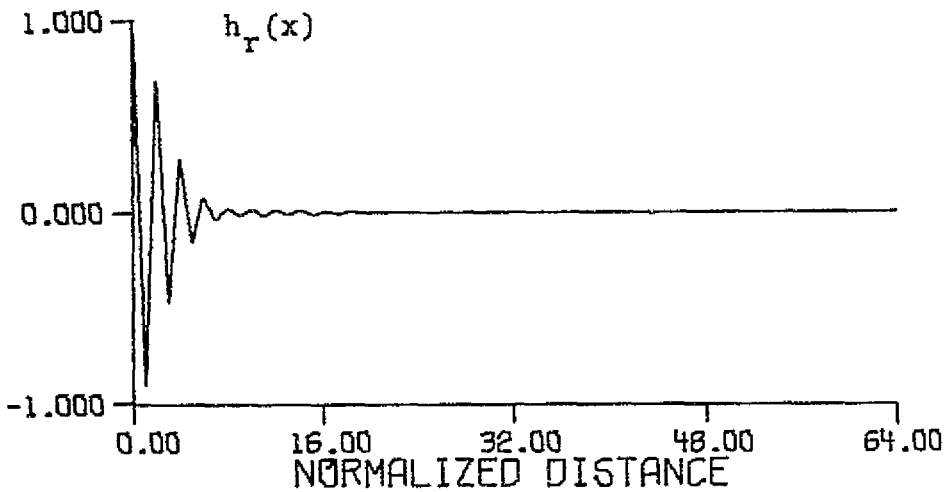

Figure 4.6 Restoration Filter Point-Spread Function Having Spectrum of Figure 4.5

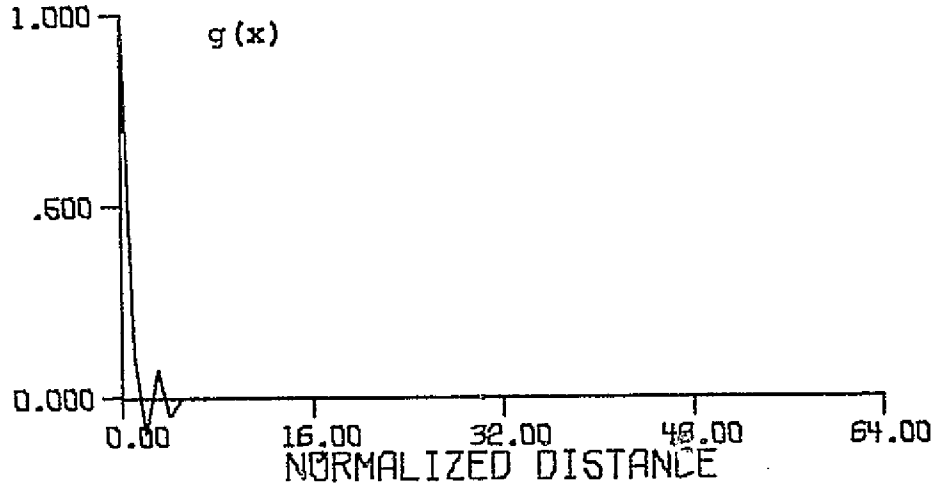

Figure 4.7 Composite System Point-Spread Function Resulting from Correcting the Blurring Aperture of Figure 4.1 with the Restoration Function of Figure 4.6

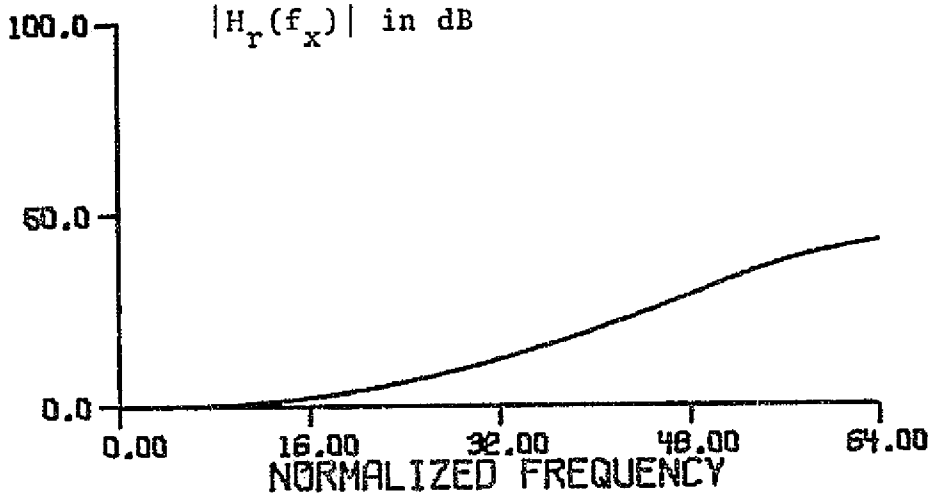

Figure 4.8 Restoration Filter Frequency Spectrum for Blurring Aperture of Figure 4.1 for $K_1 = 0.5$ Unconstrained Value and Nine Iterations with an Exponential Criterion Function

the magnitude of the primary lobe. As described in section 2.6, these secondary responses are highly undesirable since ghost images in the corrected image may result.

By applying the iteration technique described in section 2.6 to the restoration function previously described by Figure 4.5-4.7 and using nine iterations with an exponential criterion function, the resulting restoration filter frequency spectrum for the same constraint on K_1 is shown in Figure 4.8. The corresponding restoration filter point-spread function is shown in Figure 4.9 and has the same radius of gyration as the restoration function shown in Figure 4.6. The composite system point-spread function, resulting from convolving the function of Figure 4.1 with that of Figure 4.9, is shown in Figure 4.10. By comparing the composite system point-spread function shown in Figure 4.7 with that of Figure 4.10, the effectiveness of the iteration technique to suppress secondary side-lobe responses is evident. The radius of gyration of the composite system point-spread function of Figure 4.10 is approximately 74% of that the blurring aperture. Thus, as expected, the restoration function resulting from the iteration technique is somewhat less effective for image enhancement. It should be noted that although nine iterations were used, there is little change in the restoration function after about three iterations and that the iteration technique

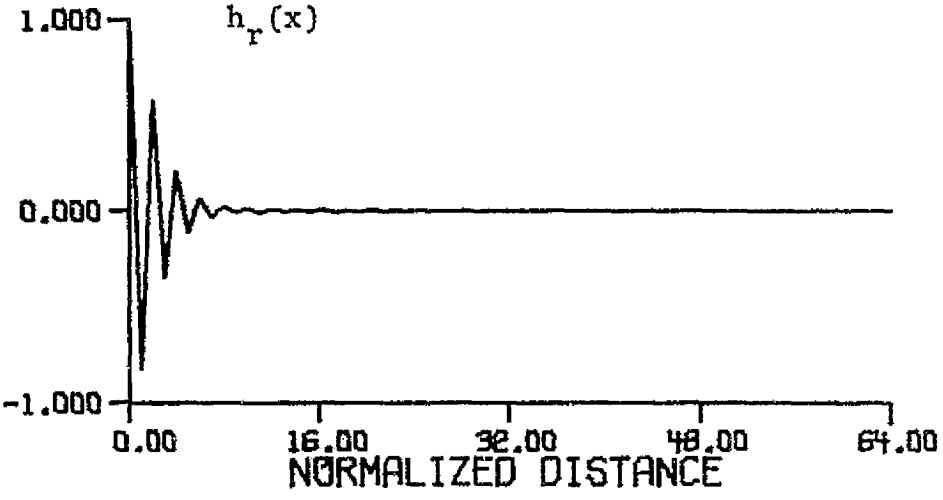

Figure 4.9 Restoration Filter Point-Spread Function Having Spectrum of Figure 4.9

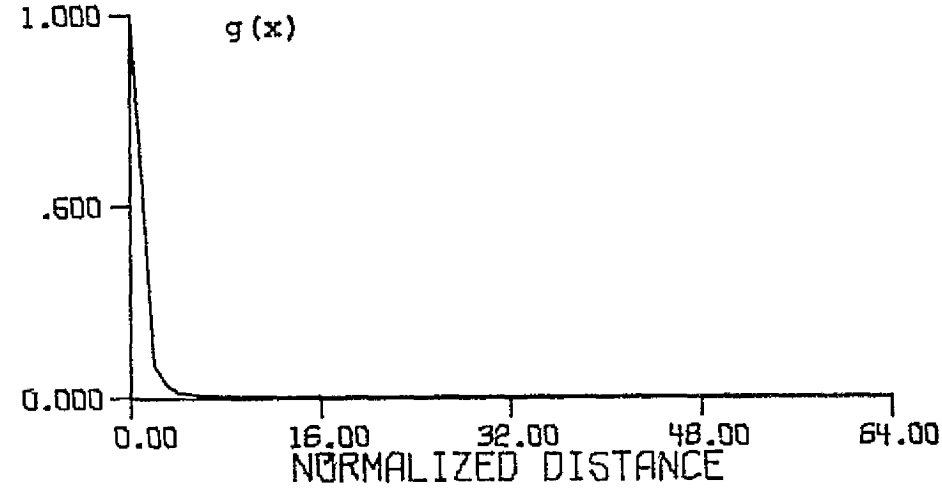

Figure 4.10 Composite System Point-Spread Function Resulting from Correcting the Blurring Aperture of Figure 4.1 with the Restoration Function of Figure 4.9

appears to converge rapidly.

Figure 4.11 through 4.16 and 4.17 through 4.22 represent the resulting restoration and composite system functions when the constraint in the radius of gyration of the restoration filter, K_1 is further reduced to 0.2 and 0.1 of the radius of gyration of the "inverse" filter, respectively. The radii of gyration of the composite system point-spread functions shown in Figure 4.13, 4.16, 4.19, and 4.22 are 81, 97, 89 and 90 percent of the radius of gyration of the blurring aperture of Figure 4.1, respectively.

The preceding figures demonstrated the effect of the constraint on the radius of gyration of the restoration filter in a noiseless environment for a Gaussian blurring aperture with a radius of gyration of one. To demonstrate the influence of noise on the restoration filter, an additive white noise with a spectral density of 10^{-5} volts^2/Hz was assumed. In addition, the output noise power constraint, K_2, was chosen to equal approximately 0.149% of the corresponding output noise power of the "inverse" filter. This particular value was chosen to approximate a signal-to-noise ratio of 20 dB when applied to the multispectral scanner data to be described in a later section. Figure 4.23 and 4.24 show the frequency spectra of the restoration filters when the constraint on the radius of gyration of the restoration filter point-spread function K_1 equals 0.5

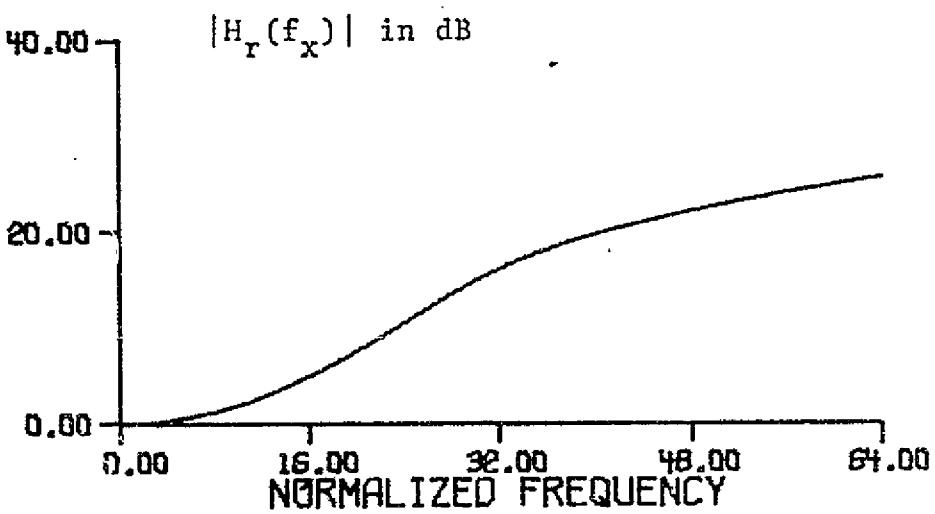

Figure 4.11 Restoration Filter Frequency Spectrum for Blurring Aperture of Figure 4.1 for $K_1 = 0.2$ Unconstrained Value with No Criterion Function Iteration

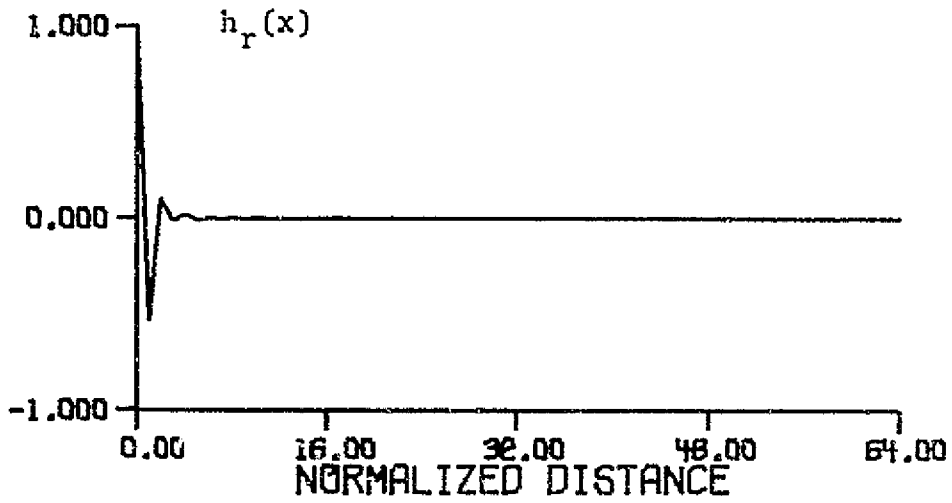

Figure 4.12 Restoration Filter Point-Spread Function Having Spectrum of Figure 4.11

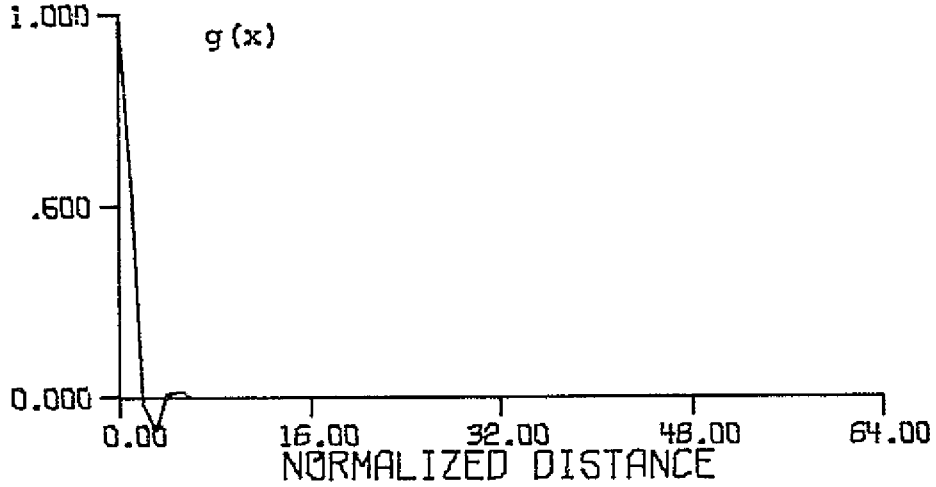

Figure 4.13 Composite System Point-Spread Function Resulting from Correcting the Blurring Aperture of Figure 4.1 with the Restoration Function of Figure 4.12

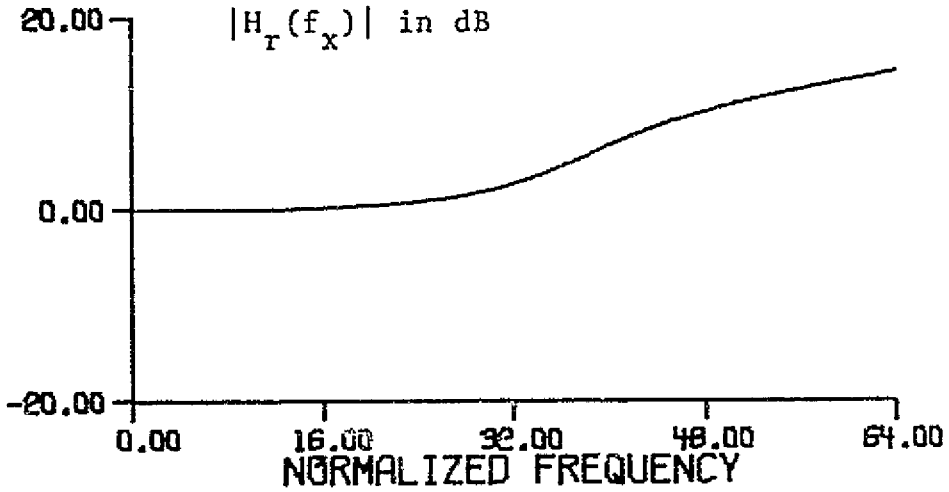

Figure 4.14 Restoration Filter Frequency Spectrum for Blurring Aperture of Figure 4.1 for $K_1 = 0.2$ Unconstrained Value with Ten Iterations Using an Exponential Criterion Function

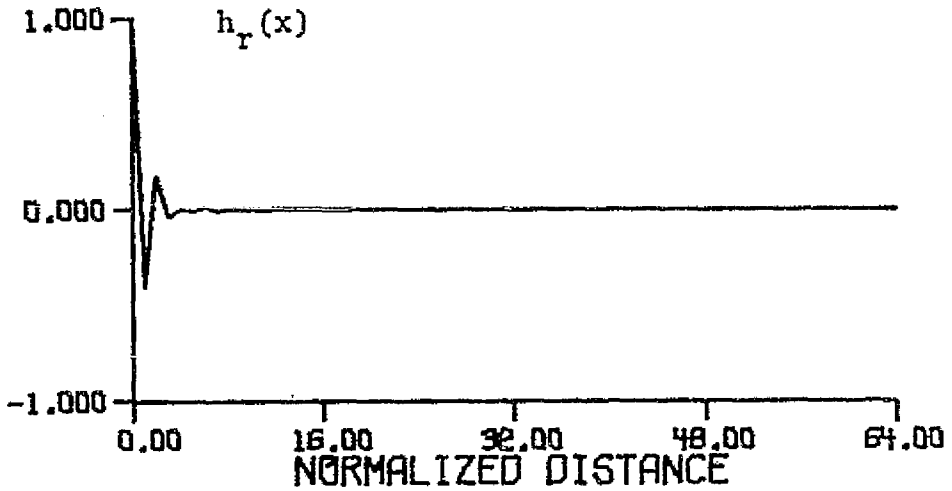

Figure 4.15 Restoration Filter Point-Spread Function Having Spectrum of Figure 4.14

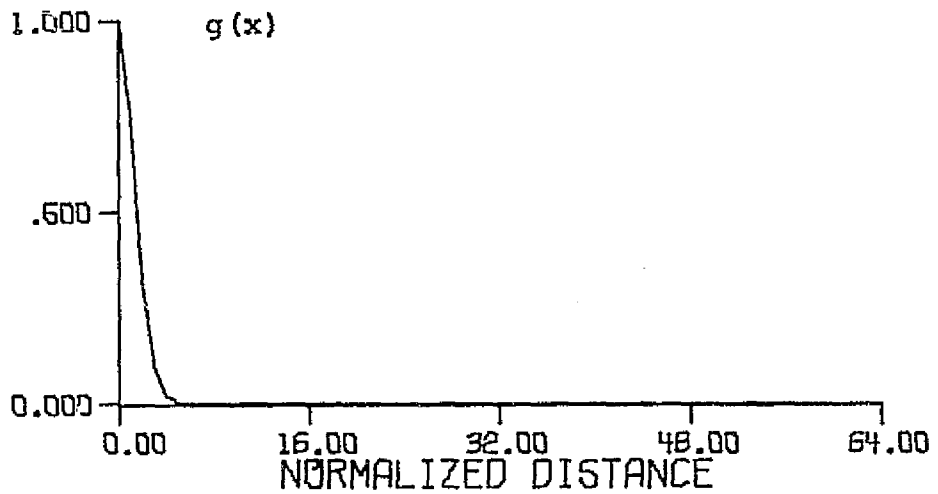

Figure 4.16 Composite System Point-Spread Function Resulting from Correcting the Blurring Aperture of Figure 4.1 with the Restoration Function of Figure 4.15

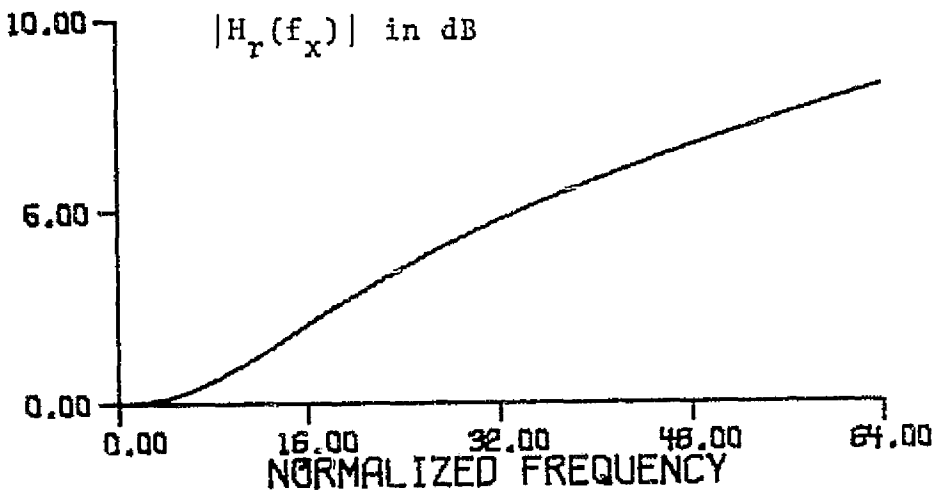

Figure 4.17 Restoration Filter Frequency Spectrum for Blurring Aperture of Figure 4.1 for K_1=0.1 Unconstrained Value With No Criterion Function Iterations

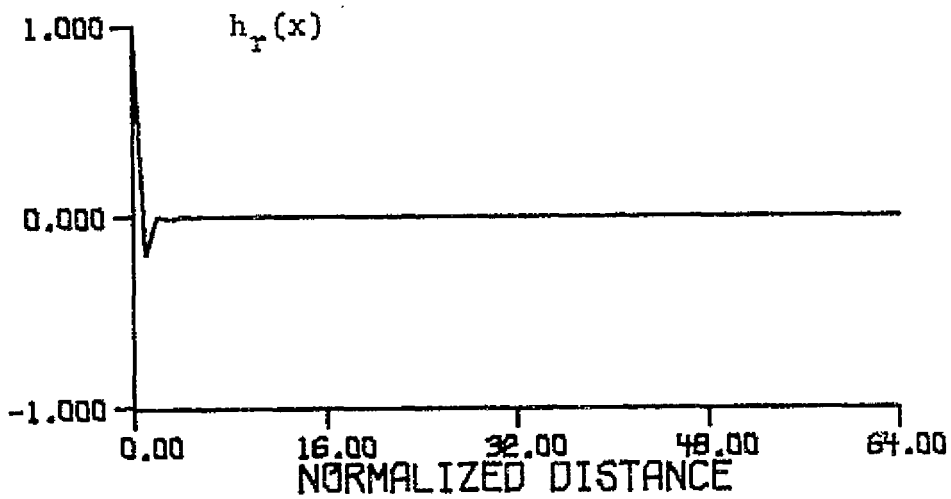

Figure 4.18 Restoration Filter Point-Spread Function Having Spectrum of Figure 4.17

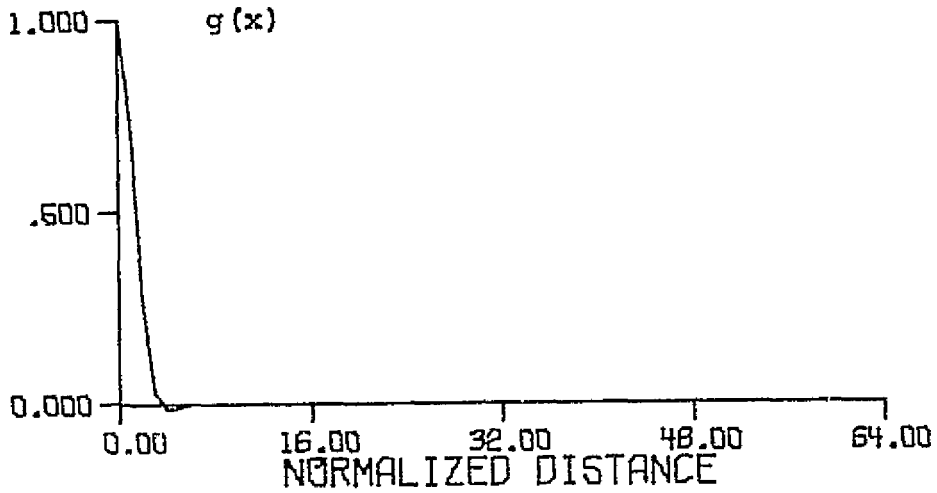

Figure 4.19 Composite System Point-Spread Function Resulting from Correcting the Blurring Aperture of Figure 4.1 with the Restoration Function of Figure 4.18

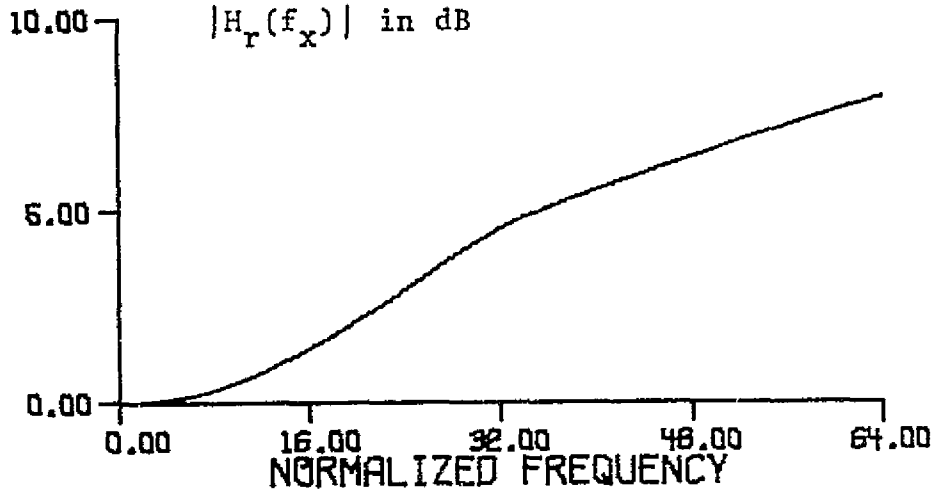

Figure 4.20 Restoration Filter Frequency Spectrum for Blurring Aperture of Figure 4.1 for $K_1 = 0.1$ Unconstrained Value with Ten Iterations Using an Exponential Criterion Function

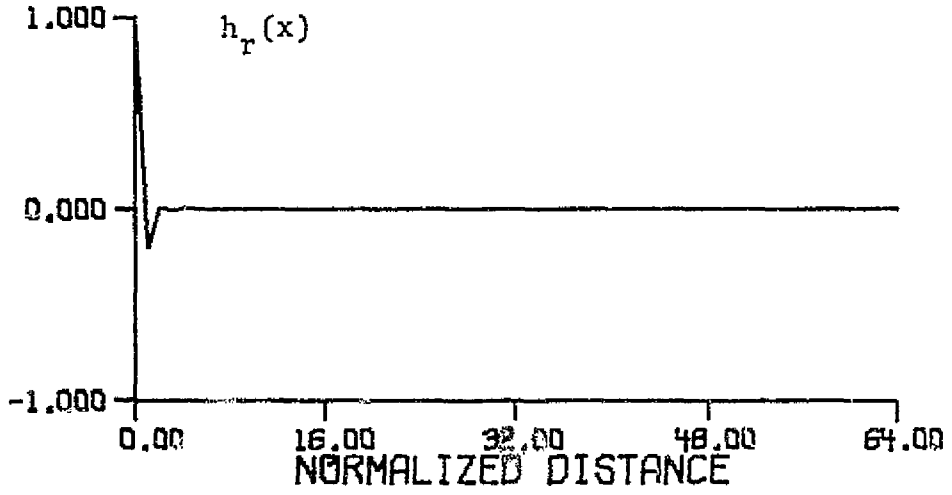

Figure 4.21 Restoration Filter Point-Spread Function Having Spectrum of Figure 4.20

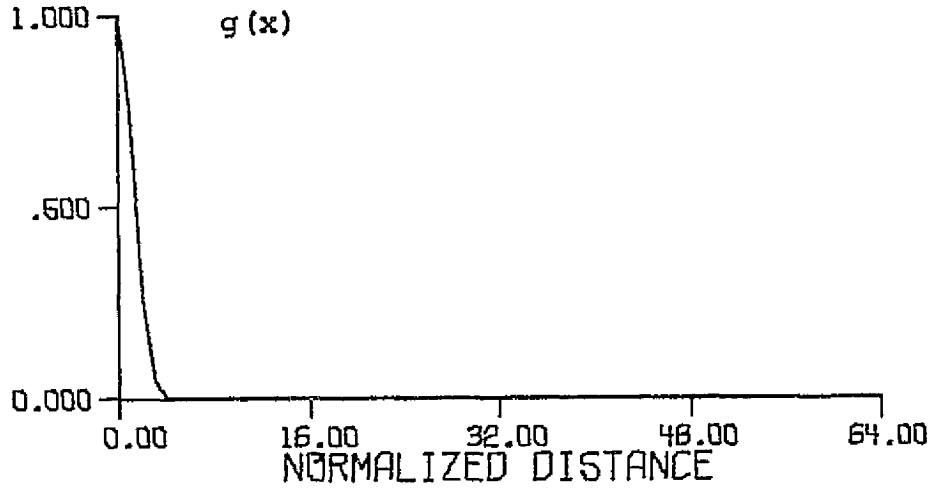

Figure 4.22 Composite System Point-Spread Function Resulting from Correcting the Blurring Aperture of Figure 4.1 with the Restoration Function of Figure 4.21

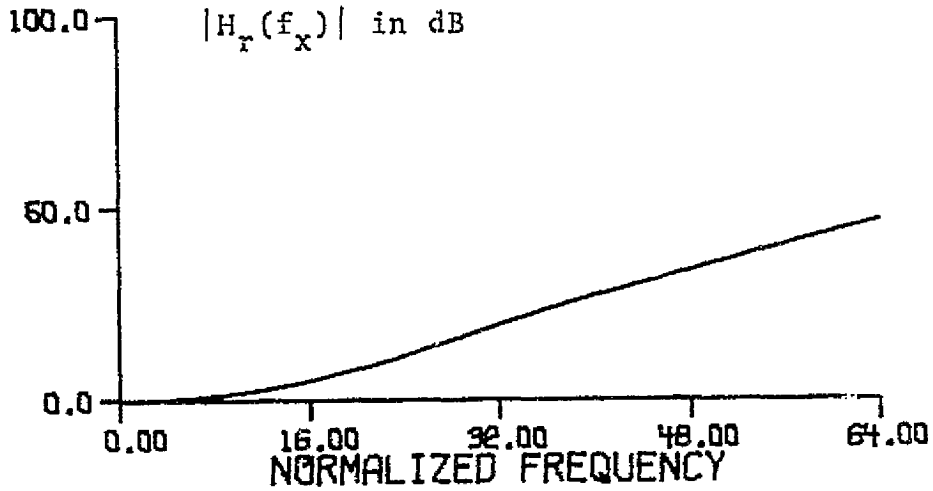

Figure 4.23 Restoration Filter Spectrum for Blurring Aperture of Figure 4.1 for $K_1 = 0.5$ and $K_2 = 0.00149$ (S/N ≈ 20dB) Unconstrained Values for a White Noise Power Spectral Density of 10^{-5} volts^2/Hz

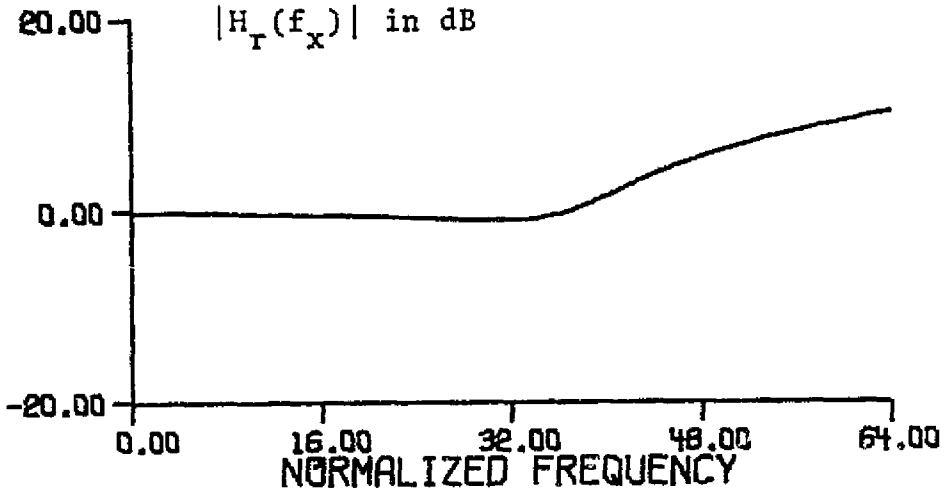

Figure 4.24 Restoration Filter Spectrum for Blurring Aperture of Figure 4.1 for $K_1 = 0.2$ and $K_2 = 0.00149$ (S/N ≈ 20dB) Unconstrained Values for a White Noise Power Spectral Density of 10^{-5} volts^2/Hz

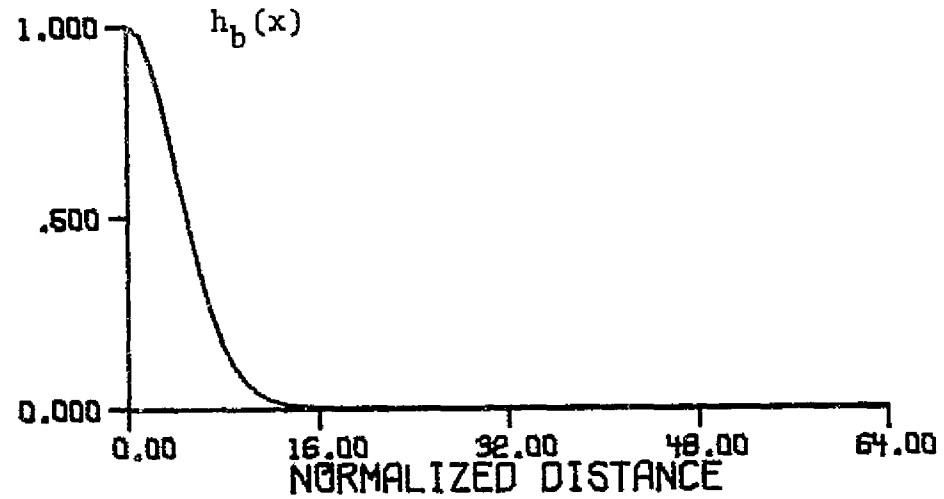

Figure 4.25 Gaussian Blurring Aperture Having a Radius of Gyration of Three

and 0.2 times the value of the "inverse" filter, respectively.

The following discussion will be with reference to a Gaussian blurring aperture with a radius of gyration of three, as shown in Figure 4.25. The restoration filter frequency spectrum, point-spread function, and the composite system point-spread function for the classical "inverse" restoration filter are shown in Figure 4.26, 4.27 and 4.28, respectively. When the radius of gyration of the restoration filter point-spread function is constrained to 0.5 of the unconstrained value, or value of the "inverse" filter, the resulting restoration and composite system functions with and without criterion function iterations are shown in Figure 4.29 to 4.34. Figure 4.35 to 4.40 show corresponding results when the radius of gyration of the restoration filter is further constrained to 0.2 of the value of the "inverse" filters. The radii of gyration of the composite system point-spread functions of Figure 4.31, 4.34, 4.37 and 4.40 are 14.3, 19.8, 88.5, and 89.3 percent of the radius of gyration of the blurring aperture of Figure 4.25.

Figure 4.41-4.52 demonstrate the effect of a white noise power spectral density upon the restoration function for the same input and output signal-to-noise ratios as employed with the filter previously considered. Figure 4.41-4.46 show the frequency spectrum of the restoration

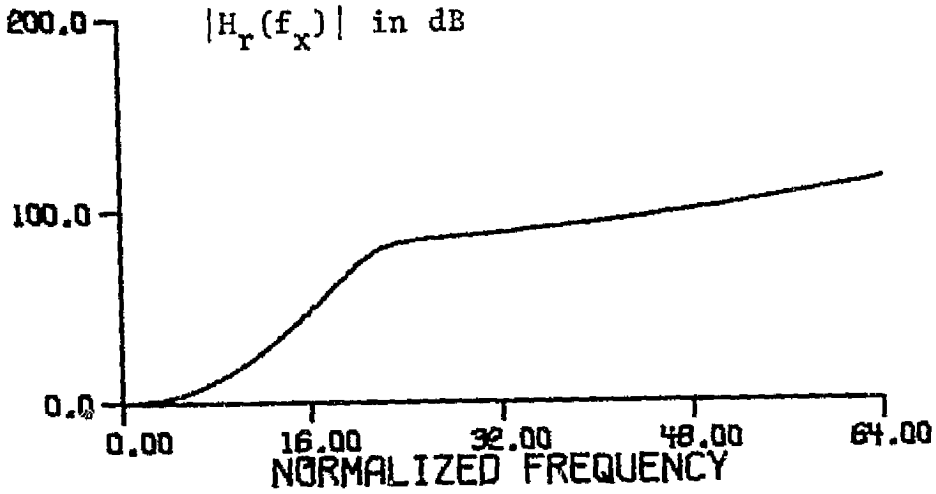

Figure 4.26 Classical "Inverse" Restoration Filter Frequency Spectrum for Blurring Aperture of Figure 4.25

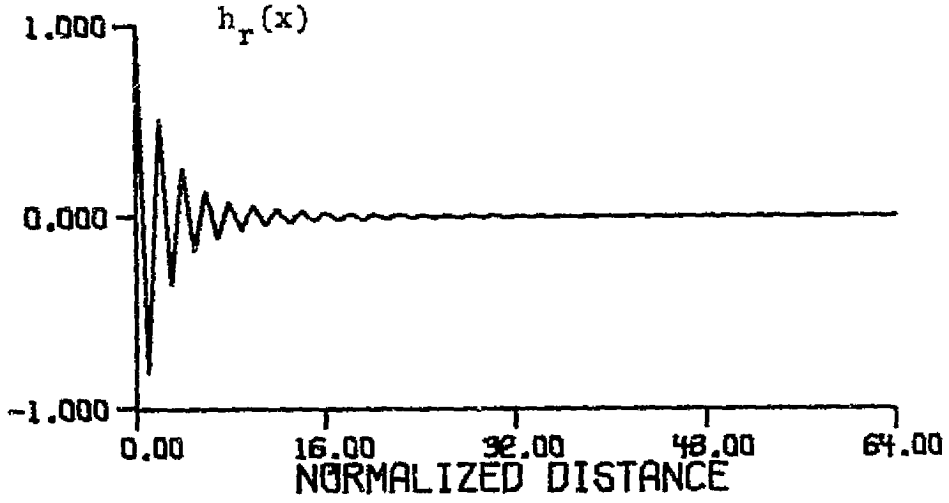

Figure 4.27 Classical "Inverse" Restoration Filter Point-Spread Function for Blurring Aperture of Figure 4.25

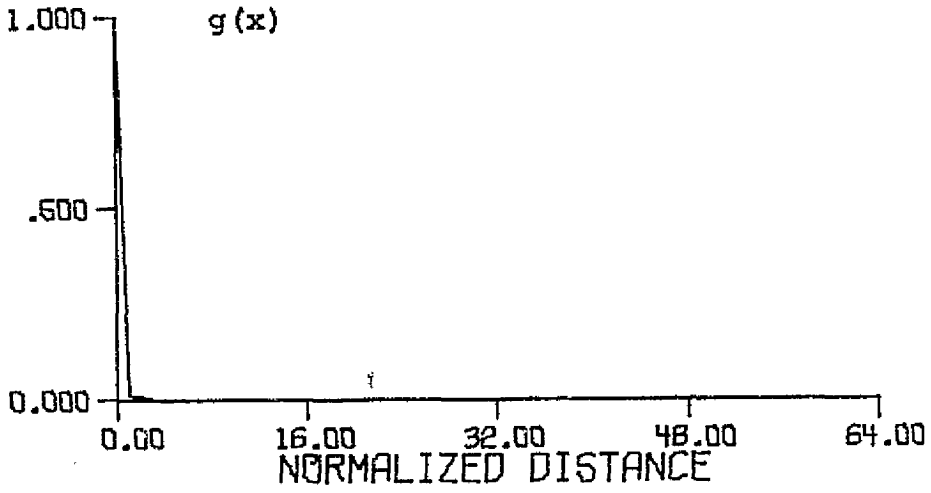

Figure 4.28 Composite System Point-Spread Function Resulting from Correcting the Blurring Aperture of Figure 4.25 with the Restoration Function of Figure 4.27

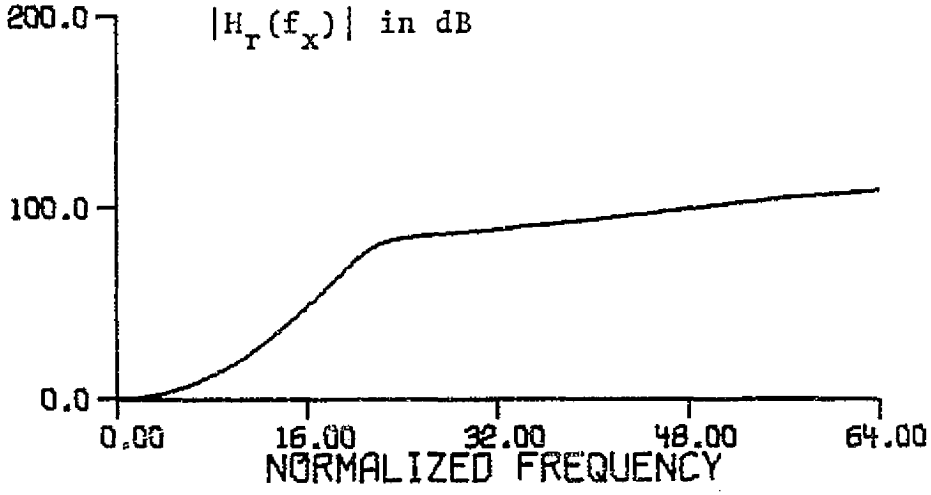

Figure 4.29 Restoration Filter Frequency Spectrum for Blurring Aperture of Figure 4.25 for $K_1 = 0.5$ Unconstrained Value with No Criterion Function Iteration

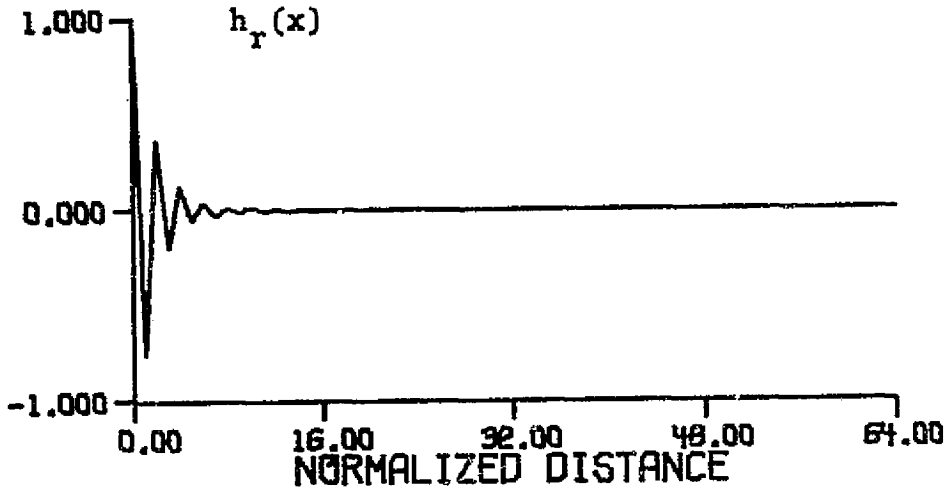

Figure 4.30 Restoration Filter Point-Spread Function Having Spectrum of Figure 4.29

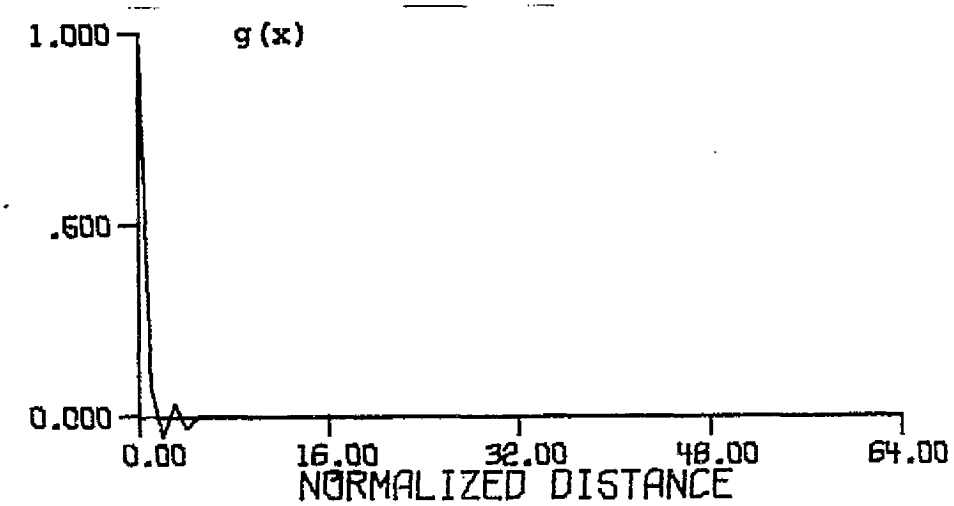

Figure 4.31 Composite System Point-Spread Function Resulting from Correcting the Blurring Aperture of Figure 4.25 with the Restoration Function of Figure 4.30

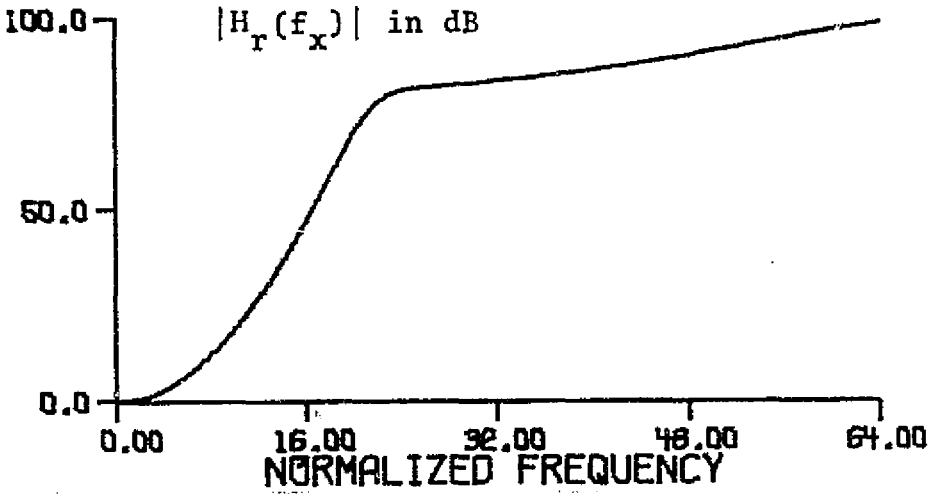

Figure 4.32 Restoration Filter Frequency Spectrum for Blurring Aperture of Figure 4.25 for $K_1 = 0.5$ Unconstrained Value and Four Iterations with an Exponential Criterion Function

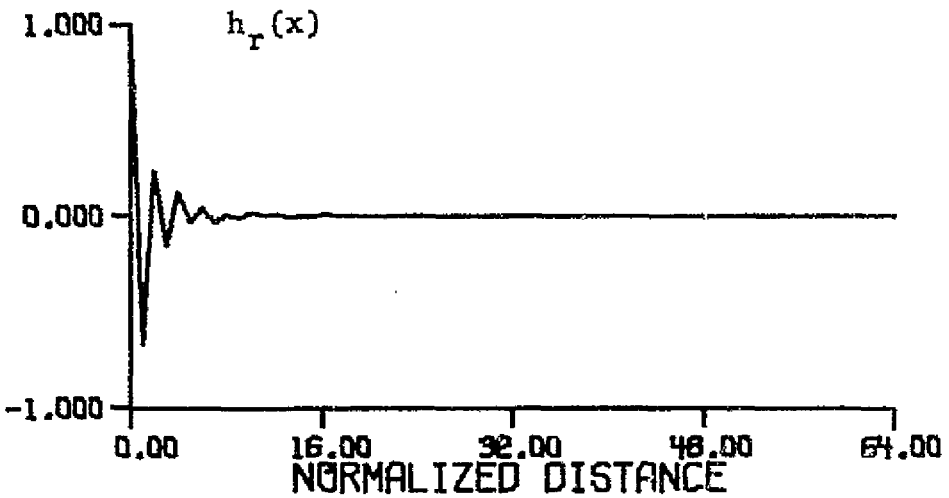

Figure 4.33 Restoration Filter Point-Spread Function Having Spectrum of Figure 4.32

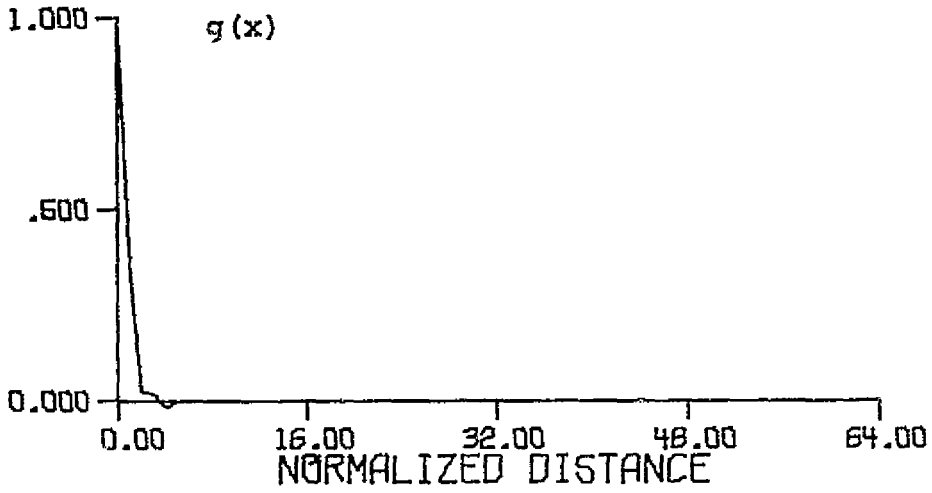

Figure 4.34 Composite System Point-Spread Function Resulting from Correcting the Blurring Aperture of Figure 4.25 with the Restoration Function of Figure 4.33

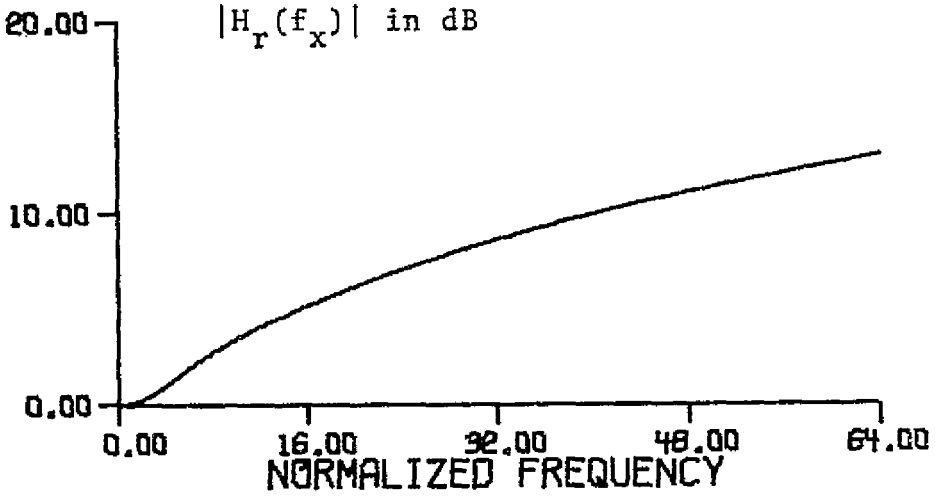

Figure 4.35 Restoration Filter Frequency Spectrum for Blurring Aperture of Figure 4.25 for $K_1 = 0.2$ Unconstrained Value with No Criterion Function Iteration

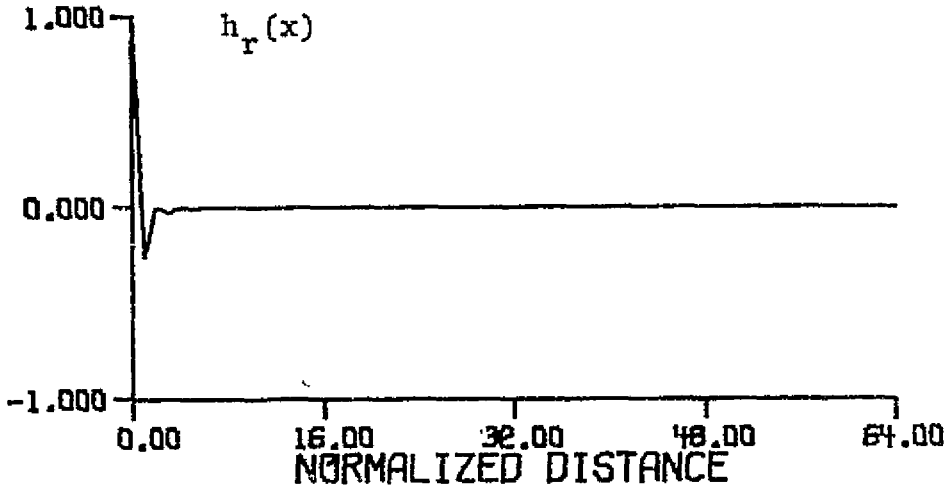

Figure 4.36 Restoration Filter Point-Spread Function Having Spectrum of Figure 4.35

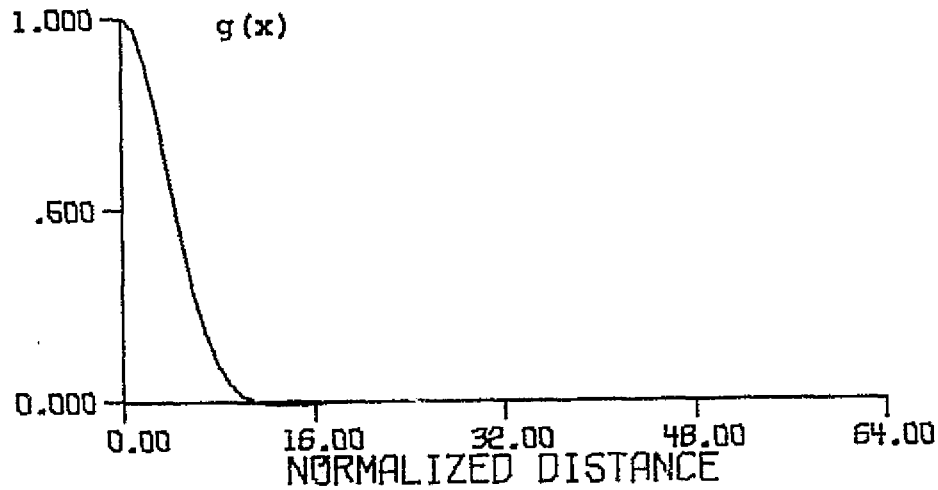

Figure 4.37 Composite System Point-Spread Function Resulting from Correcting the Blurring Aperture of Figure 4.25 with the Restoration Function of Figure 4.36

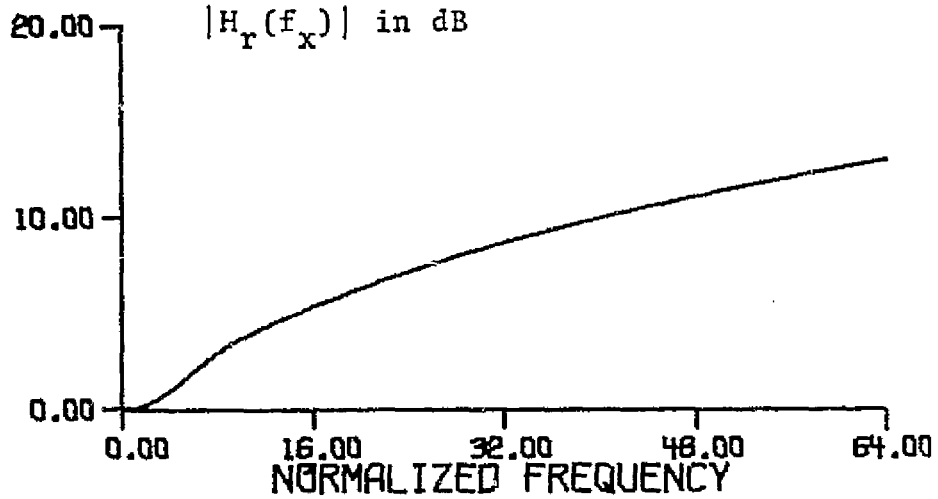

Figure 4.38 Restoration Filter Frequency Spectrum for Blurring Aperture of Figure 4.25 for $K_1 = 0.2$ Unconstrained Value and Four Iterations with an Exponential Criterion Function

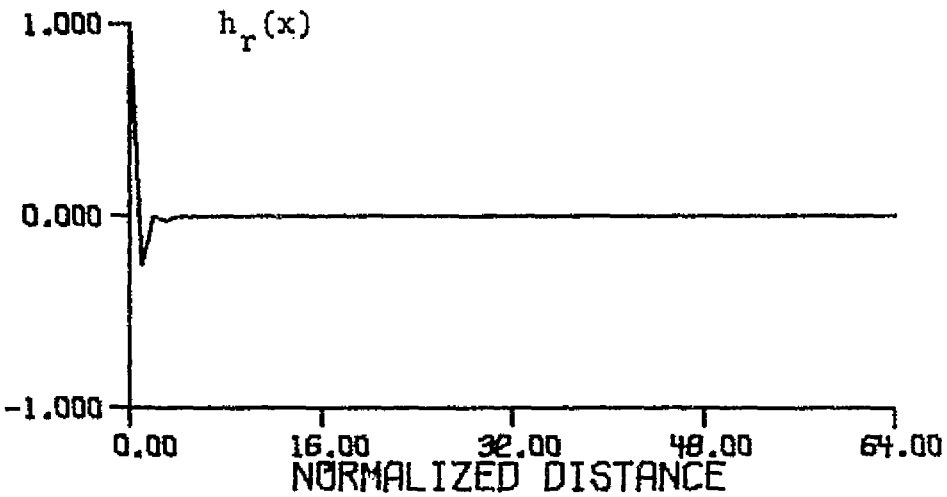

Figure 4.39 Restoration Filter Point-Spread Function Having Spectrum of Figure 4.38

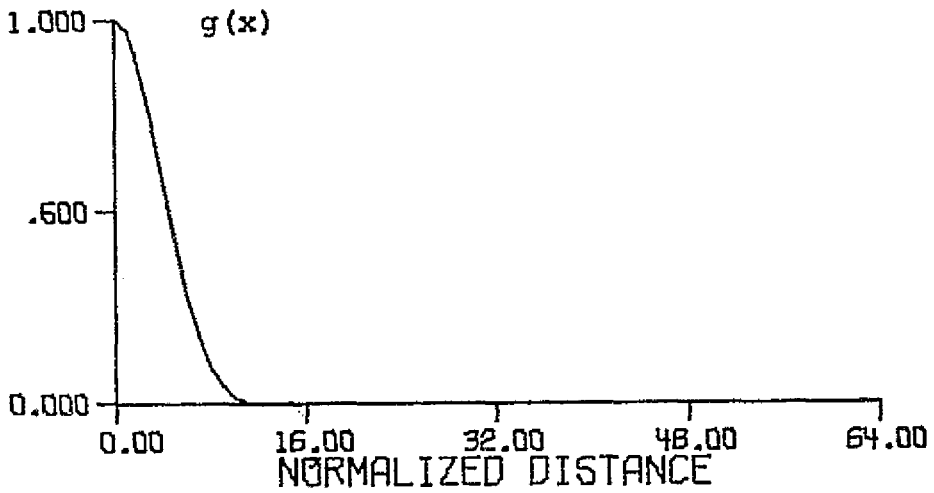

Figure 4.40 Composite System Point-Spread Function Resulting from Correcting the Blurring Aperture of Figure 4.25 with the Restoration Function of Figure 4.39

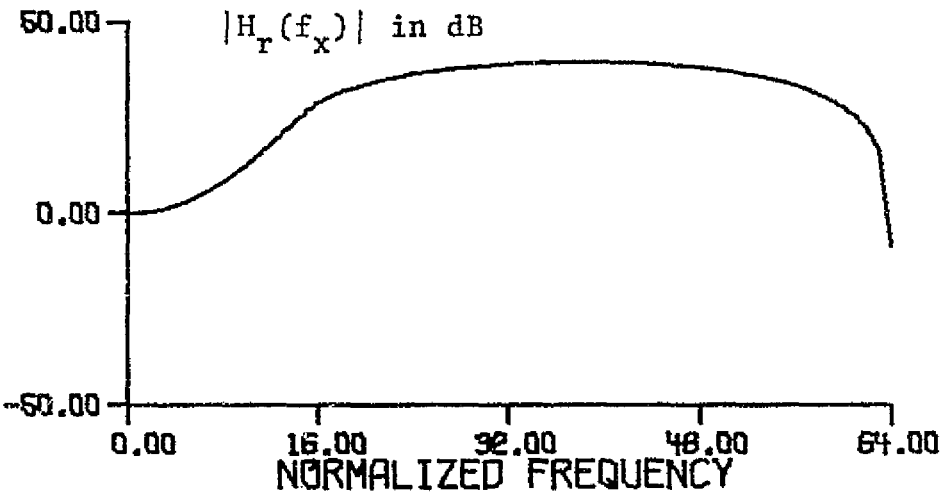

Figure 4.41 Restoration Filter Frequency Spectrum for Blurring Aperture of Figure 4.25 for $K_1 = 0.5$ and $K_2 = 1.61 \times 10^{-7}$ (S/N ≈ 20dB) Unconstrained Values for a White Noise Power Spectral Density of 10^{-5} volts^2/Hz and Four Iterations Using an Exponential Criterion Function

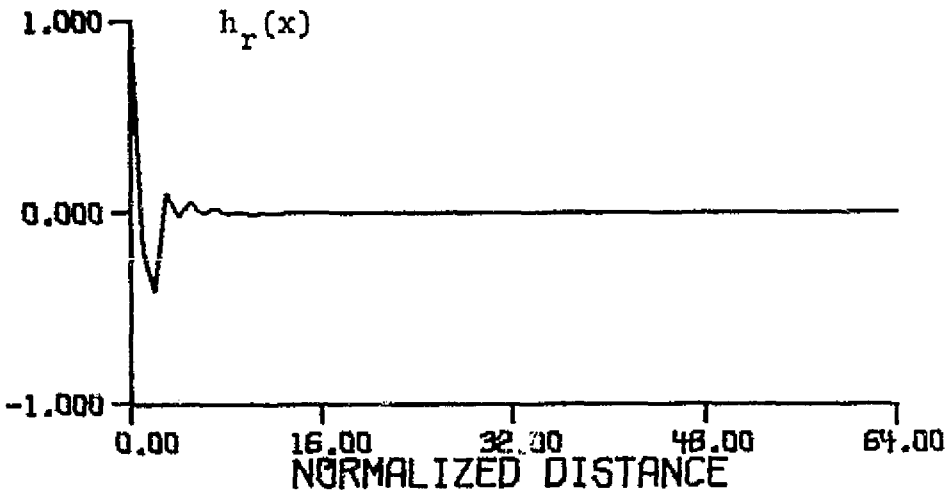

Figure 4.42 Restoration Filter Point-Spread Function Having Spectrum of Figure 4.41

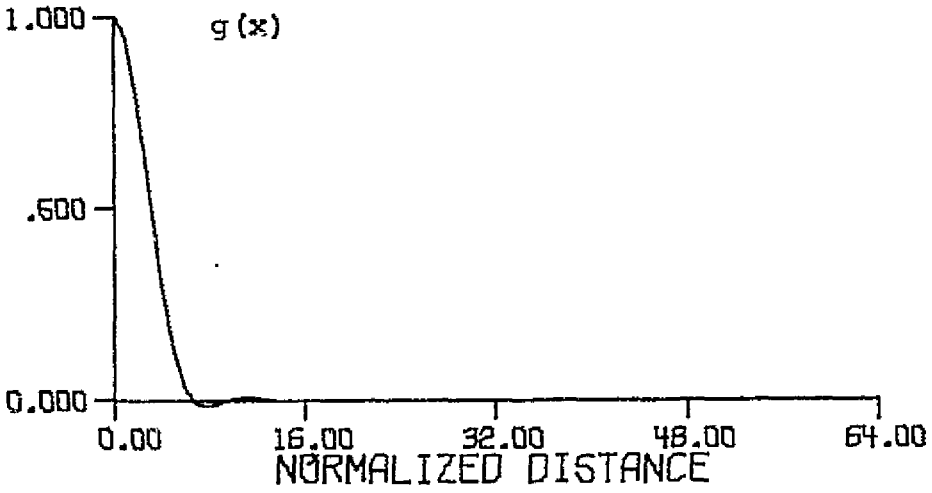

Figure 4.43 Composite System Point-Spread Function Resulting from Correcting the Blurring Aperture of Figure 4.25 with the Restoration Function of Figure 4.42

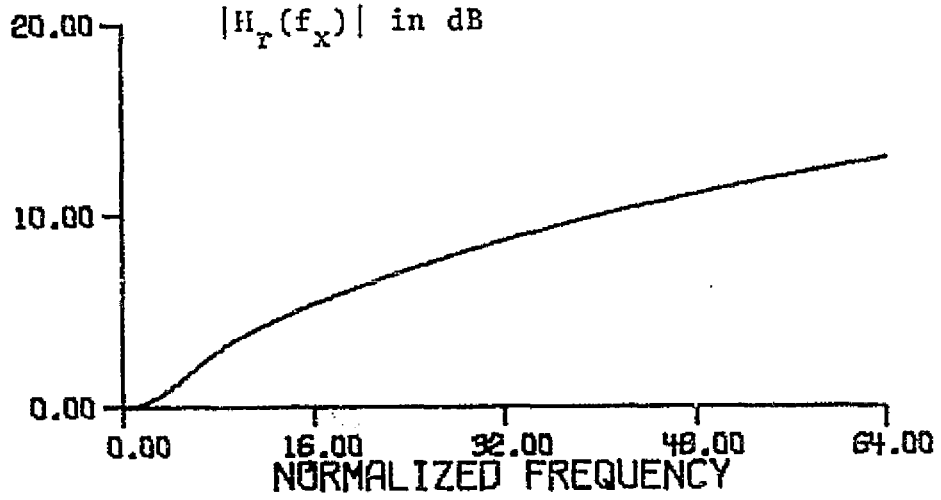

Figure 4.44 Restoration Filter Frequency Spectrum for Blurring Aperture of Figure 4.25 for $K_1 = 0.2$ and $K_2 = 1.61 \times 10^{-7}$ (S/N ≈ 20dB) Unconstrained Values for a White Noise Power Spectral Density of 10^{-5} volts^2/Hz and Four Iterations Using an Exponential Criterion Function

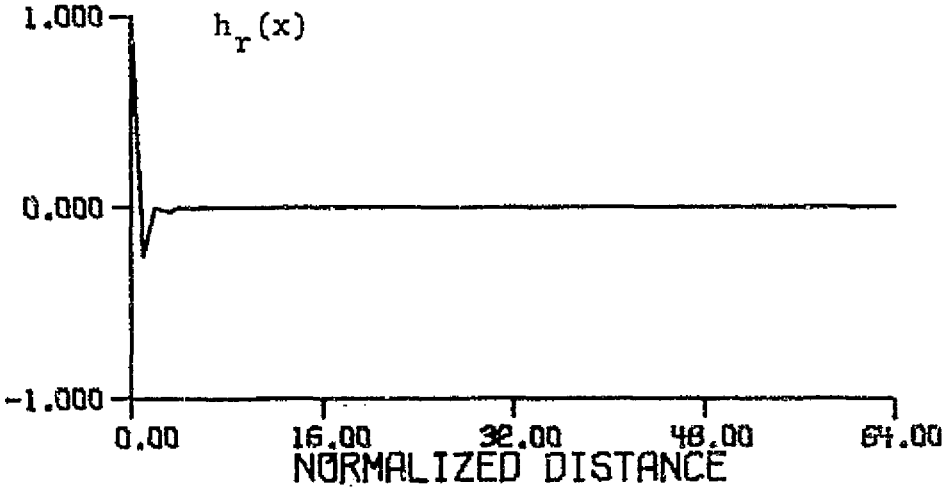

Figure 4.45 Restoration Filter Point-Spread Function Having Spectrum of Figure 4.44

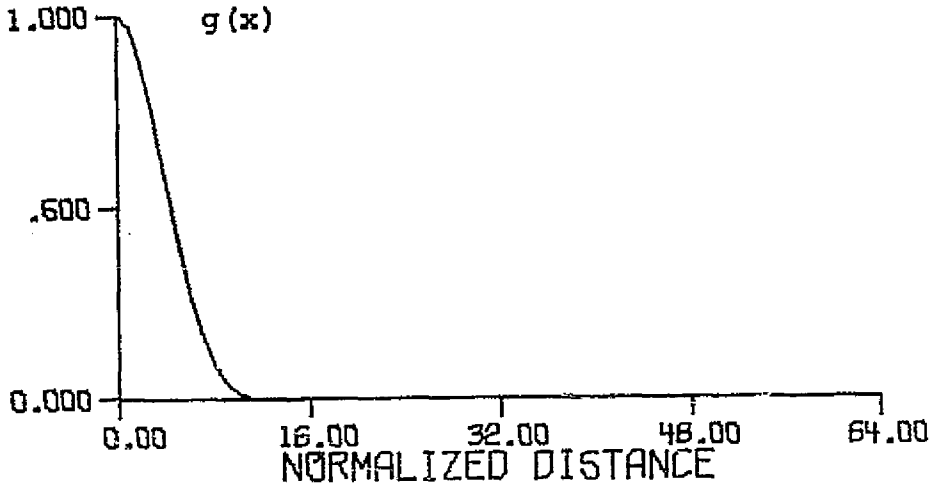

Figure 4.46 Composite System Point-Spread Function Resulting from Correcting the Blurring Aperture of Figure 4.25 with the Restoration Function of Figure 4.45

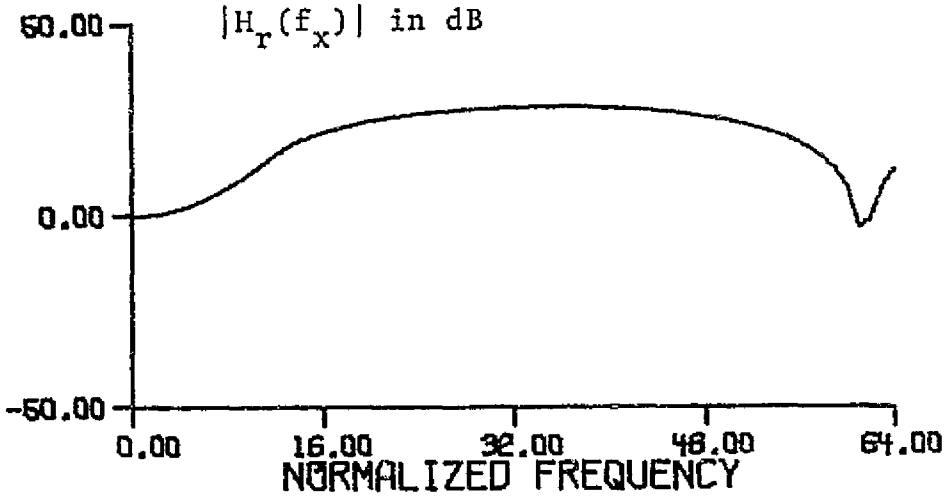

Figure 4.47 Restoration Filter Frequency Spectrum for Blurring Aperture of Figure 4.25 for $K_1 = 0.5$ and $K_2 = 1.61 \times 10^{-8}$ (S/N ≈ 20dB) Unconstrained Values for a White Noise Power Spectral Density of 10^{-4} volts^2/Hz and Four Iterations Using an Exponential Criterion Function

filter and the point-spread functions for both the restoration filter and the composite system for both K_1 = 0.5 and 0.2 of the unconstrained value for a white noise power spectral density of 10^{-5} volts^2/Hz. Figure 4.47-4.52 show the effect of increasing the noise power spectral density to 10^{-4} and 10^{-3} volts^2/Hz for K_1 = 0.5 of the unconstrained value. The radii of gyration of the composite system point-spread functions shown in Figure 4.43, 4.46, 4.49 and 4.52 are 60.2, 88.5, 66.2, and 76.9 percent of the radius of gyration of the blurring aperture of Figure 4.25.

The point-spread function for a Gaussian blurring aperture having a radius of gyration of five is shown in Figure 4.53. Figure 4.54 shows the resulting "inverse" restoration filter frequency spectrum, while the corresponding "inverse" restoration filter point-spread function is shown in Figure 4.55. The overall composite system point-spread function, resulting from correcting the blurring aperture of Figure 4.53 with the "inverse" restoration function of Figure 4.55, is shown in Figure 4.56.

When the radius of gyration of the point-spread function of the restoration filter is constrained to 0.5 of that of the "inverse" filter, the resulting restoration filter frequency spectrum, point-spread and composite system point-spread function are shown in Figure 4.57-4.59, respectively. By further reducing this constraint to 0.2 of that of the

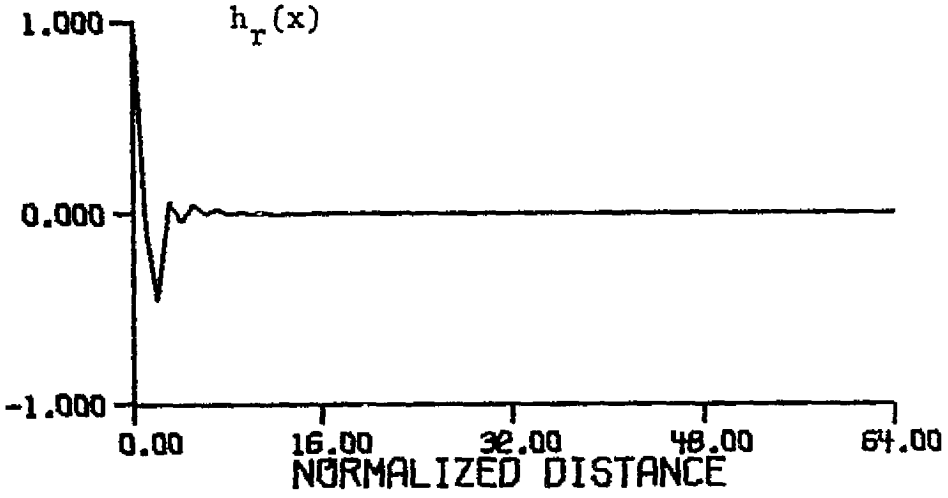

Figure 4.48 Restoration Filter Point-Spread Function Having Spectrum of Figure 4.47

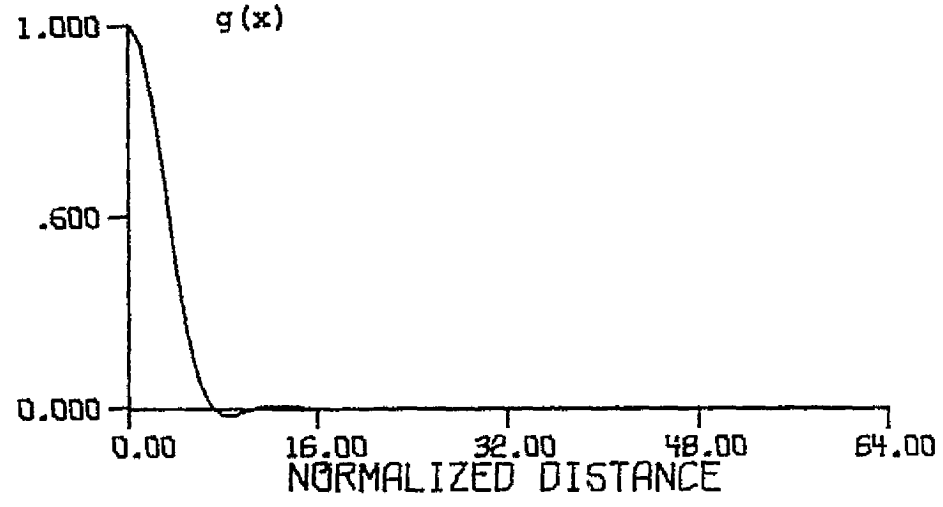

Figure 4.49 Composite System Point-Spread Function Resulting from Correcting the Blurring Aperture of Figure 4.25 with the Restoration Function of Figure 4.48

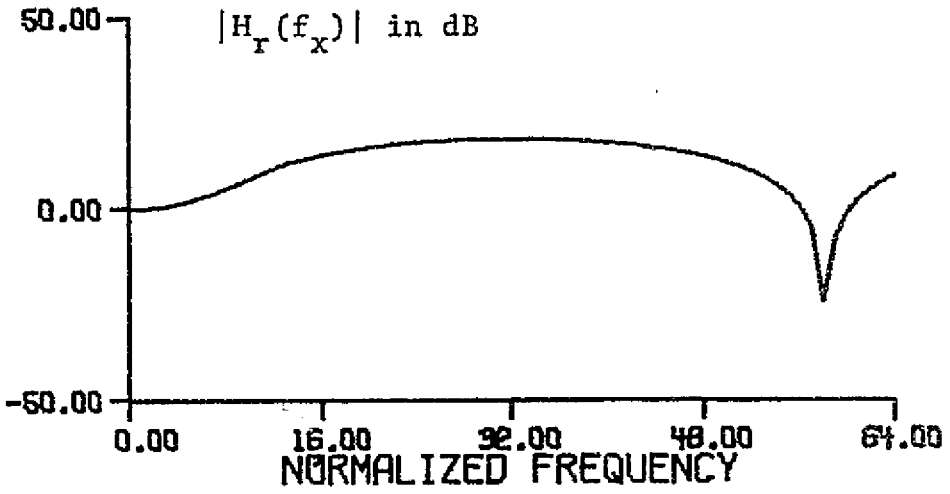

Figure 4.50 Restoration Filter Frequency Spectrum for Blurring Aperture of Figure 4.25 for $K_1 = 0.5$ and $K_2 = 1.61 \times 10^{-9}$ (S/N ≈ 20dB) Unconstrained Values for a White Noise Power Spectral Density of 10^{-3} volts^2/Hz and Two Iterations Using an Exponential Criterion Function

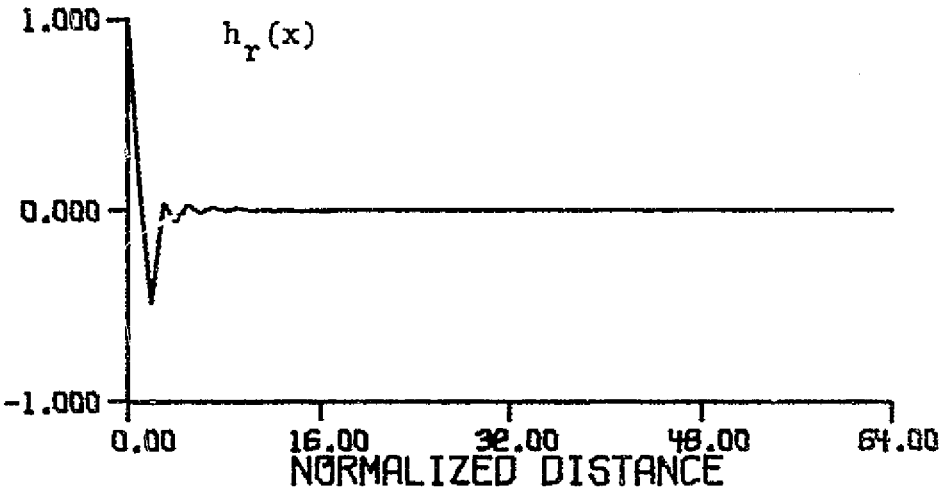

Figure 4.51 Restoration Filter Point-Spread Function Having Spectrum of Figure 4.50

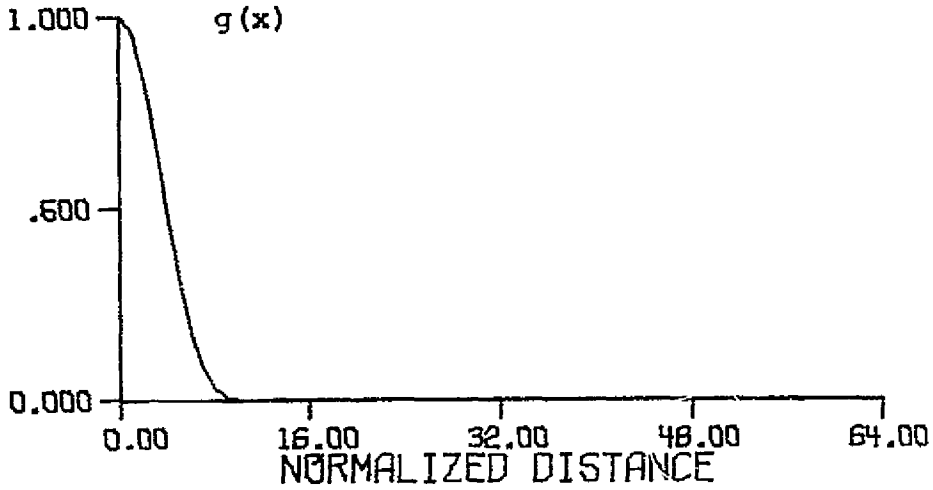

Figure 4.52 Composite System Point-Spread Function Resulting from Correcting the Blurring Aperture of Figure 4.25 with the Restoration Function of Figure 4.51

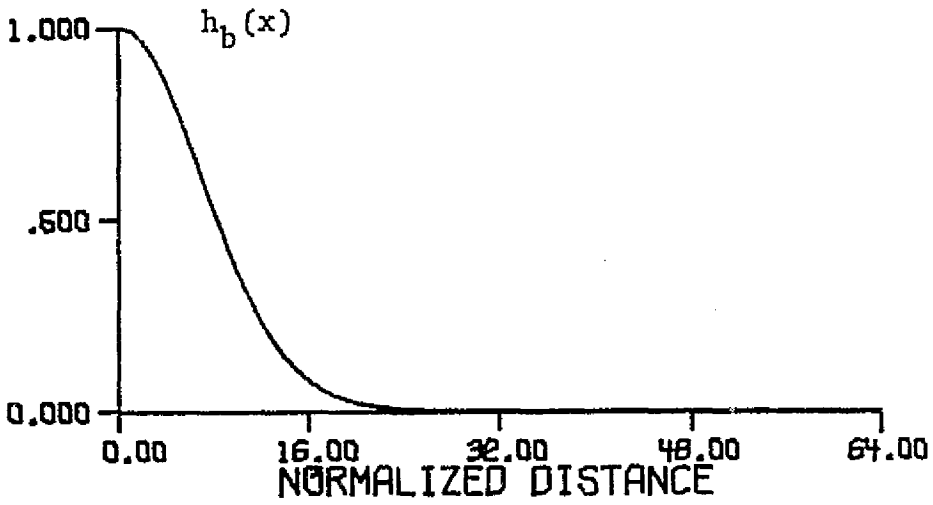

Figure 4.53 Gaussian Blurring Aperture Having a Radius of Gyration of Five

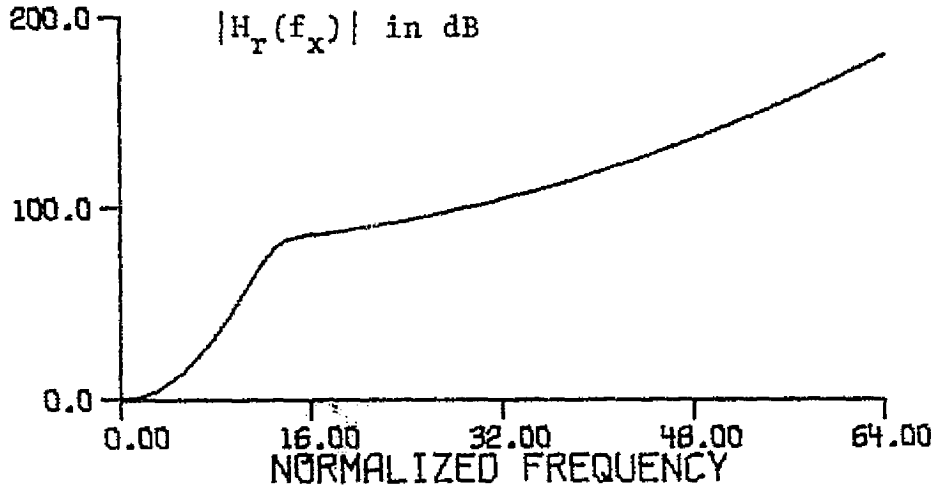

Figure 4.54 Classical "Inverse" Restoration Filter Frequency Spectrum for Blurring Aperture of Figure 4.53

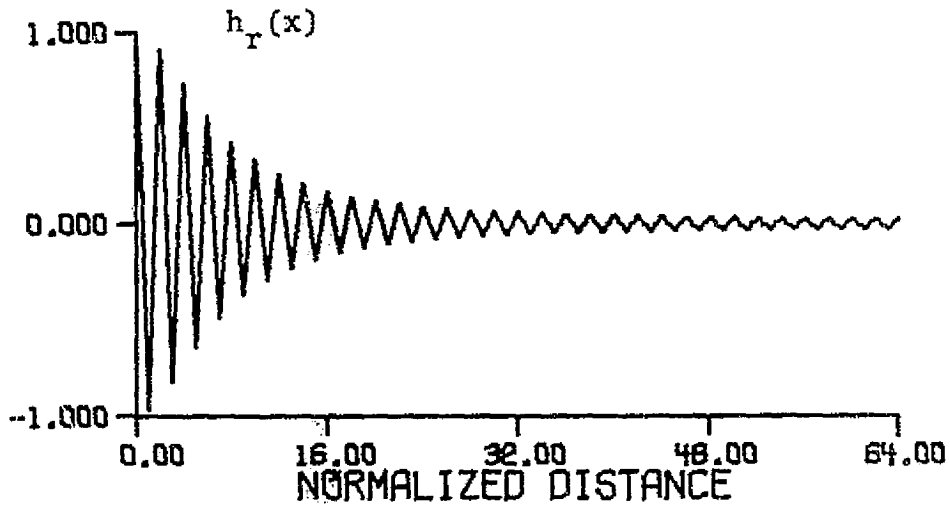

Figure 4.55 Classical "Inverse" Restoration Filter Point-Spread Function for Blurring Aperture of Figure 4.53

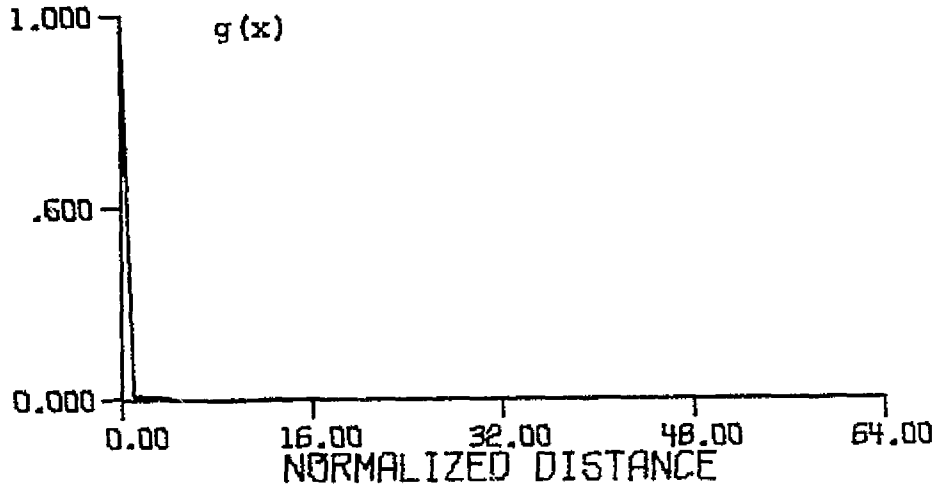

Figure 4.56 Composite System Point-Spread Function Resulting from Correcting the Blurring Aperture of Figure 4.53 with the Restoration Function of Figure 4.55

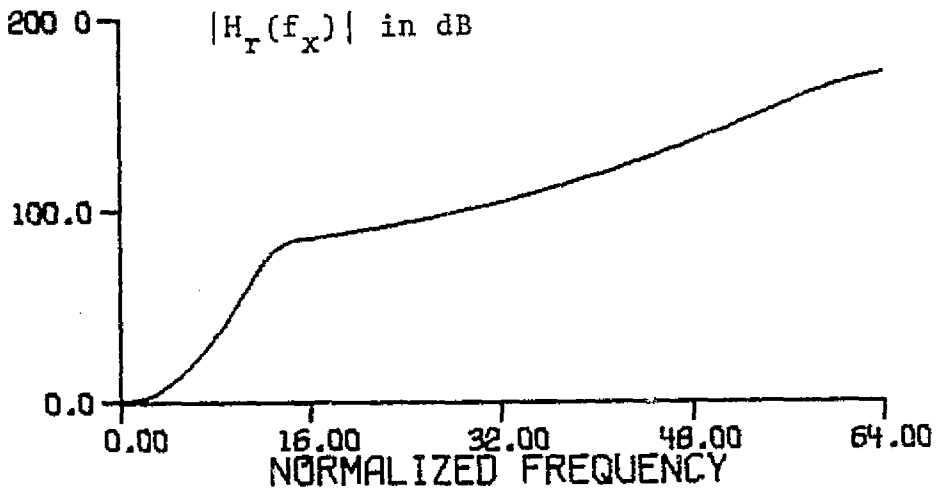

Figure 4.57 Restoration Filter Frequency Spectrum for Blurring Aperture of Figure 4.53 for K_1 = 0.5 Unconstrained Value and Two Iterations with an Exponential Criterion Function

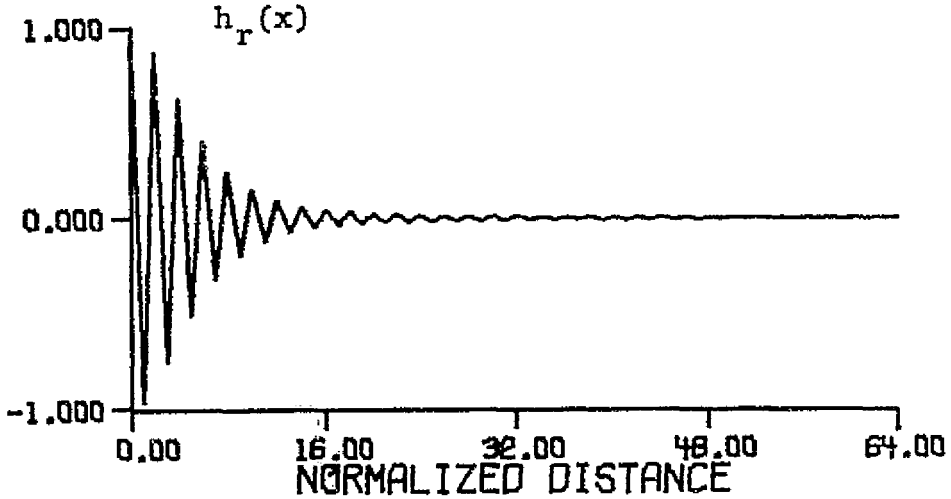

Figure 4.58 Restoration Filter Point-Spread Function Having Spectrum of Figure 4.57

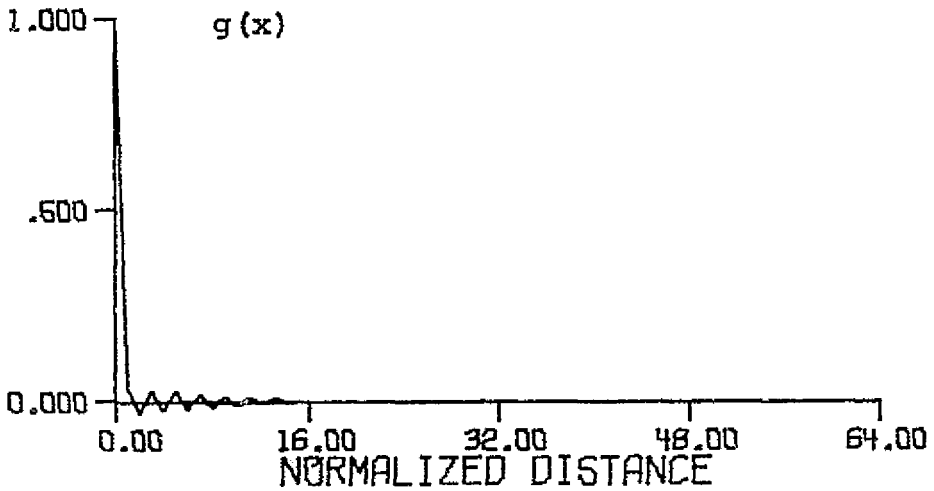

Figure 4.59 Composite System Point-Spread Function Resulting from Correcting the Blurring Aperture of Figure 4.53 with the Restoration Function of Figure 4.58

"inverse" filter, the resulting restoration filter frequency spectrum, point-spread function and composite system point-spread function are shown in Figure 4.60-4.62, respectively.

Figure 4.63-4.65 show the restoration filter frequency spectrum, point-spread function, and composite system point-spread function when the constraint on the radius of gyration of the restoration filter point-spread function is 0.1 of that of the "inverse" filter. The radii of gyration of the composite system point-spread functions shown in Figure 4.59, 4.62, and 4.65 are 15, 21, and 50 percent of the radius of gyration of the blurring aperture of Figure 4.53.

The preceding results corresponding to the blurring aperture of Figure 4.53 were for a noiseless environment. The following results are based upon two types of noise power spectral densities: white and exponentially increasing functions. The white noise power spectral density will be considered first. Results for four spectral density levels are shown: 10^{-5}, 10^{-4}, $5\text{x}10^{-4}$, and 10^{-3} volts^2/Hz. The output noise level constraint in the restored image is adjusted for a signal-to-noise ratio of approximately 20 dB. Figure 4.66-4.68 show the restoration filter frequency spectrum, point-spread function, and composite system point-spread function for K_1, the restoration filter point-spread function radius of gyration constraint equal to 0.5 that of the "inverse" filter, and K_2, the output noise

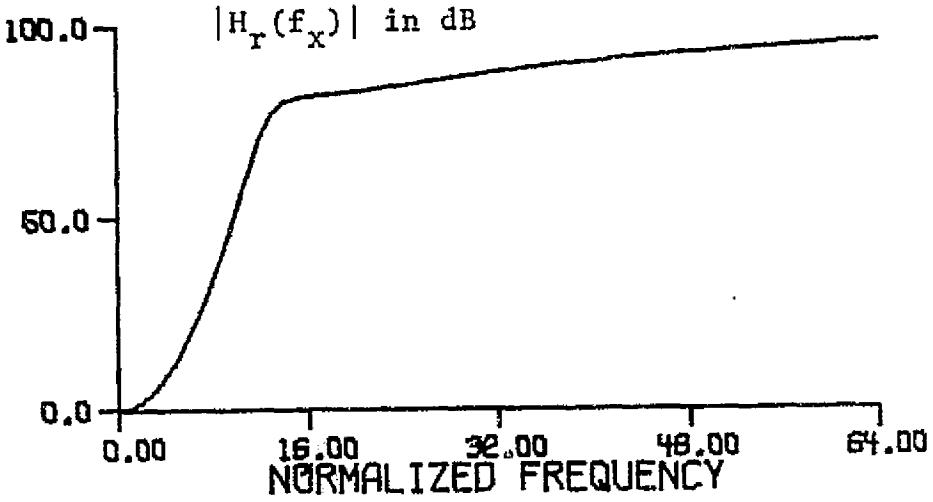

Figure 4.60 Restoration Filter Frequency Spectrum for Blurring Aperture of Figure 4.53 for K_1=0.2 Unconstrained Value and Two Iterations With An Exponential Criterion Function

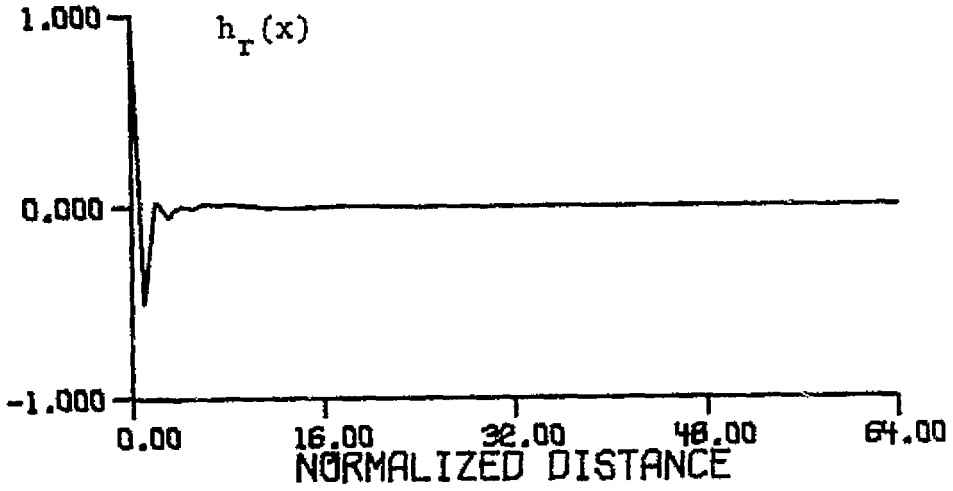

Figure 4.61 Restoration Filter Point-Spread Function Having Spectrum of Figure 4.60

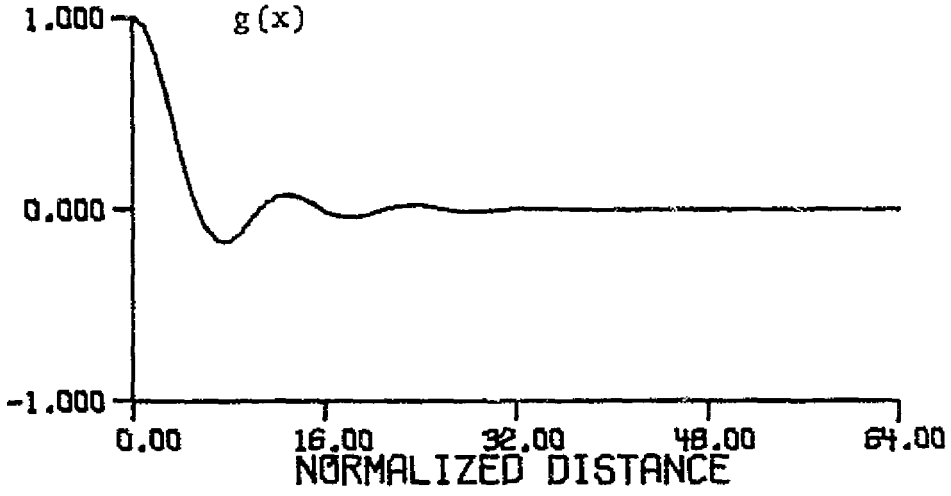

Figure 4.62 Composite System Point-Spread Function Resulting from Correcting the Blurring Aperture of Figure 4.53 with the Restoration Function of Figure 4.61

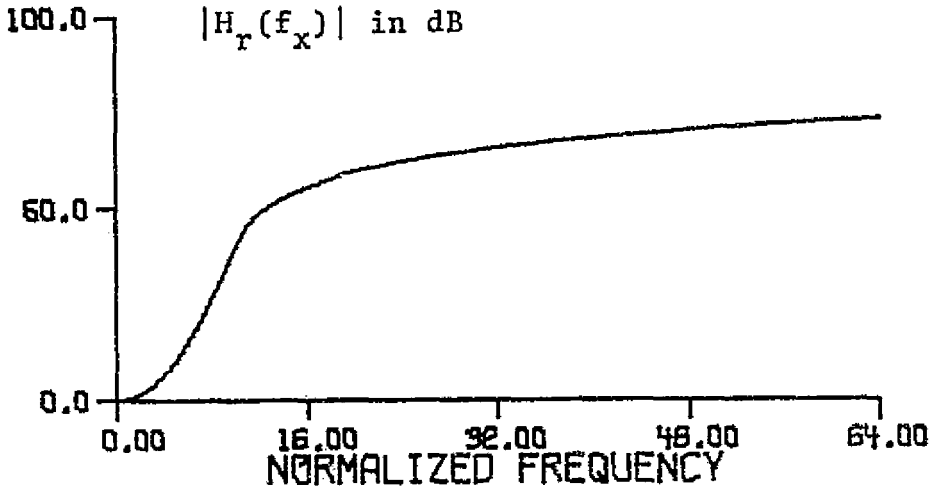

Figure 4.63 Restoration Filter Frequency Spectrum for Blurring Aperture of Figure 4.53 for $K_1 = 0.1$ Unconstrained Value and Ten Iterations with an Exponential Criterion Function

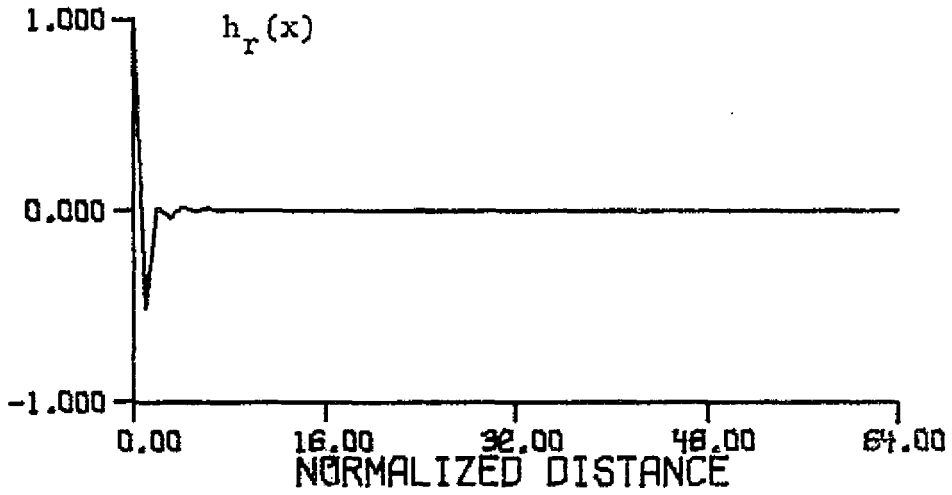

Figure 4.64 Restoration Filter Point-Spread Function Having Spectrum of Figure 4.63

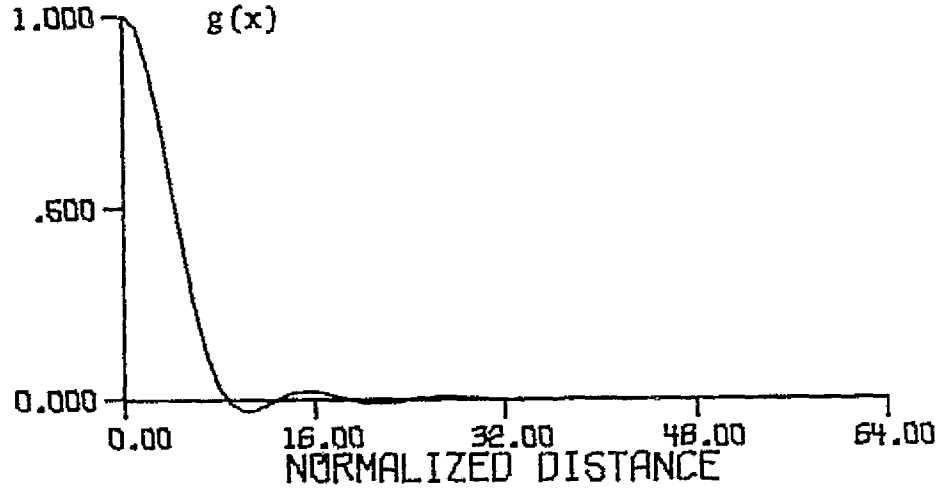

Figure 4.65 Composite System Point-Spread Function Resulting from Correcting the Blurring Aperture of Figure 4.53 with the Restoration Function of Figure 4.64

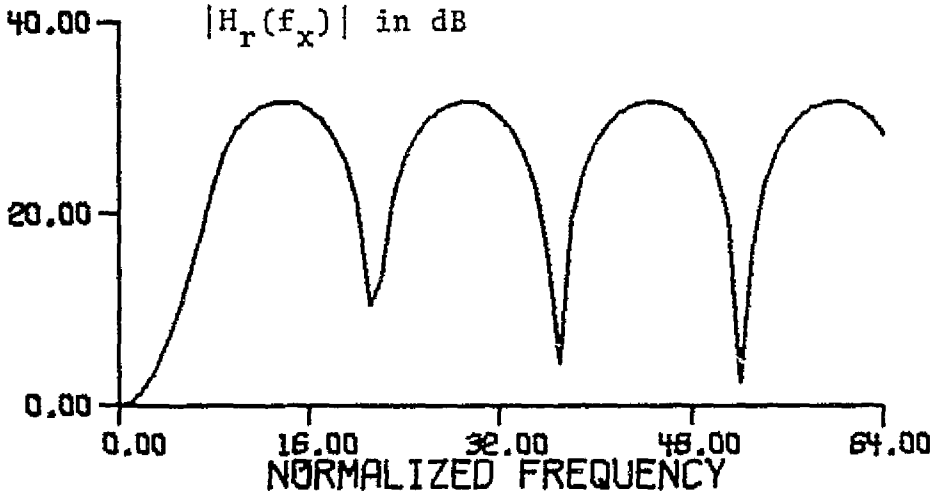

Figure 4.66 Restoration Filter Frequency Spectrum for Blurring Aperture of Figure 4.53 for $K_1 = 0.5$ and $K_2 = 2.10 \times 10^{-13}$ (S/N ≈ 20dB) Unconstrained Values for a White Noise Power Spectral Density of 10^{-5} volts^2/Hz and Ten Iterations with an Exponential Criterion Function

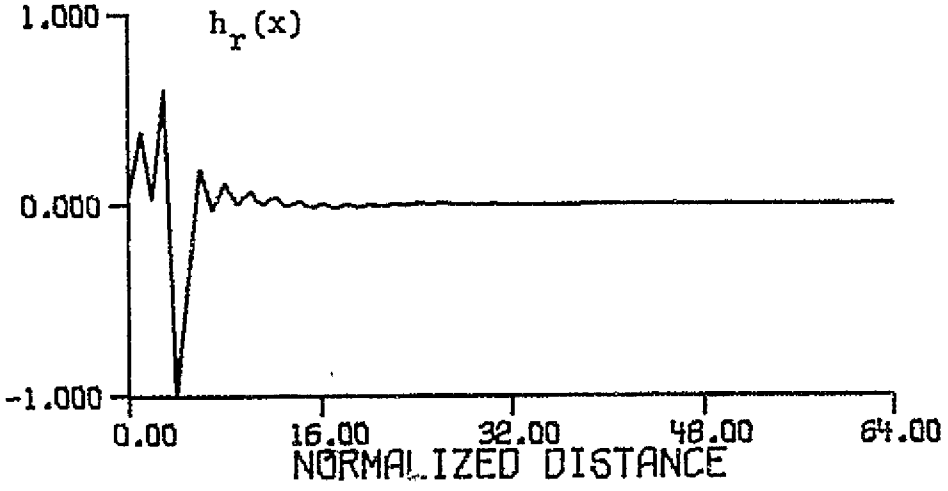

Figure 4.67 Restoration Filter Point-Spread Function Having Spectrum of Figure 4.66

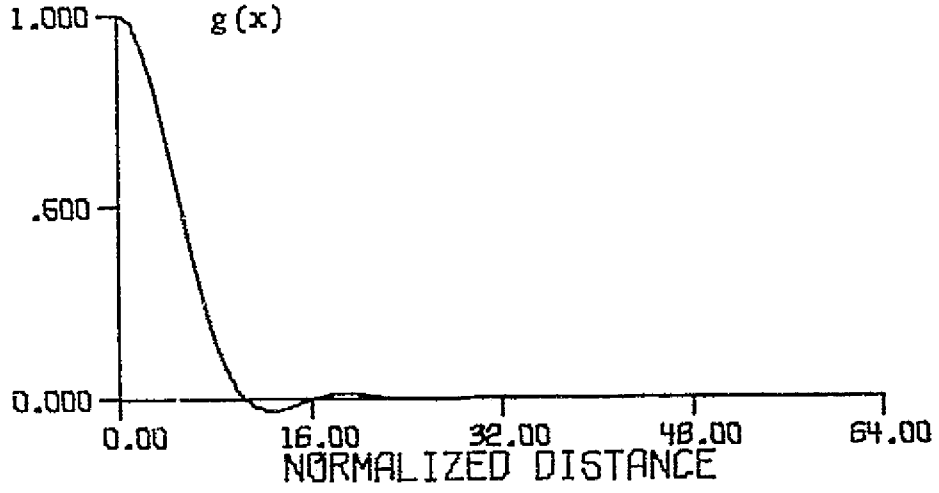

Figure 4.68 Composite System Point-Spread Function Resulting from Correcting the Blurring Aperture of Figure 4.53 with the Restoration Function of Figure 4.67

power constraint, adjusted for a 20 dB output signal-to-noise ratio when the noise power spectral density level is 10^{-5} volts^2/Hz. Figure 4.69-4.71 show similar results when $K_1 = 0.2$ that of the "inverse" filter. Figure 4.72-4.74, 4.75-4.77, and 4.78-4.80 show the restoration filter frequency spectra point-spread functions, and composite system point-spread functions for $K_1 = 0.5$ that of the "inverse" filter and for noise power spectral densities of 10^{-4}, $5x10^{-4}$, and 10^{-3} volts^2/Hz, respectively.

The exponentially increasing noise power spectral densities are shown in Figure 4.81, 4.85, and 4.89. Figure 4.82-4.84, 4.86-4.88, and 4.90-4.92 show the corresponding restoration filter frequency spectra, point-spread functions and composite system point-spread functions, respectively for $K_1 = 0.5$ that of the "inverse" filter and K_2 adjusted for a signal-to-noise ratio of 20 dB, for each noise spectrum.

Tables 4.1 and 4.2 summarize the basic restoration filter and composite system performance parameters for the constraint and noise power spectral density variations described in this section.

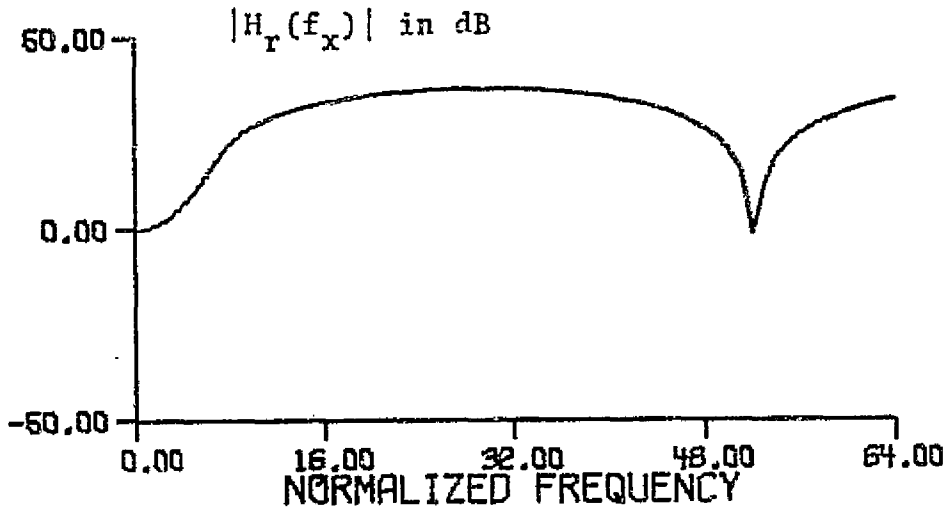

Figure 4.69 Restoration Filter Frequency Spectrum for Blurring Aperture of Figure 4.53 for $K_1 = 0.2$ and $K_2 = 2.10 \times 10^{-13}$ (S/N ≈ 20dB) Unconstrained Values for a White Noise Power Spectral Density of 10^{-5} volts^2/Hz and Four Iterations with an Exponential Criterion Function

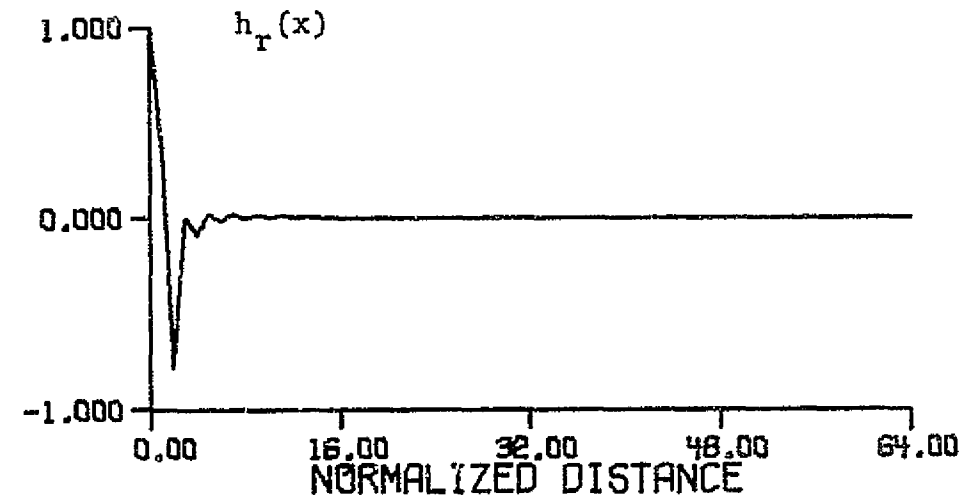

Figure 4.70 Restoration Filter Point-Spread Function Having Spectrum of Figure 4.69

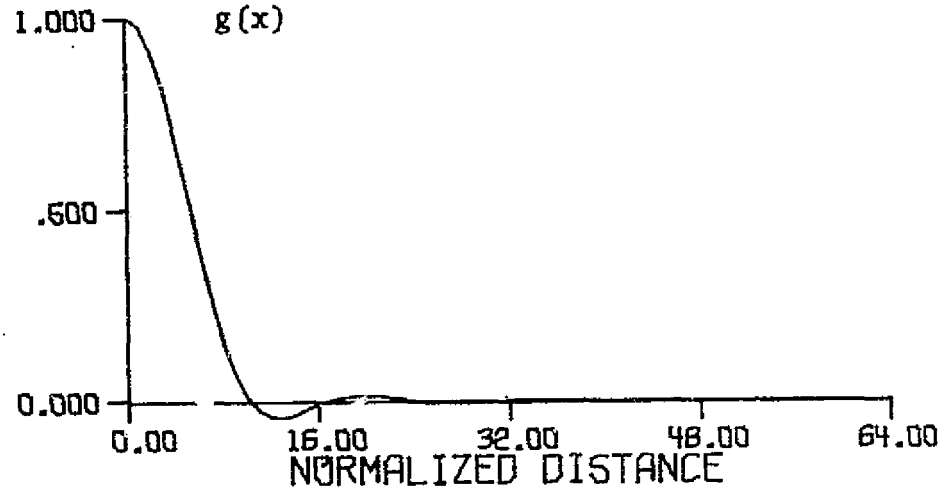

Figure 4.71 Composite System Point Spread Function Resulting from Correcting the Blurring Aperture of Figure 4.53 with the Restoration Function of Figure 4.70

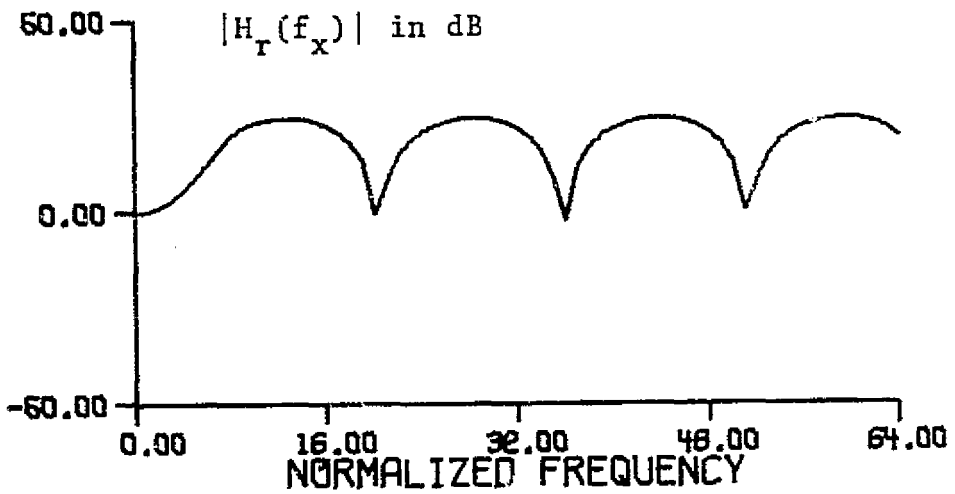

Figure 4.72 Restoration Filter Frequency Spectrum for Blurring Aperture of Figure 4.53 for $K_1 = 0.5$ and $K_2 = 2.10 \times 10^{-14}$ (S/N ≈ 20dB) Unconstrained Values for a White Noise Power Spectral Density of 10^{-4} volts^2/Hz and Four Iterations with an Exponential Criterion Function

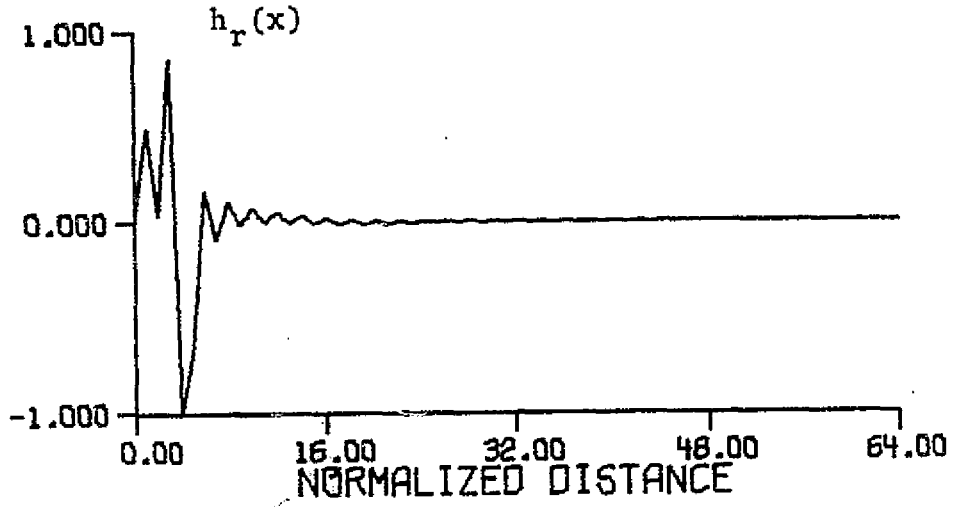

Figure 4.73 Restoration Filter Point-Spread Function Having Spectrum of Figure 4.72

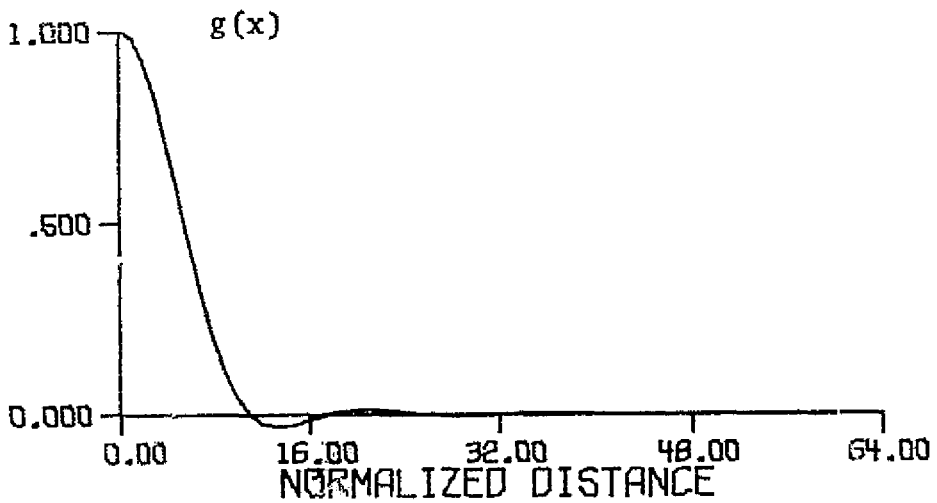

Figure 4.74 Composite System Point-Spread Function Resulting from Correcting the Blurring Aperture of Figure 4.53 with the Restoration Function of Figure 4.73

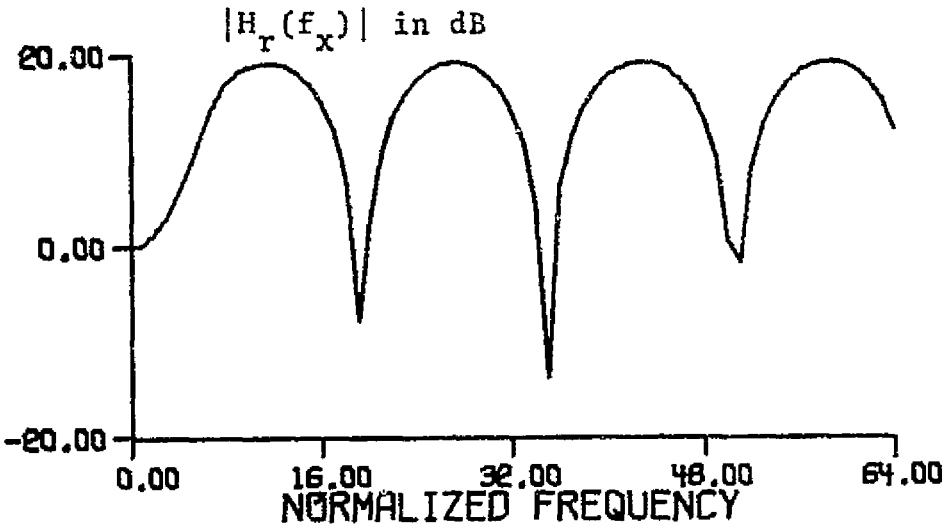

Figure 4.75 Restoration Filter Frequency Spectrum for Blurring Aperture of Figure 4.53 for $K_1 = 0.5$ and $K_2 = 1.05 \times 10^{-15}$ (S/N ≈ 20dB) Unconstrained Values for a White Noise Power Spectral Density of 5×10^{-4} volts^2/Hz and Four Iterations with an Exponential Criterion Function

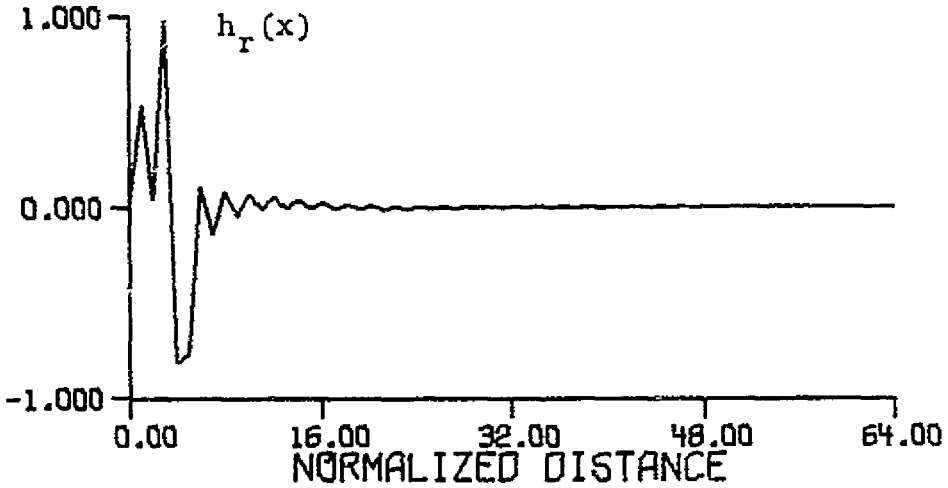

Figure 4.76 Restoration Filter Point-Spread Function Having Spectrum of Figure 4.75

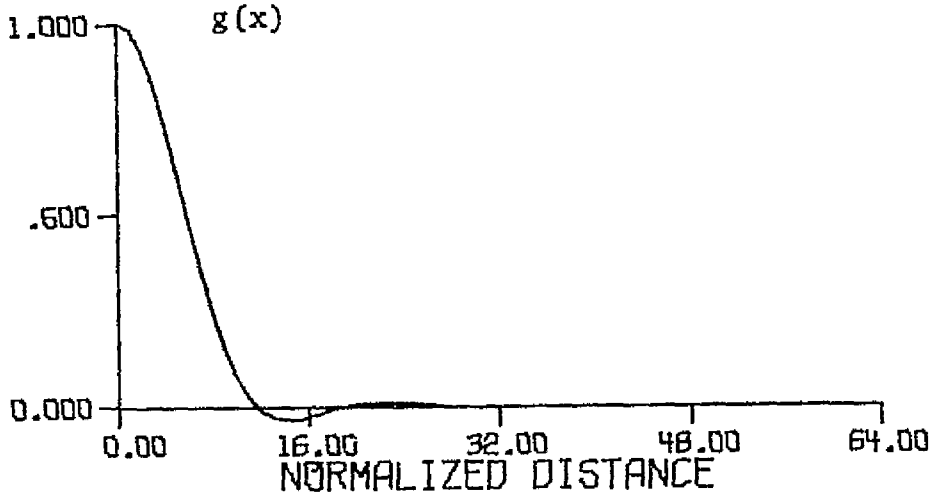

Figure 4.77 Composite System Point-Spread Function Resulting from Correcting the Blurring Aperture of Figure 4.53 with the Restoration Function of Figure 4.76

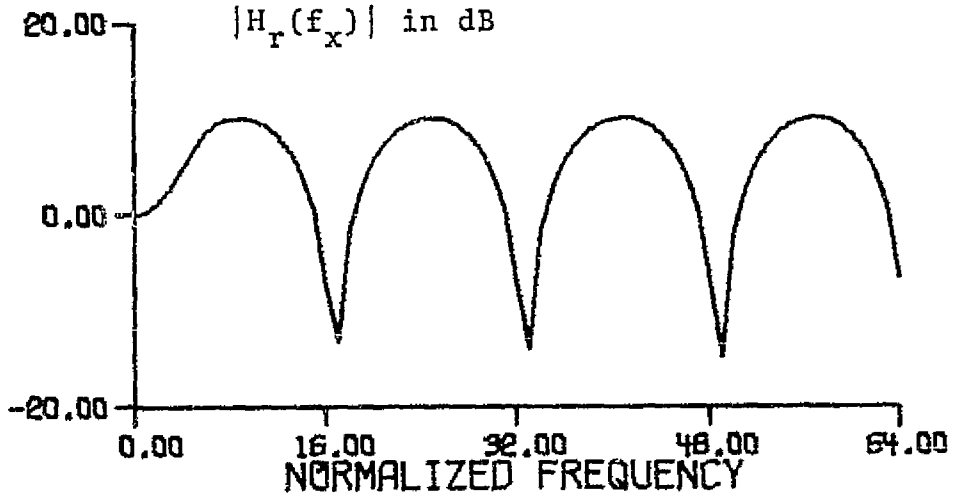

Figure 4.78 Restoration Filter Frequency Spectrum for Blurring Aperture of Figure 4.53 for $K_1 = 0.5$ and $K_2 = 2.10 \times 10^{-15}$ (S/N ≈ 20dB) Unconstrained Values for a White Noise Power Spectral Density of 10^{-3} volts^2/Hz and Four Iterations with an Exponential Criterion Function

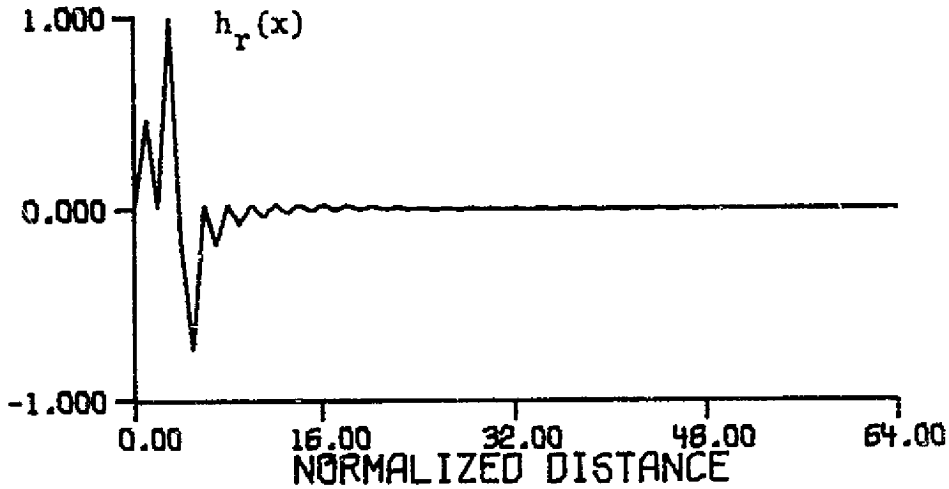

Figure 4.79 Restoration Filter Point-Spread Function Having Spectrum of Figure 4.78

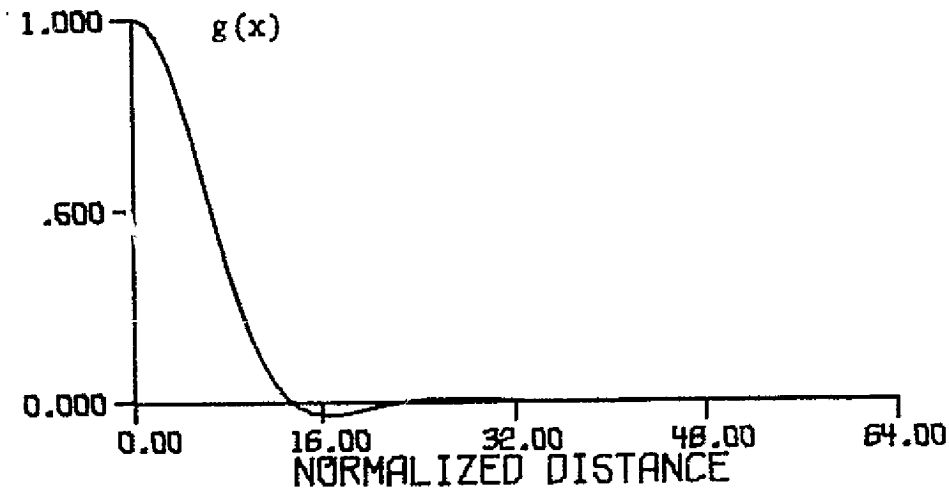

Figure 4.80 Composite System Point-Spread Function Resulting from Correcting the Blurring Aperture of Figure 4.53 with the Restoration Function of Figure 4.79

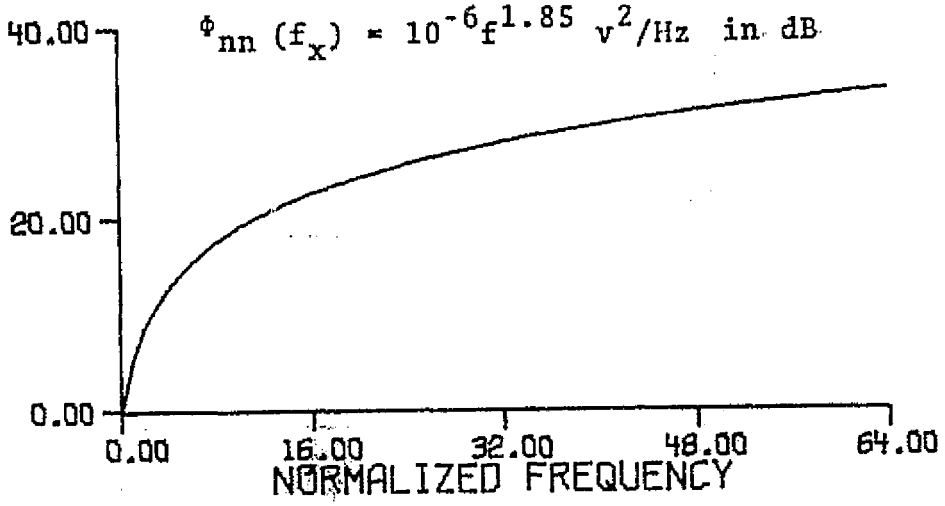

Figure 4.81 Noise Power Spectral Density for $\Phi_{nn}(f) = 10^{-6} f^{1.85}$ v^2/Hz

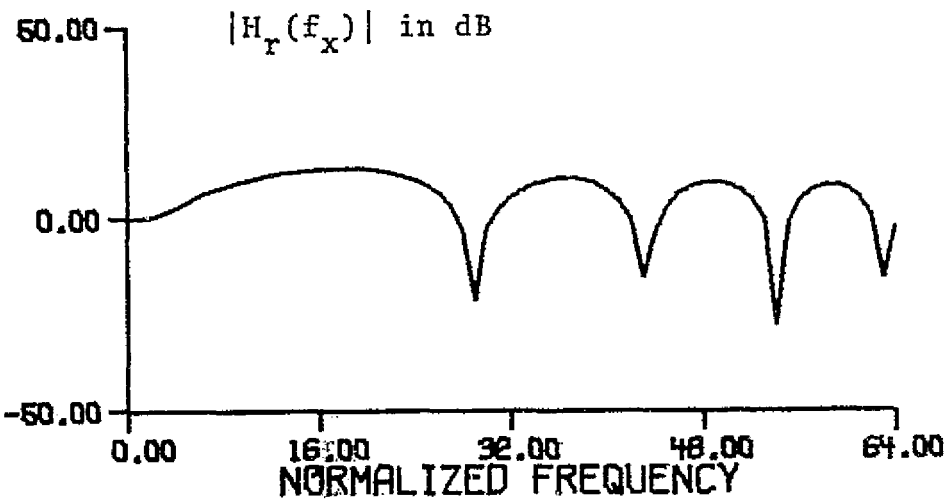

Figure 4.82 Restoration Filter Frequency Spectrum for Blurring Aperture of Figure 4.53 for Noise Power Spectral Density of Figure 4.81 and K_1 = 0.5 Unconstrained Value and K_2 = 5 (S/N ≈ 20dB) for Four Iterations with an Exponential Criterion Function

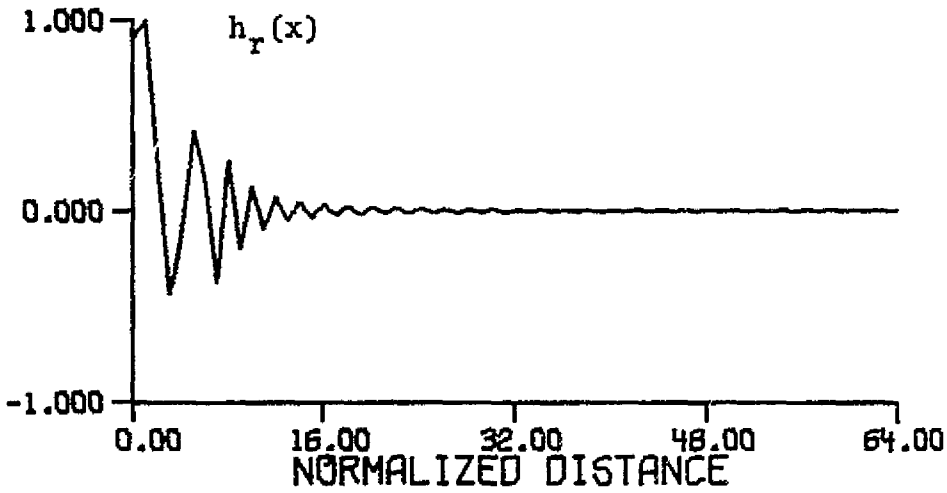

Figure 4.83 Restoration Filter Point-Spread Function Having Spectrum of Figure 4.82

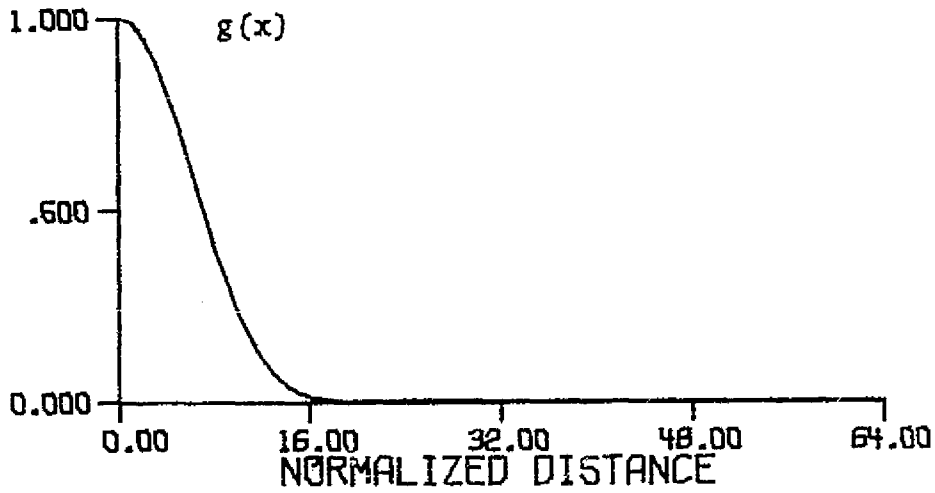

Figure 4.84 Composite System Point-Spread Function Resulting from Correcting the Blurring Aperture of Figure 4.53 with the Restoration Function of Figure 4.83

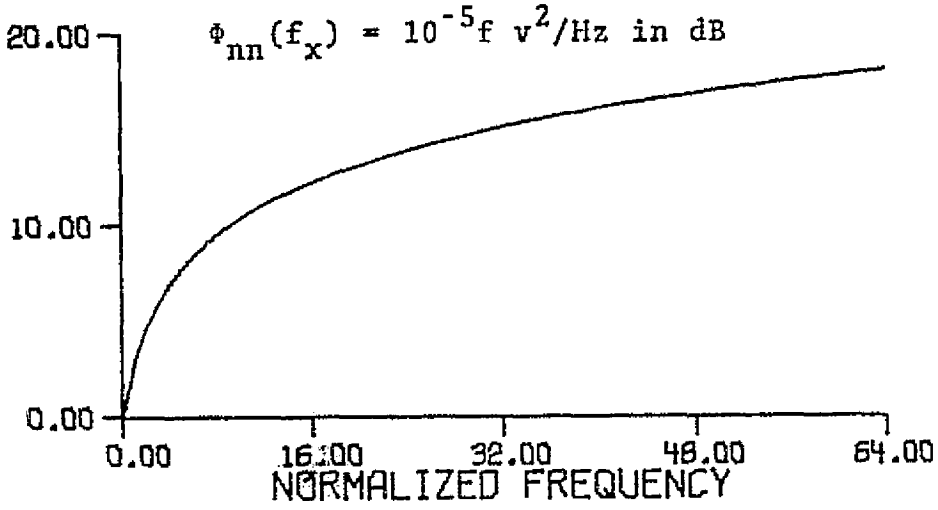

Figure 4.85 Noise Power Spectral Density for $\Phi_{nn}(f) = 10^{-5}$ f v^2/Hz

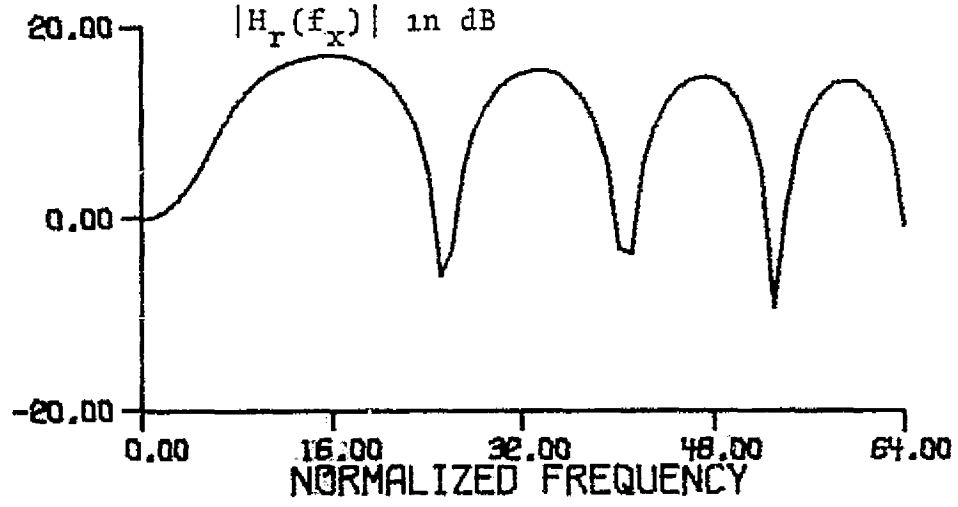

Figure 4.86 Restoration Filter Frequency Spectrum for Blurring Aperture of Figure 4.53 for Noise Power Spectral Density of Figure 4.85 and K_1 = 0.5 Unconstrained Value and K_2 = 5 (S/N ≈ 20dB) for Four Iterations with an Exponential Criterion Function

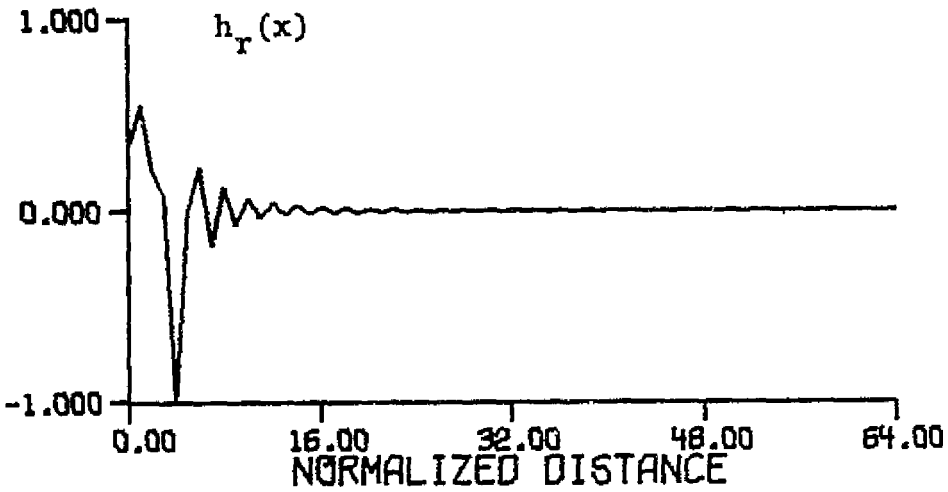

Figure 4.87 Restoration Filter Point-Spread Function Having Spectrum of Figure 4.86

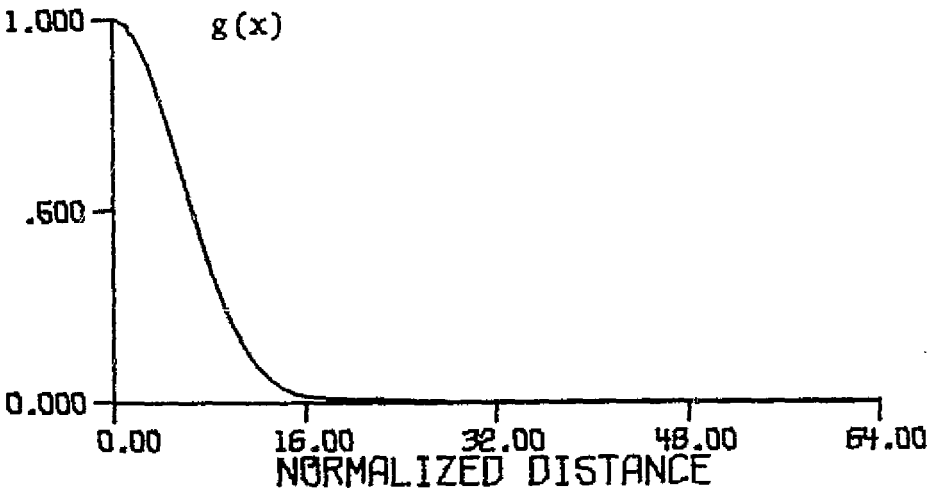

Figure 4.88 Composite System Point-Spread Function Resulting from Correcting the Blurring Aperture of Figure 4.53 with the Restoration Function of Figure 4.87

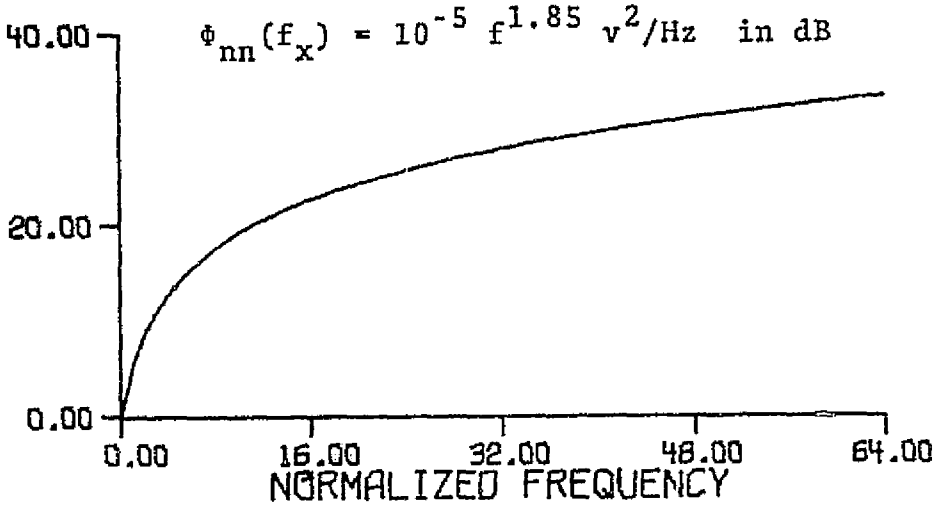

Figure 4.89 Noise Power Spectral Density for $\Phi_{nn}(f) = 10^{-5}\ f^{1.85}\ v^2/Hz$

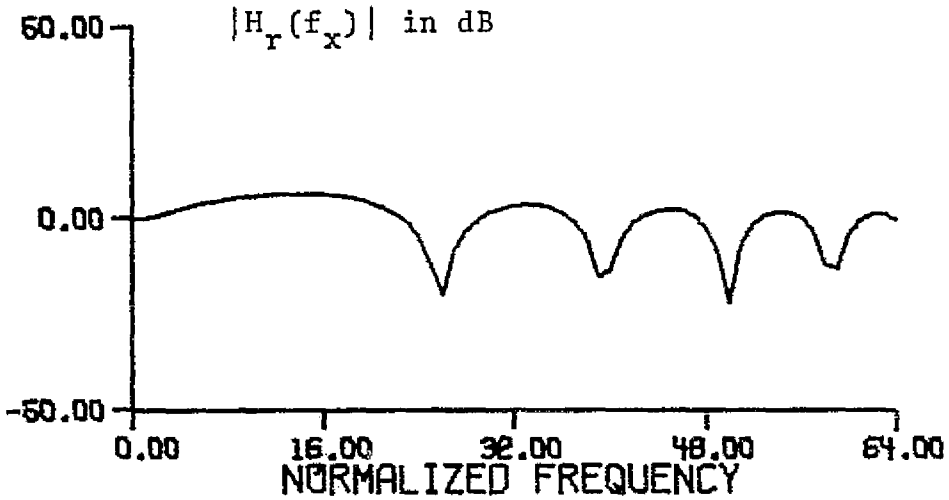

Figure 4.90 Restoration Filter Frequency Spectrum for Blurring Aperture of Figure 4.53 for Noise Power Spectral Density of Figure 4.89 and $K_1 = 0.5$ Unconstrained Value and $K_2 = 5$ $(S/N \approx 20dB)^{-1}$ for Four Iterations with an Exponential Criterion Function

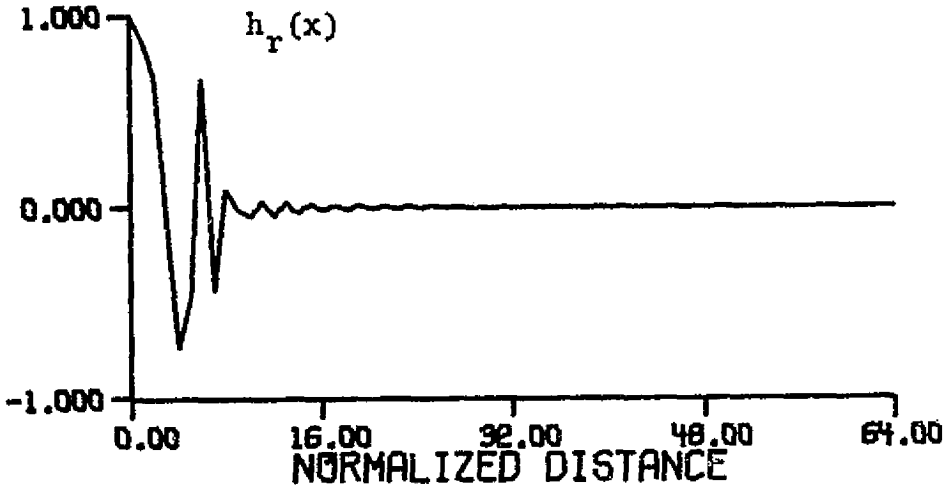

Figure 4.91 Restoration Filter Point-Spread Function Having Spectrum of Figure 4.90

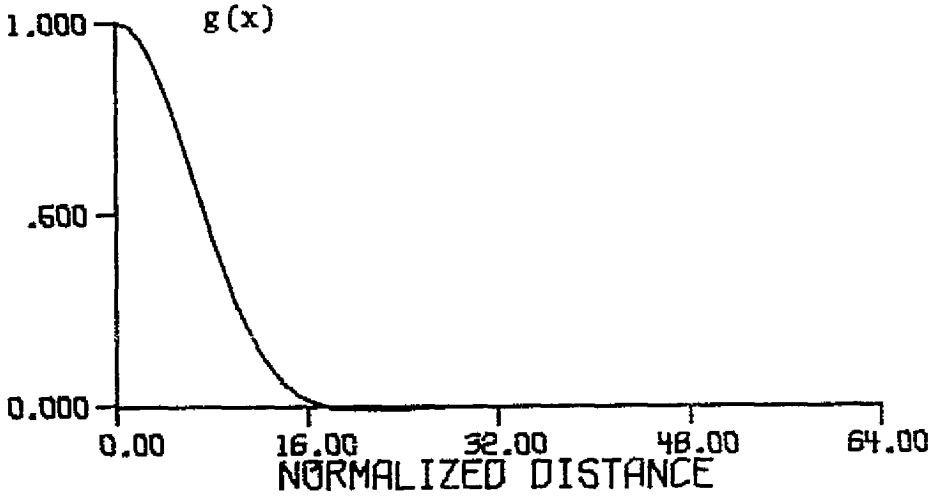

Figure 4.92 Composite System Point-Spread Function Resulting from Correcting the Blurring Aperture of Figure 4.53 with the Restoration Function of Figure 4.91

Table 4.1: Basic Restoration Filter and Co
Performance Parameters As A Fun
and White Noise Spectral Densit

blurring aperture radius of gyration	1		1	
K_1 constraint as a fraction of the unconstrained value	0.5		0.2	
K_2 constraint for approximate 20dB output signal-to-noise ratio	Unconstrained		Unconstrained	
input signal-to-noise ratio for specified white noise power spectral density amplitude	∞, 0		∞, 0	
criterion function iteration	none	4, exponential	none	4,
composite system radius of gyration as percentage of blurring aperture radius of gyration	67	74	81	
maximum peak of secondary oscillations as percentage of primary lobe in composite system point-spread function	-6.3	-5.2×10^{-3}	-9.0	

blurring aperture radius of gyration	3		3	
K_1 constraint as a fraction of the unconstrained value	0.5		0.5	
K_2 constraint for approximate 20dB output signal-to-noise ratio	5		5	
input signal-to-noise ratio for specified white noise power spectral density amplitude	52.84dB, 10^{-4} v^2/Hz		42.84dB, 10^{-3}	
criterion function iteration	none	4, exponential	none	2,
composite system radius of gyration as percentage of blurring aperture radius of gyration	60	66.2	72.7	
maximum peak of secondary oscillations as percentage of primary lobe in composite system point-spread function	-12.4	-2.06	-4.08	

blurring aperture radius of gyration	3		3	
K_1 constraint as a fraction of the unconstrained value	0.5		0.2	
K_2 constraint for approximate 20dB output signal-to-noise ratio	5		5	
input signal-to-noise ratio for specified white noise power spectral density amplitude	62.84dB, 10^{-5} v^2/Hz		62.84dB, 10^{-5}	
criterion function iteration	none	4, exponential	none	4,
composite system radius of gyration as percentage of blurring aperture radius of gyration	59.8	60.2	75.8	
maximum peak of secondary oscillations as percentage of primary lobe in composite system point-spread function	-15.5	-1.74	-1.35	

...ation Filter and Composite System ...Parameters As A Function of Constraint ...oise Spectral Density Variations

	1		1		1			
	0.2		0.1		0.2			
	Unconstrained		Unconstrained		5			
	∞, 0		∞, 0		62.84dB, 10^{-5} v^2/Hz			
al	none	4, exponential	none	4, exponential	none	4, exponential		
	81	97	89	90	82	97		
10^{-3}	-9.0	-10^{-3}	-1.7	-8.7×10^{-2}	-9.2	-3.6×10^{-3}		

	3		3		3			
	0.5		0.5		0.2			
	5		Unconstrained		Unconstrained			
	42.84dB, 10^{-3} v^2/Hz		∞, 0		∞, 0			
ial	none	2, exponential	none	4, exponential	none	4, exponential		
	72.7	76.9	14.3	19.8	88.5	89.3		
	-4.08	-0.55	7.6	-2.03	-1.18	-0.84		

	3							
	0.2							
	5							
	62.84dB, 10^{-5} v^2/Hz							
ial	none	4, exponential						
	75.8	88.5						
	-1.35	-0.84						

Table 4.1, cont.

blurring aperture radius of gyration	5		5	
K_1 constraint as a fraction of the unconstrained value	0.2		0.5	
K_2 constraint for approximate 20dB output signal-to-noise ratio	5		5	
input signal-to-noise ratio for specified white noise power spectral density amplitude	62.84dB, 10^{-5} v^2/Hz		52.84dB, 10^{-4}	
criterion function iteration	none	4, exponential	none	4, e
composite system radius of gyration as percentage of blurring aperture radius of gyration	61.4	70.7	54.4	
maximum peak of secondary oscillations as percentage of primary lobe in composite system point-spread function	-12.9	-4.3	-7.16	

blurring aperture radius of gyration	5		5	
K_1 constraint as a fraction of the unconstrained value	0.5		0.2	
K_2 constraint for approximate 20dB output signal-to-noise ratio	Unconstrained		Unconstrained	
input signal-to-noise ratio for specified white noise power spectral density amplitude	∞, 0		∞, 0	
criterion function iteration	none	2, exponential	none	2,
composite system radius of gyration as percentage of blurring aperture radius of gyration	13.3	15	16.6	
maximum peak of secondary oscillations as percentage of primary lobe in composite system point-spread function	-14.5	3.36	-16.2	

Table 4.1, cont.

5	5	5
0.5	0.5	0.5
5	5	5
52.84dB, 10^{-4} v^2/Hz	45.85dB, 5 x 10^{-4} v^2/Hz	42.84dB, 10^{-3} v^2/Hz
1 none / 4, exponential	none / 4, exponential	none / 4, exponential
54.4 / 61.6	59.4 / 67.2	66.9 / 70.1
-7.16 / -3.4	-13 / -3.6	-3.9 / -3.4

5	5	5
0.2	0.1	0.5
Unconstrained	Unconstrained	5
∞, 0	∞, 0	62.84dB, 10^{-5} v^2/Hz
ial none / 2, exponential	none / 10, exponential	none / 10, exponential
16.6 / 21	47 / 50	50.1 / 54.3
-16.2 / -0.3	-14.9 / -2.9	-14.1 / -3.4

FOLDOUT FRAME

Table 4.2: Basic Restoration Filter and
Performance Parameters As A
and Exponential Noise Spectr

blurring aperture radius of gyration	5	
K_1 constraint as a function of the unconstrained value	0.5	
K_2 constraint for approximate 20dB output signal-to-noise ratio	5	
power spectral density function	$\Phi_{nn}(f) = 10^{-6} f^{1.85}$ v^2/Hz	
input signal-to-noise ratio	29.57dB	
criterion function iteration	none	4, exponential
composite system radius of gyration as percentage of blurring aperture radius of gyration	60	66
maximum peak of secondary oscillations as percentage of primary lobe in composite system point-spread function	-1.38	-0.38

n Filter and Composite System
meters As A Function of Constraints
Noise Spectral Density Variations

	5		5	
	0.5		0.5	
	5		5	
v^2/Hz	$\Phi_{nn}(f) = 10^{-5}\ f\ v^2/Hz$		$\Phi_{nn}(f) = 10^{-5}\ f^{1.85}\ v^2/Hz$	
	47.72dB		19.57dB	
exponential	none	4, exponential	none	4, expcnential
66	65	73	89	94
-0.38	-1.42	-0.39	-0.62	-3.4×10^{-3}

FOLDOUT FRAME

4.3 The Effect Of Error Between Actual And Assumed Gaussian Blurring Apertures On Composite System Performance

The results of the preceding section assumed that the blurring aperture function was explicitly known. When this function is not known, the composite system performance based upon an erroneous blurring function can deviate significantly from the optimal response. The purpose of this section is to demonstrate the effect upon the composite system point-spread function produced when a restoration filter computed for a Gaussian blurring aperture of specified radius of gyration is used to correct data blurred by a Gaussian aperture having a different radius of gyration.

Figure 4.93-4.96 show both the composite system frequency spectra and point-spread functions when restoration filters computed for Gaussian blurring apertures having radii of gyration of three and five, respectively, are used to correct a Gaussian blurring aperture having a radius of gyration of one. Figure 4.97 and 4.98 show the composite system frequency sepctrum and point-spread functions when a restoration filter computed for a Gaussian blurring aperture having a radius of gyration of five is used to correct a Gaussian blurring aperture having a radius of gyration of three. These preceding mismatch combinations of actual and assumed blurring apertures correspond to an overcorrection of the data as demonstrated by the peaks in the com-

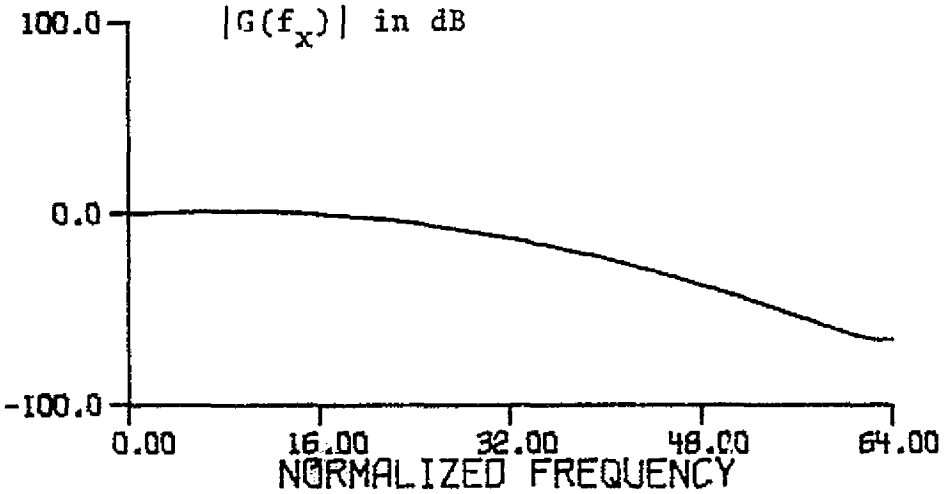

Figure 4.93 Composite System Frequency Spectrum Resulting from Correcting the Blurring Aperture of Figure 4.1 with the Restoration Filter of Figure 4.45

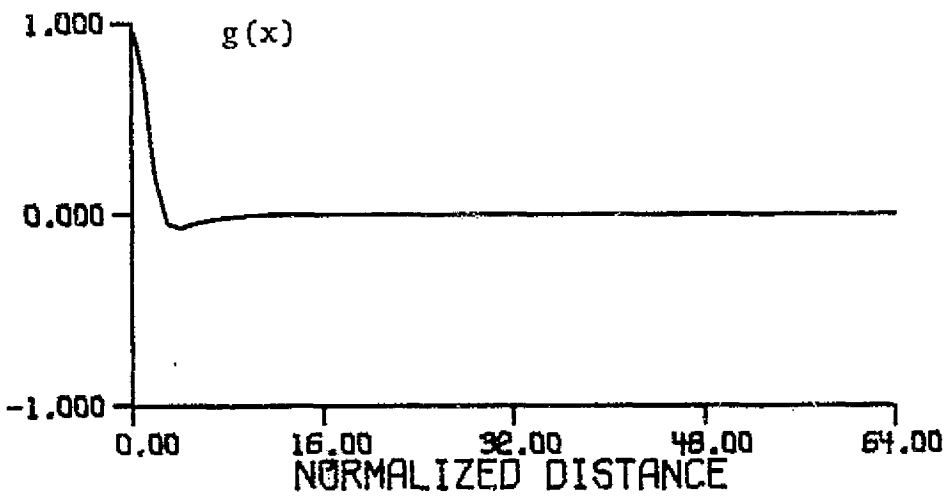

Figure 4.94 Composite System Point-Spread Function Having Spectrum of Figure 4.93

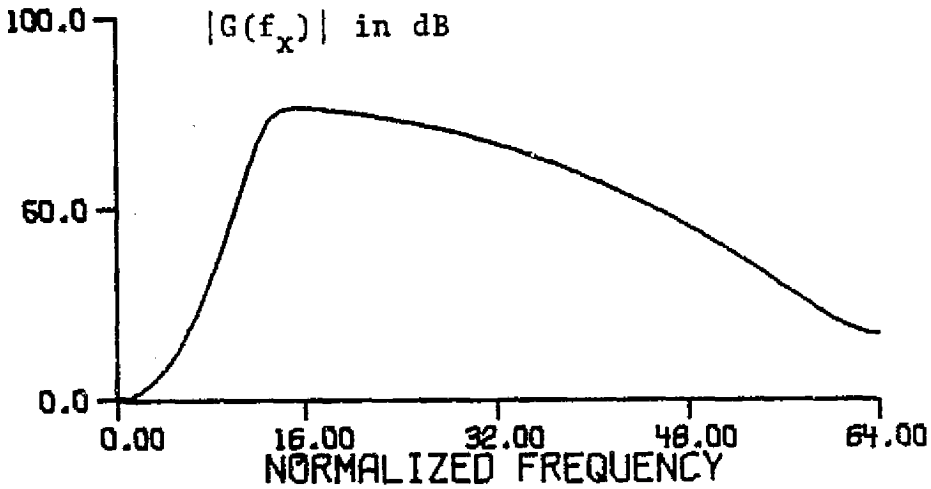

Figure 4.95 Composite System Frequency Spectrum Resulting from Correcting the Blurring Aperture of Figure 4.1 with the Restoration Filter of Figure 4.70

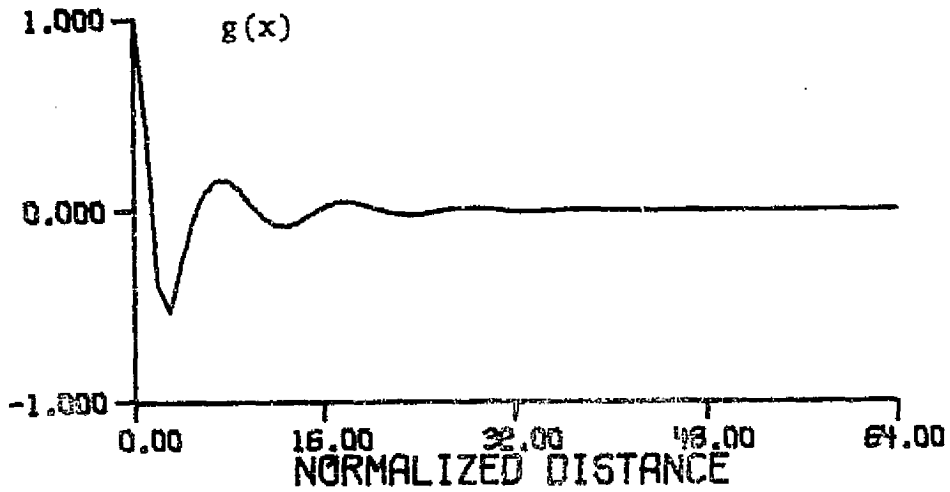

Figure 4.96 Composite System Point-Spread Function Having Spectrum of Figure 4.95

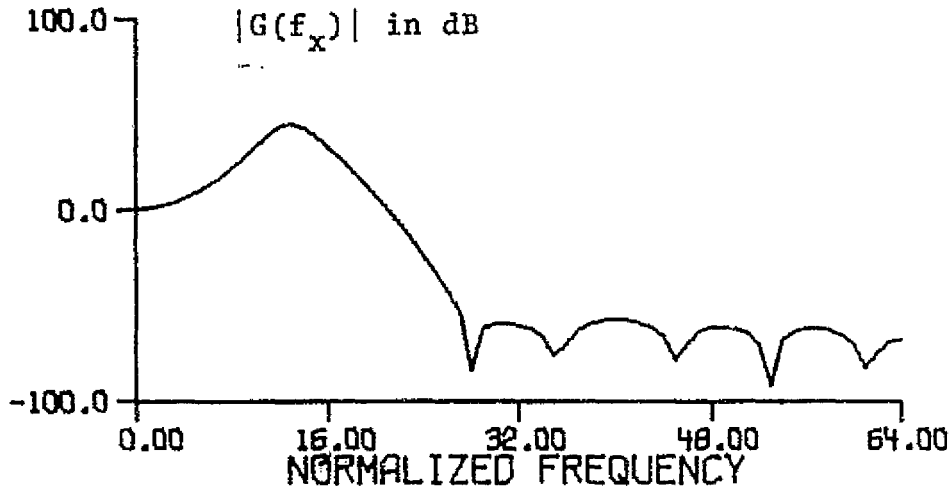

Figure 4.97 Composite System Frequency Spectrum Resulting from Correcting the Blurring Aperture of Figure 4.25 with the Restoration Filter of Figure 4.70

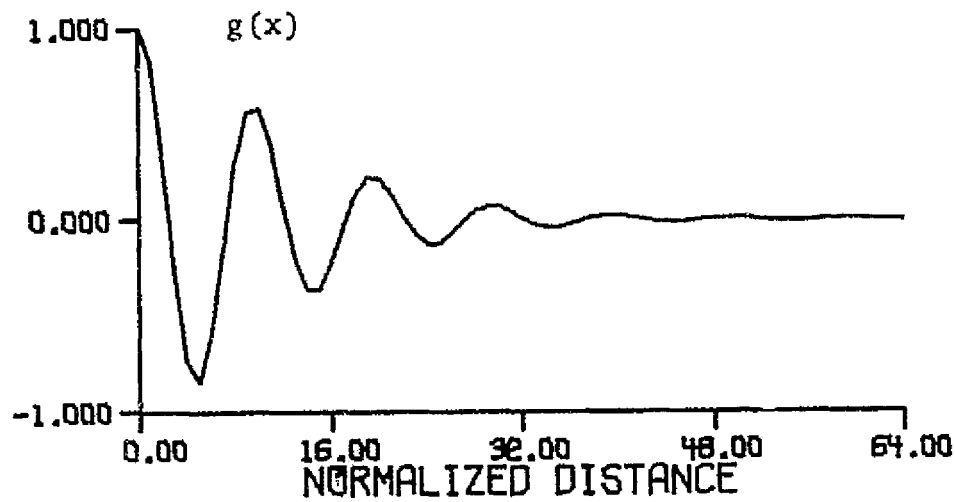

Figure 4.98 Composite System Point-Spread Function Having Spectrum of Figure 4.97

posite system frequency spectra of Figure 4.93, 4.95, and 4.97. The resulting composite system point-spread functions, as shown in Figure 4.94, 4.96, and 4.98 are highly oscillatory - the greater the assumed blurring aperture relative to the actual, the greater the oscillations in the composite system point-spread functions.

Figure 4.99-4.104 show corresponding composite system spectra and point-spread functions for the opposite situation, where the radius of gyration of the actual blurring aperture is larger than that of the assumed aperture. These blurring aperture mismatch combinations correspond to undercorrection of the data.

Of the two types of mismatch conditions considered, the least desirable is the overcorrection condition; since it would introduce ghosts into the "corrected" image. In contrast, the undercorrected condition produces a stable system response which would not introduce any oscillatory error; however, less than optimal image enhancement could be expected.

The recognition of the overcorrection condition by a peak in the frequency spectrum of the "corrected" data or by the presence of oscillations about transients in the "corrected" image could provide a criterion for determining when a blurring aperture match has been achieved for data where the radius of gyration of the actual Gaussian-shaped aperture is unknown.

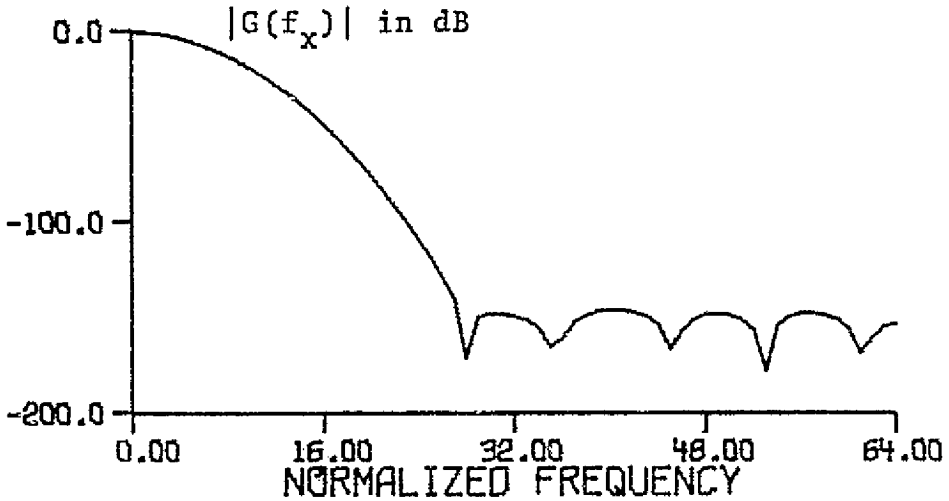

Figure 4.99 Composite System Frequency Spectrum Resulting from Correcting the Blurring Aperture of Figure 4.25 with the Restoration Filter of Figure 4.24

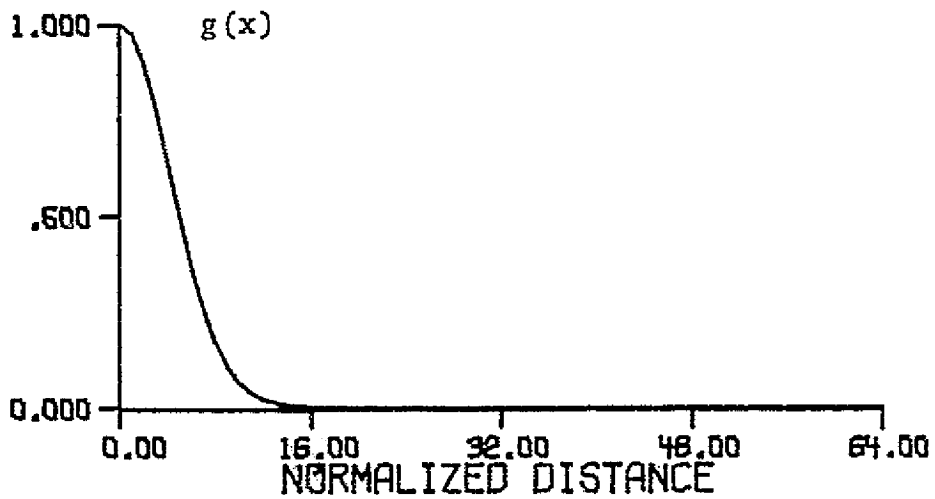

Figure 4.100 Composite System Point-Spread Function Having Spectrum of Figure 4.99

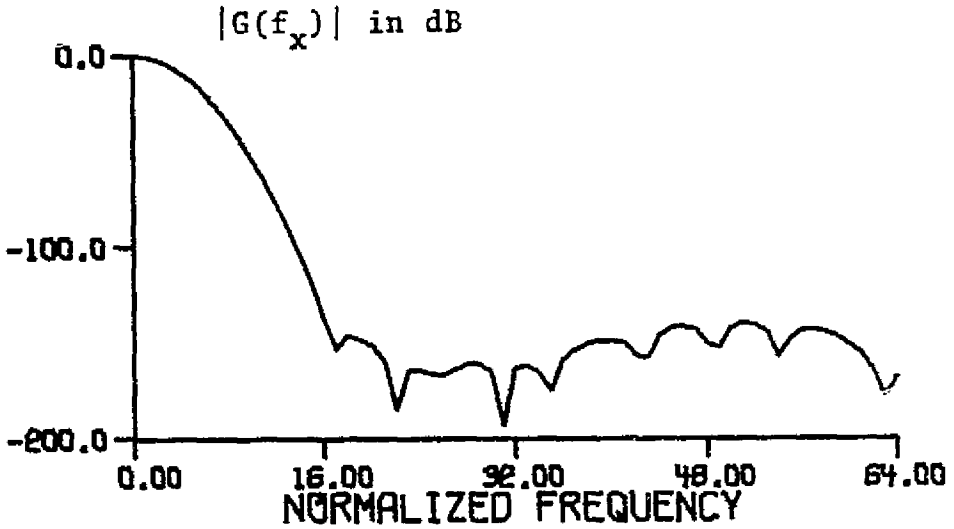

Figure 4.101 Composite System Frequency Spectrum Resulting from Correcting the Blurring Aperture of Figure 4.53 with the Restoration Filter of Figure 4.24

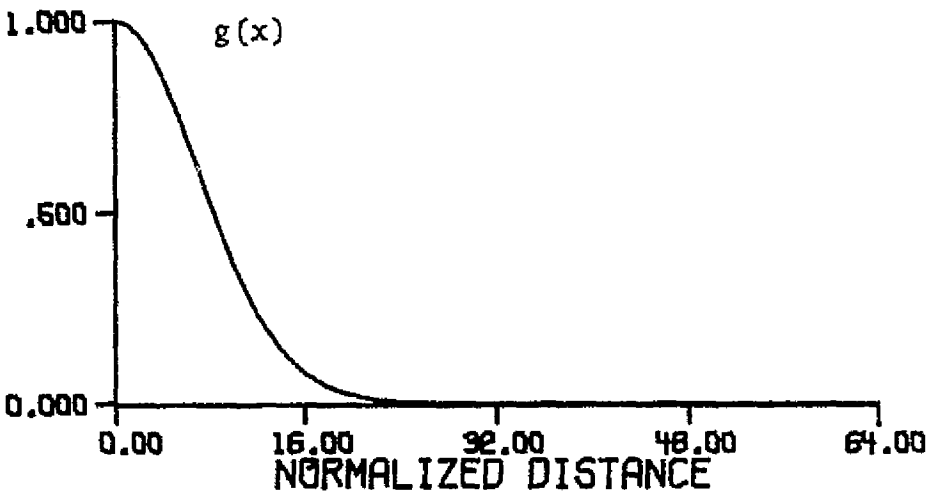

Figure 4.102 Composite System Point-Spread Function Having Spectrum of Figure 4.101

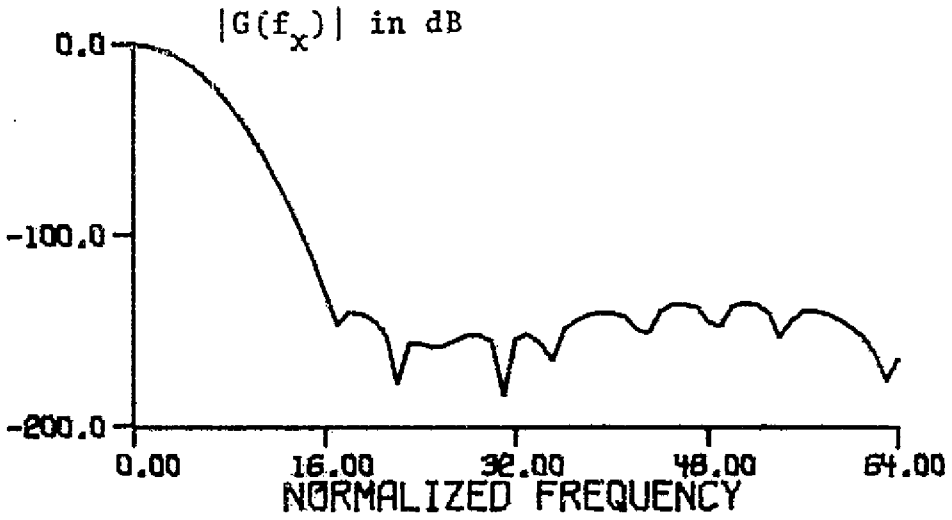

Figure 4.103 Composite System Frequency Spectrum Resulting from Correcting the Blurring Aperture of Figure 4.53 with the Restoration Filter of Figure 4.45

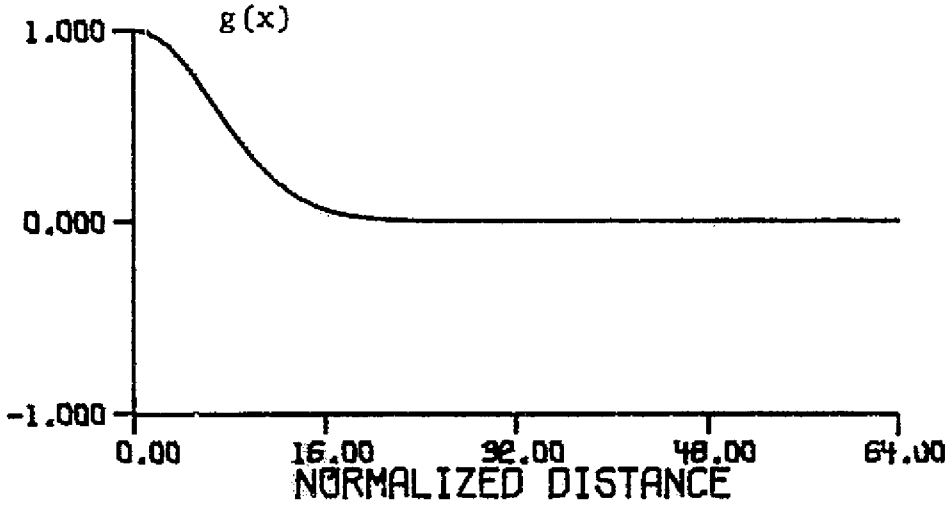

Figure 4.104 Composite System Point-Spread Function Having System of Figure 4.103

4.4 Application of the Restoration Filter to Images Blurred by a Known Gaussian Aperture

The data presented in this section was chosen to qualitatively demonstrate the fundamental properties of the optimum restoration function as previously described analytically in Chapter 2 and experimentally presented in section 2 of this chapter. Figure 4-105 thru 107 demonstrate the resolution improvement possible when a given test pattern initially blurred by a known aperture function is reconstructed under essentially noiseless conditions. It should be mentioned that round-off errors within the restoration program, resulting principally from FORT, are primarily responsible for the noise present. The input image to the blurring system is shown in Figure 4-105. This pattern is described by a two dimensional array of 512 x 512, as are all the images shown and is composed of a series of rectangular wedges whose periodicity ranges from 16 pixels/cycle to 2 pixels/cycle in 2 integer increments. This frequency variation was chosen to provide a simple qualitative comparison of the resolution of the blurred image to that of the restored image. In addition, the 8 increment grey level pattern was included to demonstrate any changes to the dynamic range of the blurred and restored images. Figure 4-106 represents the output of an imaging system having a Gaussian blurring aperture with a radius of gyration of 3, as shown in Figure 4-25. It is evident from this figure that the constrast of even the lowest frequency wedge has

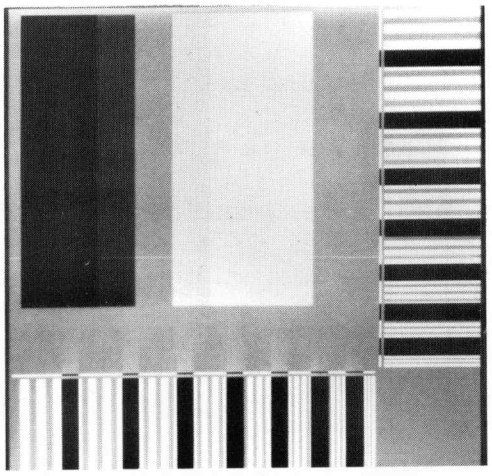

Figure 4.105 Resolution Bar Test Pattern

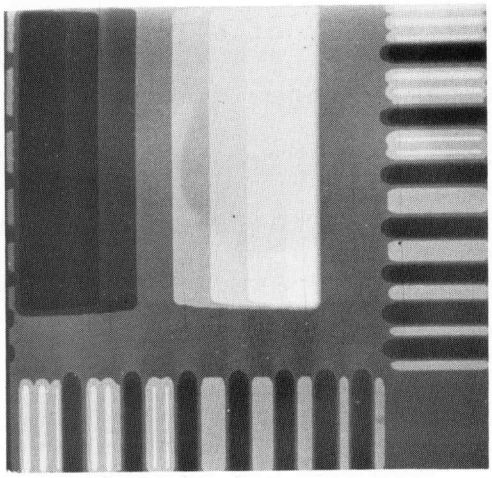

Figure 4.106 Figure 4.105 Blurred by a Gaussian Aperture with a Radius of Gyration of Three

been significantly reduced and that the highest frequency present in this pattern has a period of approximately 12 pixels/cycle. By applying the restoration function of Figure 4-42 to the data of Figure 4-106 a significant improvement in picture quality is produced as shown in Figure 4-107. The highest frequency present in the restored image has a period between 6 and 4 pixels/cycle, thus providing more than a 2 to 1 resolution improvement.

The restoration function chosen for this resolution improvement test provided a high output signal-to-noise ratio, over 40dB, for the round-off error noise introduced by the restoration program. Had the round-off error noise been less, a more powerful restoration filter could have been employed giving a greater improvement in resolution for the same output signal-to-noise ratio. It should also be noted that had no round-off error noise been present, the classical "inverse" filter would have provided perfect restoration of the blurred image.

The test results shown in Figure 4-108 thru 111 demonstrate the "ghost" effect produced by restoring a blurred image with a restoration function not specifically designed to control secondary oscillations about the origin of the composite system point-spread function. This control, as described in Chapter 2, was obtained by application of the criterion function iteration procedure. The input image, Figure 4-108, represents a bar pattern having a period of

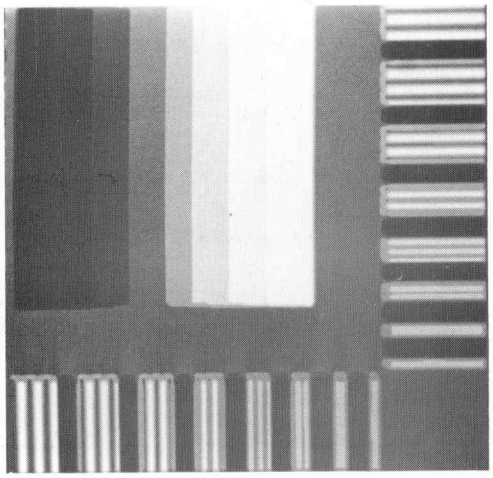

Figure 4.107 Figure 4.106 Restored by the Restoration Function of Figure 4.42

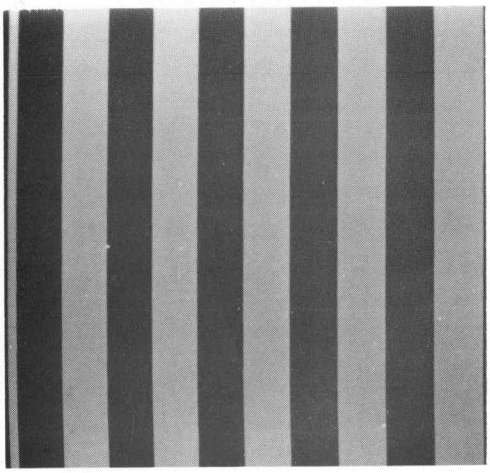

Figure 4.108 Low Frequency Square Bar Pattern

100 pixels/cycle. Figure 4-109 represents the output of an imaging system having a Gaussian blurring aperture with a radius of gyration of 3, the same as used in the previous set of figures. Figure 4-110 represents a restoration of Figure 4-109 with the noniterated version of the restoration function of Figure 4-42. A "ghost" image or oscillation on each side of the discontinuities of the bar pattern is apparent. However, when the iterated restoration function of Figure 4-42 is used to correct the image of Figure 4-109, the resulting image, Figure 4-111, shows no evidence of any "ghosts".

The final fundamental property of the optimum restoration filter, and possibly the most significant is the reduction of truncation error as compared to that produced by the classical "inverse" filter and which is produced by restoration of a truncated version of the original blurred image. This effect will first be demonstrated by a one-dimensional example. Figure 4-112 represents a rectangular test function which when blurred by the Gaussian aperture of Figure 4.53 having a radius of gyration of 5 produces the data of Figure 4-113. Figure 4-114 is obtained by truncating, or setting to zero, the first 10 points of Figure 4-113. By applying the classical "inverse" restoration filter of Figure 4-55 to the truncated data set of Figure 4-114, the data of Figure 4-115 results. At no point in the data record does the truncation error become small enough to resolve the original

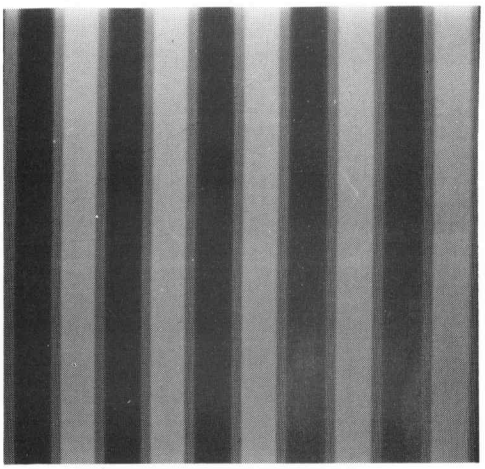

Figure 4.109 Figure 4.108 Blurred by a Gaussian Aperture with a Radius of Gyration of Three

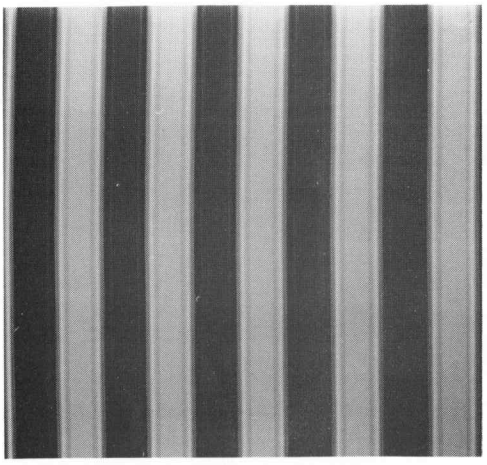

Figure 4.110 Figure 4.109 Restored by the Uniterated Version of the Restoration Function of Figure 4.42

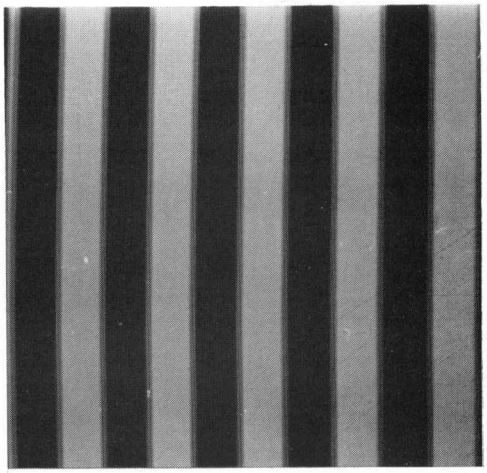

Figure 4.111 Figure 4.109 Restored by the Restoration Function of Figure 4.42

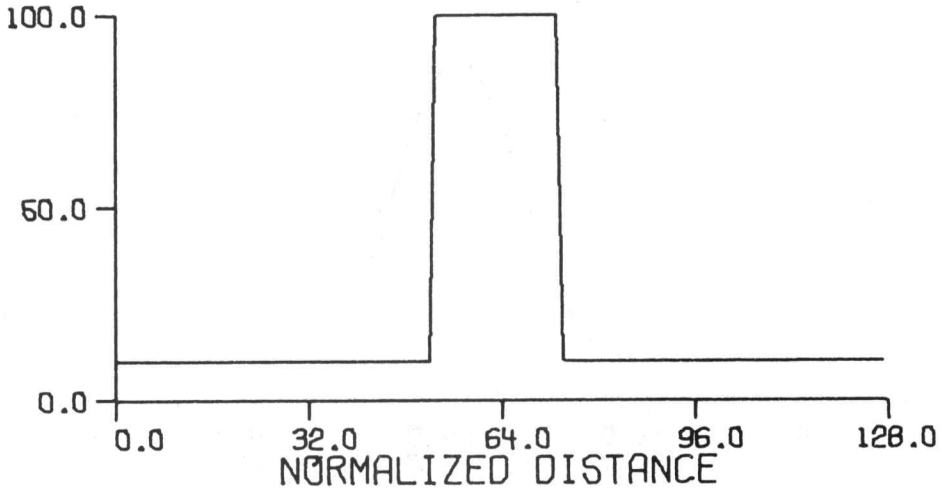

Figure 4.112 Rectangular Test Function

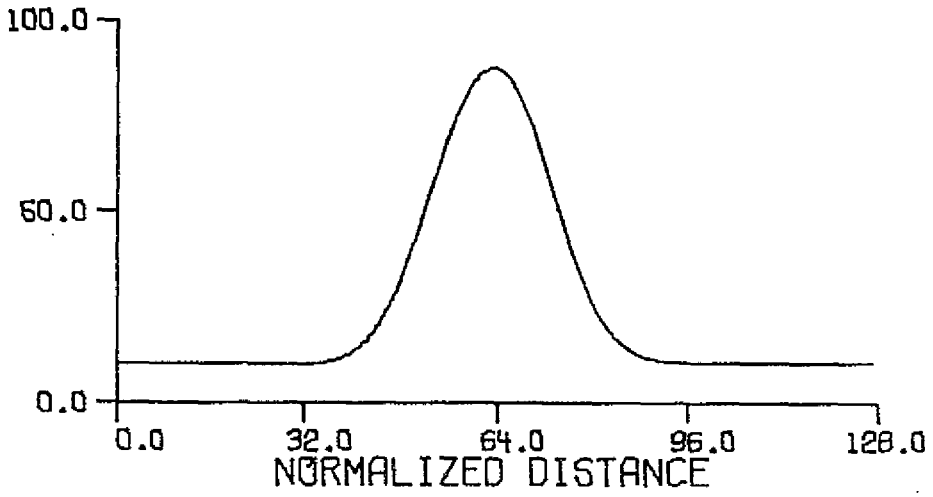

Figure 4.113 Convolution of the Function of Figure 4.112 with the Function of Figure 4-53

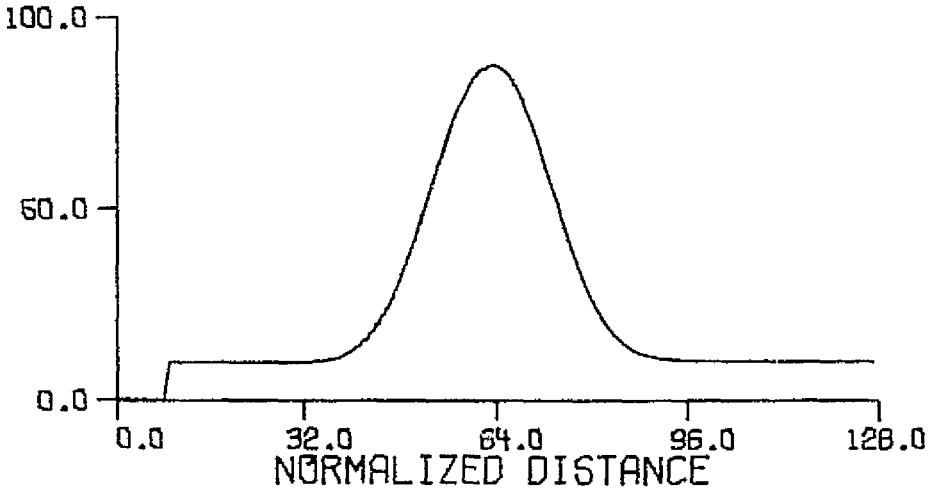

Figure 4.114 Truncation of First 10 Points of Figure 4.113

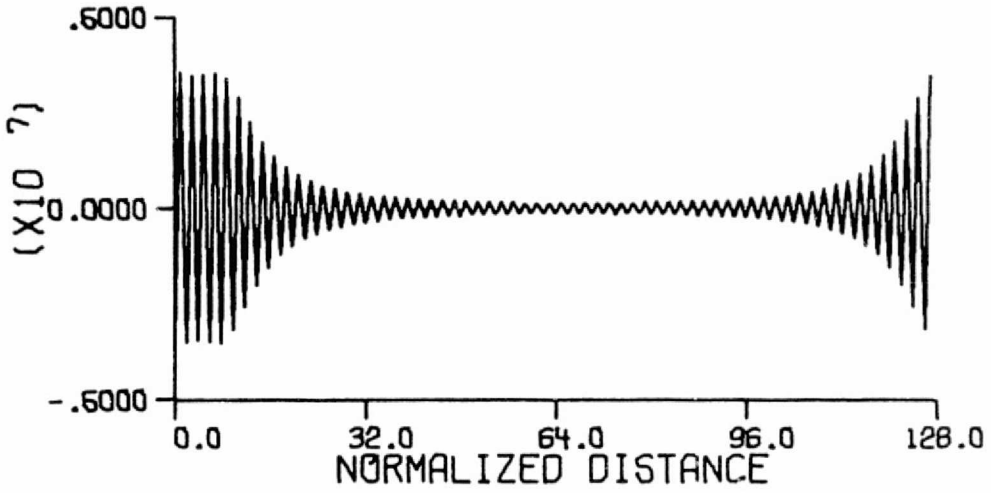

Figure 4.115 "Restored" Function Obtained By Correcting the Truncated Data of Figure 4.114 With the Classical "Inverse" Restoration Function of Figure 4.55

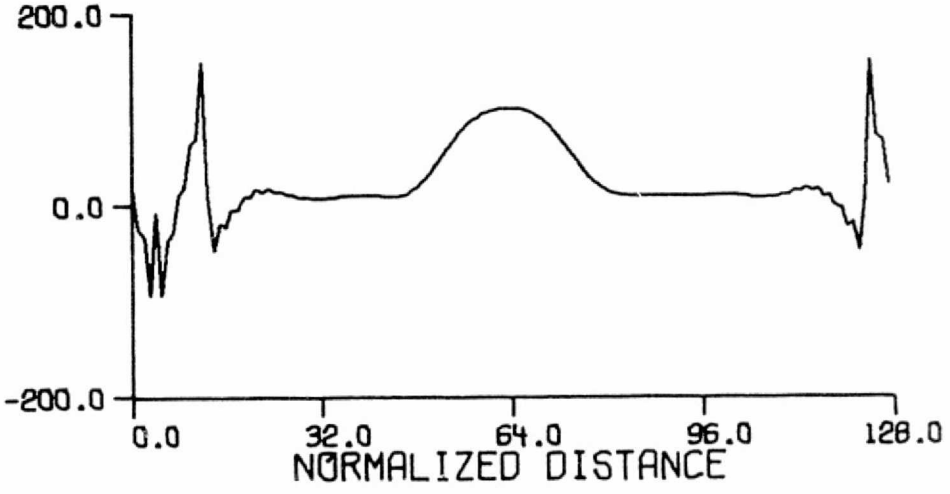

Figure 4.116 Correction of Truncated Data of Figure 4.114 by the Restoration Function of Figure 4.67

test function. When the restoration function of Figure 4-67 is applied to the same truncated data set of Figure 4-114 the result, shown in Figure 4-116, is obtained and indicates significant error at the edges of the restoration. However, because the radius of gyration of the restoration filter point-spread function was constrained negligible error is present at the center of the data record.

Figure 4-117 thru 4-120 demonstrate this same effect for a two-dimensional example. Figure 4-117 represents a bar pattern with a spatial period of 10 pixels/cycle. When the Gaussian aperture of Figure 4-25 is used to blur the image of Figure 4-117, the result is shown in Figure 4-118. By truncating, i.e. setting to zero, all but the center 256 x 256 portion of Figure 4-118 and applying the classical "inverse" restoration filter to the result, the image of Figure 4-119 is produced. Although the truncation error is smallest at the center of this image, no significant restoration of the original bar pattern is apparent. However, when the restoration function of Figure 4-42 is applied to the same truncated version of Figure 4-118, the result is shown in Figure 4-120. It is clearly evident that the truncation error rapidly becomes negligible inside the center 256 x 256 portion of this figure and that significant restoration of the original bar pattern is apparent.

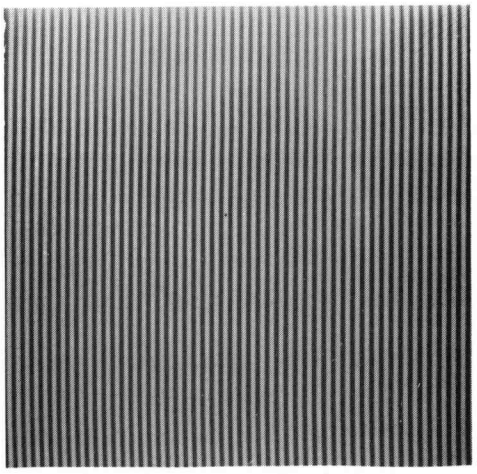

Figure 4.117 High Frequency Square Bar Pattern

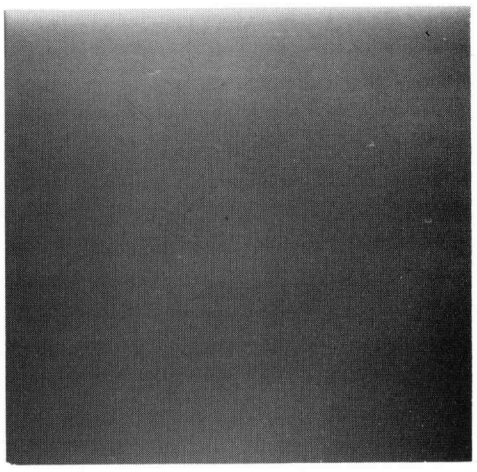

Figure 4.118 Figure 4.117 Blurred by a Gaussian Aperture with a Radius of Gyration of Three

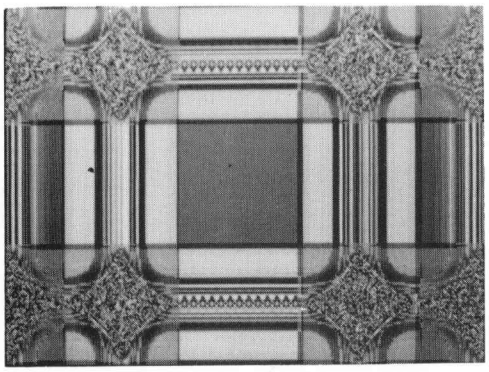

Figure 4.119 Restoration of a 256^2 Center Portion of Figure 4.118 by the Classical "Inverse" Restoration Function of Figure 4.27

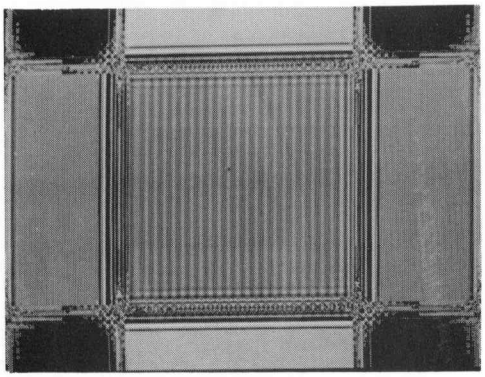

Figure 4.120 Restoration of a 256^2 Center Portion of Figure 4.118 by the Restoration Function of Figure 4.42

CHAPTER 5

APPLICATION OF OPTIMUM IMAGE RESTORATION FILTER TO ERTS MULTISPECTRAL SCANNER DATA

5.1 Introduction

The primary motivation for this research was the development of an optimal resolution enhancement technique for application to remotely sensed multispectral scanner data. The fundamental properties of the resulting optimal restoration filter examined in the previous chapter indicated that the shortcomings of the classical "inverse" filter, which formed the basis for defining most of these properties as discussed in Chapter 2, had been resolved. However, until this restoration technique was applied to actual ERTS data, it would not be known whether there existed any significant deficiencies which had not been previously anticipated.

This chapter describes the application of this restoration technique to a specific ERTS data set. The problems encountered in estimating the multispectral scanner blurring aperture, defining the noise present in the data, and performing the correction to the data are examined. Finally conclusions are drawn concerning the quality of the restoration achieved and the effect of numerical error both in the calculation and implementation of the restoration function. An IBM 360 model 67 computer was used to compute the restoration filters of Chapter 4 and to apply these

corrections to the selected ERTS data set.

5.2 Estimation of Blurring Aperture

As mentioned earlier, since no specific information concerning the blurring aperture of the multispectral scanner was available, a mathematical model had to be defined. As discussed in the introduction to Chapter 4, a Gaussian model was ultimately chosen in order to make possible certain simplifying assumptions. These assumptions include defining a separable blurring process to substantially reduce processing cost and time and to permit explicit computation of the blurring aperture spectrum, so that numerical round-off errors may be reduced.

It should also be noted that an alternative to choosing a model for the blurring aperture would be the estimation of the aperture directly from the data. However, in view of the extremely large quantization noise present in all the ERTS data examined and which will be discussed shortly, it seemed unlikely that this procedure would provide any better estimate of the blurring process.

By re-examining the results of Table 4.1 and 4.2, it is apparent that the more data samples per blurring aperture width, the more effective the restoration procedure for a given set of constraints. For example in the extreme case where the blurring aperture is described by only one sample point, then regardless of the constraints on the restoration filter the resulting composite system point-spread function

can contain no less than one sample point. Thus for this case it is clear that no resolution improvement is possible. However, if the blurring aperture could be sampled more often, increasing the number of sample points per blurring width, then a resolution improvement should be possible.

This problem of having relatively few samples per blurring aperture width exits with the ERTS data. The scanner aperture has an effective ground diameter of approximately 80 meters. The data is collected so that a rectangular array of points is generated with an effective ground distance between adjacent vertical points in the array of 79 meters and an effective ground distance between adjacent horizontal points in the array of 56 meters. Thus it is unlikely that there are more than 3 sample points within a circle of three σ radius centered at the blurring aperture. In order to obtain significant resolution improvement, it is necessary to have a larger number of samples per blurring width than this. One way to obtain more samples is to interpolate additional values between the original data points. The idea is not to create information where no information originally existed buth rather to provide sufficient sample values to allow use of an effective restoration filter function. The procedure that will be used is to increase the number of points per blurring aperture until they correspond to one of the aperture functions for which the optimum restoration filter has been determined. The

The restoration can then be carried out and the final data set can be compressed back to the original size if desired. The use of interpolation allows the data set to be matched to the restoration function experimentally which is very desirable because precise values for the actual blurring function are not known.

At the same time that the interpolation is performed to increase the number of points per blurring aperture, the scale factor differences of the vertical and horizontal image axes can be corrected. This scale factor difference arises from the fact that the effective ground distances between adjacent points along the vertical and horizontal axes are not equal. If these points are displayed as if these distances were equal, then resulting distortion produces an image which is compressed vertically. Thus to correct this distortion, a somewhat greater degree of interpolation, or magnification, is required along the vertical axis. By magnifying the vertical axis, 79/56 with respect to the horizontal axis, this distortion should be corrected.

A third-order polynominal interpolation function was used because of its relative smoothness compared to other forms, including trigonometric and sinc functions. The restoration filter corresponding to a blurring aperture of radius of gyration of 5 is the largest that has been computed due to limitations imposed by round-off errors in the computations. In this blurring function, there are approx-

imately 45 samples (pixels) within the 1% amplitude levels of the blurring function along each axis. Therefore, it is necessary to interpolate the ERTS data to obtain this same number of points in the estimated width of the ERTS aperture. As a first approximation, the width of the ERTS aperture was taken to be 3 as discussed above and accordingly the required interpolation factor is 45/3 = 15. In addition, to correct the geometric distortion, the ratio of the vertical to horizontal interpolation factors should be 79/56 ≈ 1.411. The only integer ratio which satisfied both the interpolation factor for matching the effective data scanner aperture to a Gaussian blurring aperture with a radius of gyration of five and the geometric distortion correction interpolation ratio was 17/12 ≈ 1.417. In other words, an interpolation of 17 along the vertical axis and 12 along the horizontal axis would not only correct the geometric distortion but also approximately match the effective ERTS data scanner aperture to the restoration function computed for a Gaussian aperture with a radius of gyration of five. Several additional interpolation ratios were used to determine whether a better aperture match could be obtained. However, as will be explained later, this ratio provided the best performance.

It appears likely that restoration functions computed for larger radii of gyration then five would provide even better results when matched to the ERTS data by appropriate interpolation factors. However, because of the excessive

round-off errors encountered in the restoration function computation program, the largest radius of gyration which would provide reliable results was five. In addition, excessive interpolation of under sampled data may be desirable because of the effect of aliasing errors on the interpolation accuracy. However, for the ratios chosen, this error did not appear significant.

5.3 Composite System Noise

The composite system noise is defined as the total noise process including both the noise introduced by the ERTS data collection system and that introduced by the restoration process. The noise introduced by the ERTS data collection system arises from three primary sources: the sensors of the multispectral scanner, the signal conditioning electronics, and the A/D conversion process. The noise introduced by the restoration process arises principally from numerical round-off errors.

The predominant data collection system noise source is introduced in the quantization stage of the A/D process. The data is quantized into six bits producing a signal dynamic range from 0 to 63. The total noise power, n^2, introduced by uniform quantization may be approximated by the expression [3,6]

$$n^2 = \frac{\Delta v}{12} \qquad (5\text{-}1)$$

where Δv represents the quantization increment, in this case it is 1 unit. Thus the total quantization noise power is approximately

$$n^2 = \frac{1}{12} \simeq 0.08333 \text{ volts}^2. \qquad (5\text{-}2)$$

This noise process may be shown to have an essentially flat spectrum extending to many times the sampling frequency. A conservative estimate of the power spectrum density of the quantization noise can be obtained by assuming that it lies entirely within the band occupied by the signal. The

resulting one sided noise spectral density is given by

$$\Phi_{nn}(f) \leq \frac{1}{12(f_s)} = \frac{1}{6f_s}, \qquad f \geq 0 \qquad (5\text{-}3)$$

where f_s is the sampling frequency of the A/D process. The magnitude of f_s depends on the units of measurement being employed. For convenience it will be assumed that $f_s = 128$ which is the number of samples used to define the restoration filters along each axis. With this convention the noise spectral density is then

$$\Phi_{nn}(f) \leq \frac{1}{6(128)} = 1.302 \times 10^{-3}. \qquad (5\text{-}4)$$

Because the ERTS data does not occupy the full 64 level dynamic range defined by the quantization process, the quantization noise is made even more significant due to the reduced input signal-to-noise ratio. The ERTS data sets examined have a dynamic range of approximately $\pm$ 15 units, producing an input signal-to-noise ratio of less than 34 dB. In view of the fact that the restoration process will be enhancing the high frequency components of the ERTS data and from the assumption that the quantization noise spectral density is flat, the quantization noise presents a very serious problem to obtain significant restoration and a high signal-to-noise ratio in the deblurred image.

The second source of composite system noise is introduced by computational round-off errors. These errors arise principally within the FORT Fast Fourier Transform algorithm. A double precision version of this algorithm is employed both

in the computation of the restoration function and in the application of this function to a blurred image. This algorithm is used to perform the spatial deconvolution by multiplication of the spectral components of the blurred image with the corresponding components of the restoration function and then talking the inverse Fourier transform of the product. By using this algorithm to compute the spectrum of one of the Gaussian blurring apertures previously described in Chapter 4 which should also be Gaussian shaped, it was found that the magnitudes of the resulting spectrum never become less then approximately 10^{-5} when normalized with respect to the DC term. Consequently, this noise process is assumed to have a flat spectral density of approximately 10^{-5} below the DC level of the data being corrected. Since the ERTS data sets examined typically had a DC value of approximately 30, the round-off error noise spectral density amplitude was assumed to be approximately 10^{-4} v^2/Hz.

The severity of this problem is made evident by considering the application of the classical "inverse" restoration filter to the image of Figure 4.106 as discussed in Section 4.4. Using the exact inverse one would expect to obtain a perfect restoration. However, because of the noise introduced by the round-off errors within the FORT algorithm, the actual restoration obtained consisted only of a random noise pattern with none of the original features being evident.

Since this noise source appears to be a function of the numerical accuracy of the computations within the FORT algorithm it is probable that it could be reduced to a negligible level by increasing the precision of the computations. However, it was not possible to employ more than double precision accuracy because of computer limitations.

5.4 Resolution Enhancement of ERTS Data

The ERTS data set to be enhanced had to satisfy two primary criteria. The first, and possibly the most important, was that the data set had to be free of any obvious noise so as to permit maximum restoration. The second was that the data set had to include a known topographical feature to provide a degree of "a priori" knowledge of the original image before blurring by the multispectral scanne. for comparison to the restored results. Figure 5.1 and 5.2 show the ERTS data set selected. This data was taken from ERTS frame ID no. 1080-15192 collected on October 11, 1972, and reformatted as LARS run number 7^041900, Ch. 3, lines 916-1427, columns 986-1497. This area includes a portion of Washington, D.C. The topographical feature selected for enhancement was the Pentagon Building which appears at the center of Figure 5.1 and the upper center of Figure 5.2, a 2X linear magnification of Figure 5.1. This feature was chosen not only because its shape is well defined but also because the luminance intensity of a single scan line passing through the center of the building for a scanner with

Figure 5.1 ERTS Multispectral Scanner Data of Washington, D.C. Area with Pentagon at Center (LARS Run No. 72041900, Ch 3, Lines 916-1427, Columns 986-1497)

Figure 5.2 2X Linear Enlargement of Figure 5.1 Showing Pentagon in Upper Center

infinite resolution would appear as two closely spaced rectangular pulses with the level between the pulses representing the "hole" in the center of the building. Thus by comparing the luminance signal for a single scan line passing through this area, a qualitative measure of the resolution enhancement is possible.

Figure 5.3 shows the Pentagon and surroundings of Figure 5.1 after the application of a third-order two-dimensional polynomial interpolation. As previously discussed, in order to correct the axis scale factor difference and also to approximately match the ERTS scanner aperture to the most powerful restoration functions computed for a Gaussian blurring aperture with a radius of gyration of five, the horizontal axis was interpolated or magnified by a factor of 12 while the vertical axis was interpolated by a factor of 17. Figure 5.4 represents a 2X linear enlargement of the upper left quadrant of Figure 5.3.

Figure 5.5 represents a plot of the luminance level for a scan line passing through the center of the Pentagon of Figure 5.3, i.e. data line 110. The left most side of the Pentagon is centered at the 60th sample, the "hole" at the 85th sample, and the right most side at the 110th sample. The frequency spectrum corresponding to this line is shown in Figure 5.6. The information provided by these two graphs will form the primary basis for selecting the "best" restoration function of those computed in Chapter 4 for a Gaussian

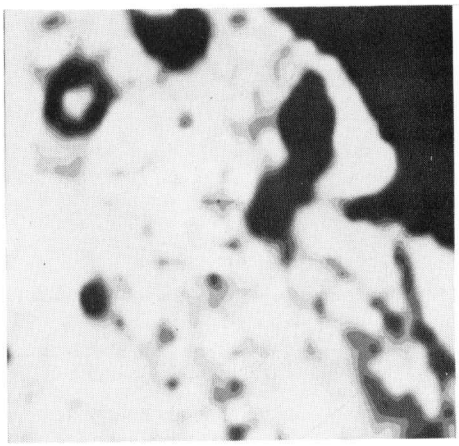

Figure 5.3 Polynomial Interpolation of Figure 5.1 Using an Interpolation Factor of 17 for the Vertical Axis and 12 for the Horizontal Axis

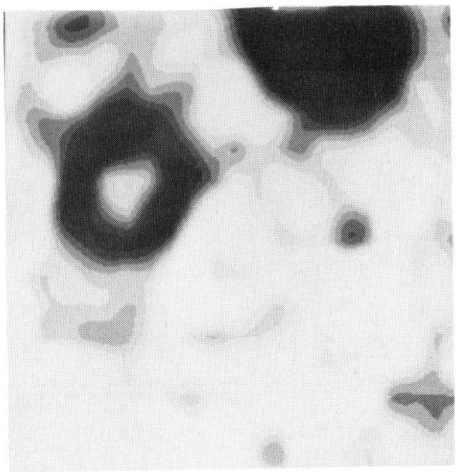

Figure 5.4 2X Linear Enlargement of the Upper Left Quadrant of Figure 5.3

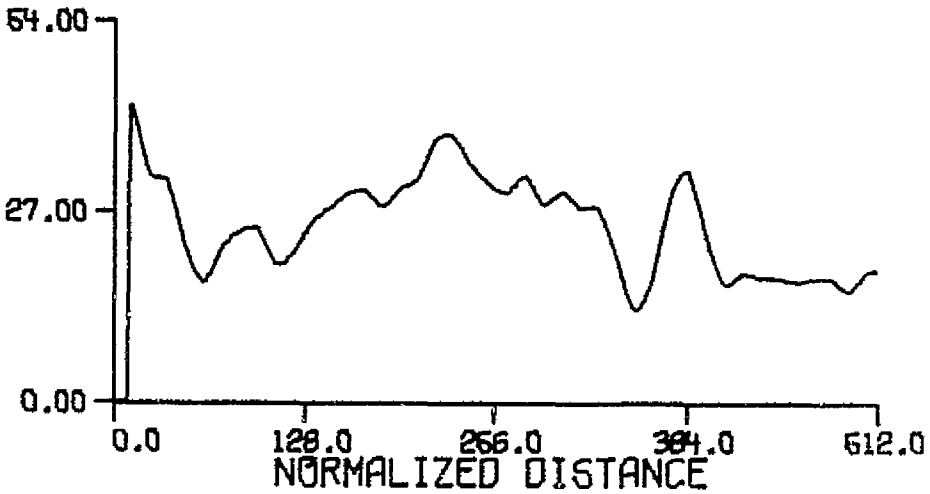

Figure 5.5 Graph of Data Line 110 of Figure 5.3

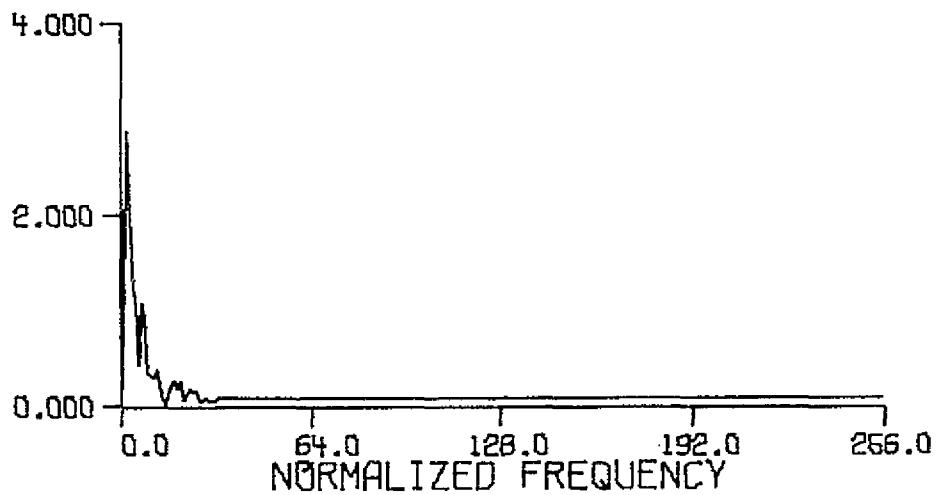

Figure 5.6 Frequency Spectrum of Data Line 110 of Figure 5.5

aperture with a radius of gyration of five.

The restoration function selection procedure was as follows. Several restoration functions were computed based upon white noise spectral density amplitudes approximating the spectral density amplitude estimates of the system noise processes previously described. The data of Figure 5.3 was restored by each function. Then the graph of data line 110 and the corresponding frequency spectrum were compared to those of Figure 5.5 and 5.6. The spectrum of line 110 for each restoration was examined to determine if the fundamental frequency components of Figure 5.5, approximately the first 22 normalized frequency components of Figure 5.6, had been amplified without introducing higher frequency noise components of comparable magnitude. In addition, the graphs of data line 110 for each restoration were compared to that of Figure 5.5 to determine the degree of resolution enhancement by estimating the rise time associated with the luminance level change between the left most side and the "hole" of the Pentagon.

Figure 5.7 and 5.8 represent the graphs of data line 110 and its spectrum when the restoration function based on flat noise spectrum $\Phi_{nn}(f) = 10^{-5}$ (Figure 4.67) is applied to the data of Figure 5.5. The spectrum shown in Figure 5.8 indicates that significant high frequency spectral components have been introduced during the restoration procedure. Since these high frequency components have the same general

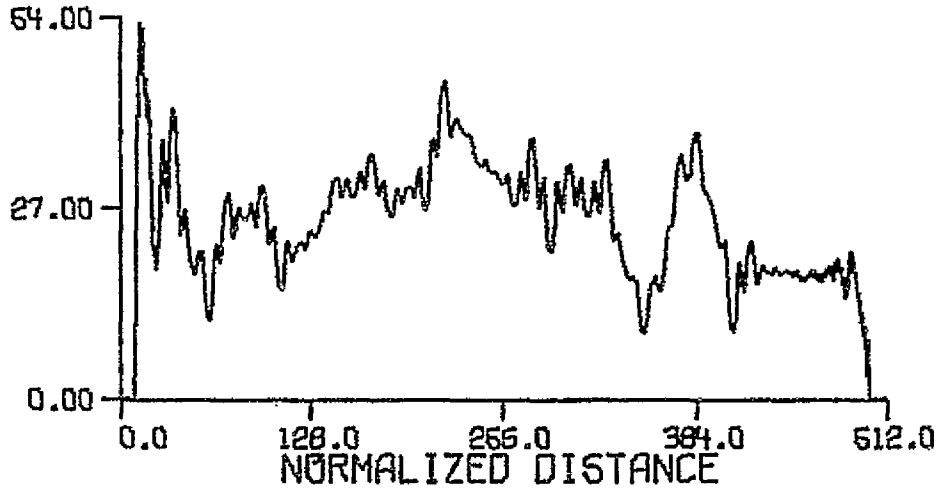

Figure 5.7 Graph of Data Line 110 of Figure 5.5 after Restoration with the Filter of Figure 4.67

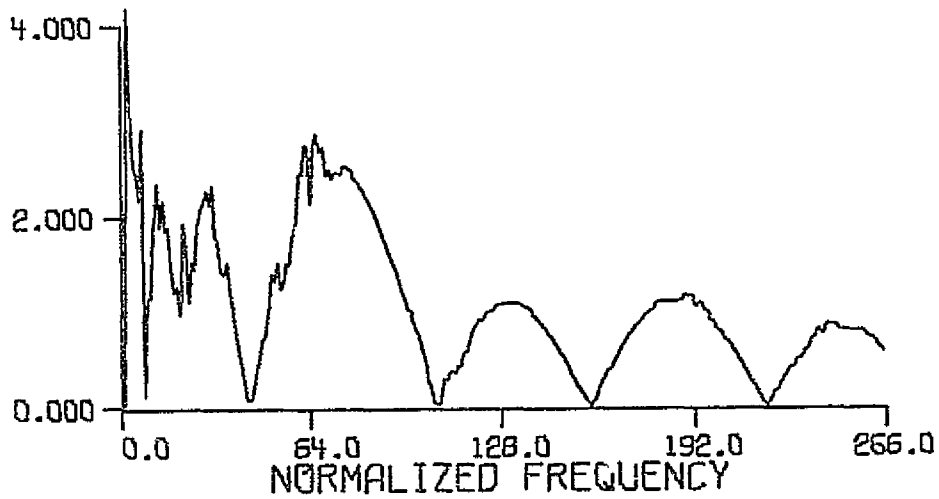

Figure 5.8 Frequency Spectrum of Data Line 110 of Figure 5.7

shape as the spectrum of the restoration filter, shown in Figure 4.65, it is reasonable to assume that these spectral components are the result of amplification of the system noise by the restoration filter. In other words, the assumed noise spectral density amplitude of 10^{-5} for the computation of this filter was much less than that of the composite system noise process. Figure 5.9 shows the result of this restoration to Figure 5.3. Figure 5.10 is a 2X linear magnification of the upper left quadrant of Figure 5.9.

By increasing the assumed noise spectral density amplitude to 10^{-4} a new restoration function shown in Figure 4.73 is obtained. Figure 5.11 and 5.12 show the graph of data line 110 and its corresponding spectrum when this restoration function is applied to Figure 5.3. It is clear that the high frequency noise components, shown in Figure 5.12, are of less amplitude then those of Figure 5.8. It should again be noted that the shape of the noise spectrum in Figure 5.12 is determined by the spectrum of the restoration filter. Figure 5.13 represents the result of applying the restoration function of Figure 4.73 to the data of Figure 5.3. Figure 5.14 is a 2X linear magnification of the upper left quadrant of Figure 5.13.

By further increasing the noise spectral density amplitude to 10^{-3}, the restoration function of Figure 4.79 is obtained. Figure 5.15 and 5.16 represent the graphs of data line 110 and its corresponding frequency spectrum when

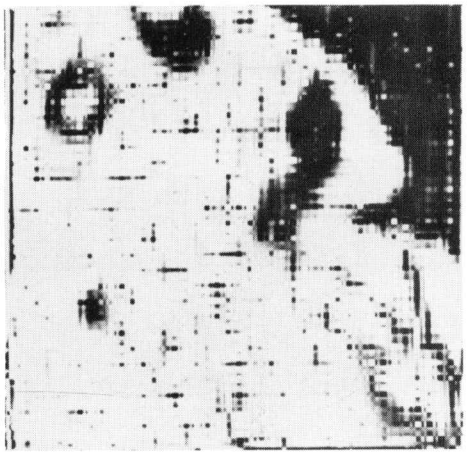

Figure 5.9 Restoration of Figure 5.3 with the Filter of Figure 4.67

Figure 5.10 2X Linear Enlargement of the Upper Left Quadrant of Figure 5.9

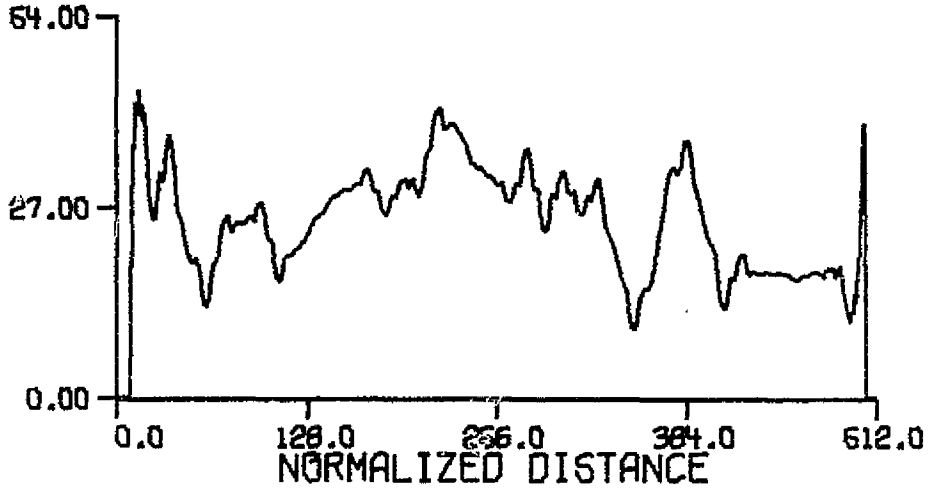

Figure 5.11 Graph of Data Line 110 of Figure 5.5 after Restoration with the Filter of Figure 4.73

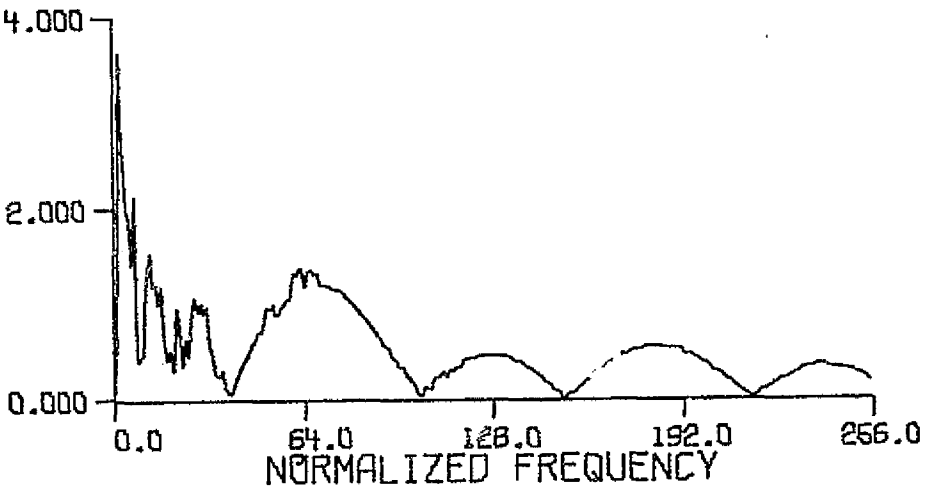

Figure 5.12 Frequency Spectrum of Data Line 110 of Figure 5.11

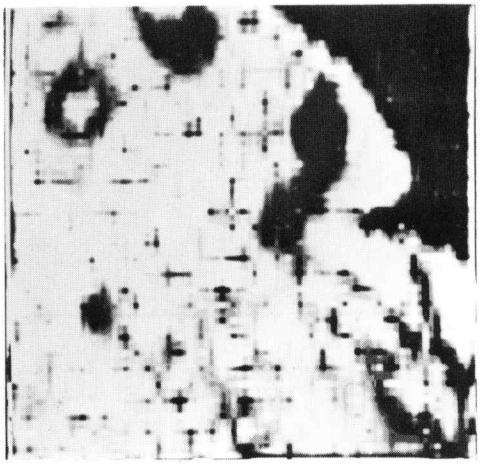

Figure 5.13 Restoration of Figure 5.3 with the Filter of Figure 4.73

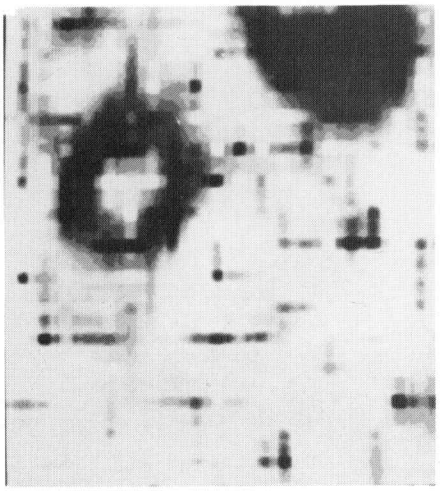

Figure 5.14 2X Linear Enlargement of the Upper Left Quadrant of Figure 5.13

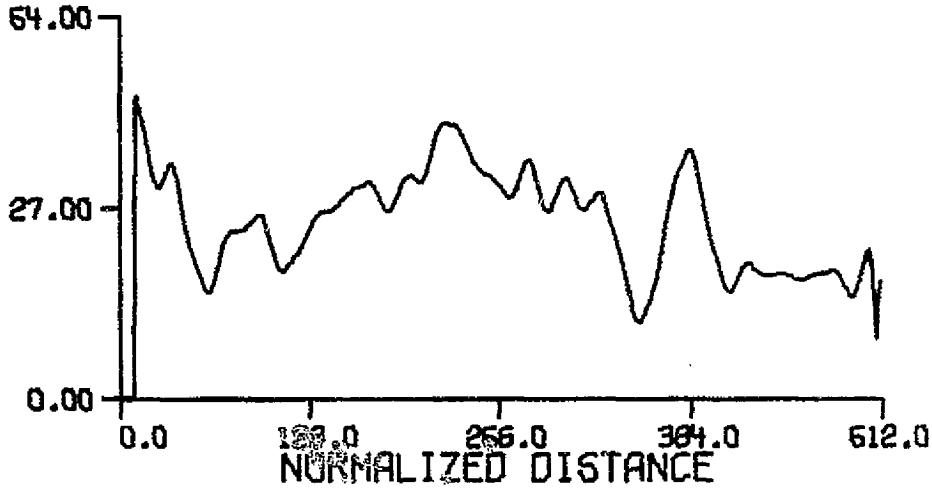

Figure 5.15 Graph of Data Line 110 of Figure 5.5 after Restoration with the Filter of Figure 4.79

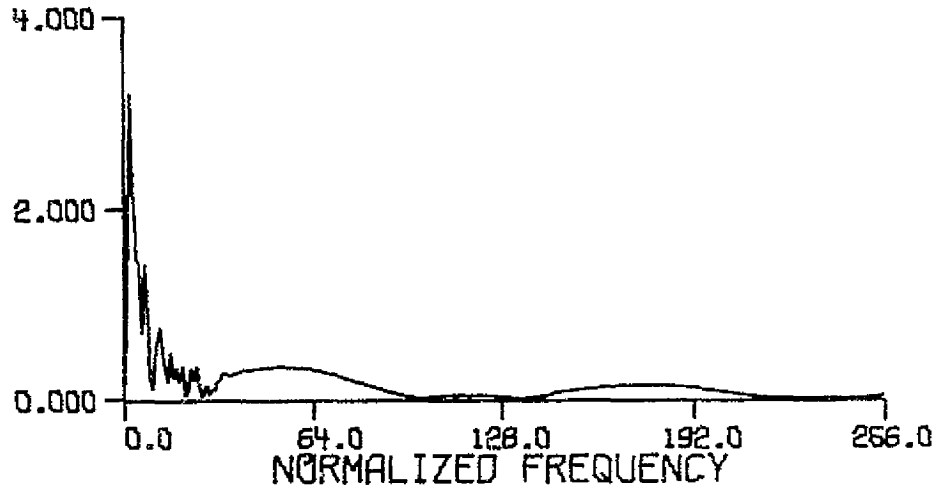

Figure 5.16 Frequency Spectrum of Data Line 110 of Figure 5.15

the restoration function of Figure 4.79 is applied to the data of Figure 5.3. Although the high frequency noise components are still evident in Figure 5.16, the effect on the data, as shown in Figure 5.15, appears negligible. Figure 5.17 represents the restoration of Figure 5.3 by the restoration function of Figure 4.79. Figure 5.18 is a 2X linear magnification of the upper left quadrant of Figure 5.17.

Additional restoration functions were computed based on various other amplitudes and shapes of the noise spectral density. These correspond to Figure 4.70, 4.73, 4.75, 4.83, 4.87, and 4.91, and each was applied to the data of Figure 5.3. However, no significant improvement was achieved compared to the results of Figure 5.17 and 5.18 obtained by the restoration function of Figure 4.79. It should also be noted that additional interpolation ratios were applied to the image of Figure 5.1 to determine if a better "match" could be obtained than that of 17 for the vertical axis and 12 for the horizontal axis. These ratios included 10/7, 14/10, and 20/14. However, no improvement was obtained over the 17/12 ratio for any of the restoration functions previously discussed.

A comparison of the graph of data line 110 for this restoration, Figure 5.15, with that of the original interpolated image, Figure 5.5, shows that the rise time for the restoration as measured for the transition between the left most side of the Pentagon and the "hole" is approximately one

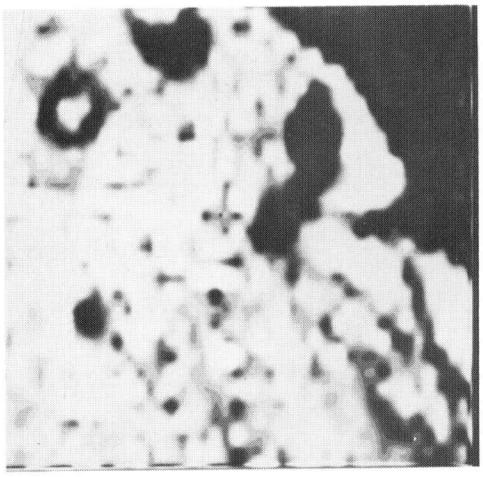

Figure 5.17 Restoration of Figure 5.3 with the Filter of Figure 4.79

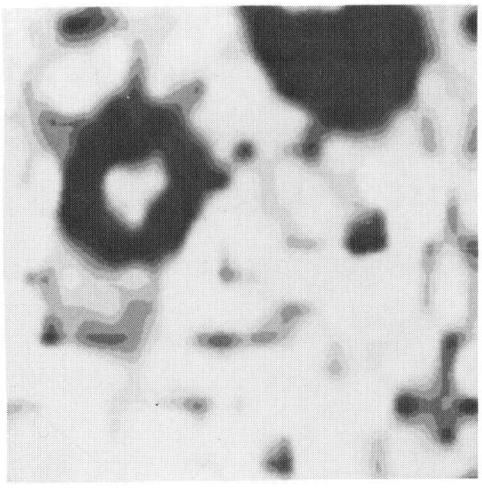

Figure 5.18 2X Linear Enlargement of the Upper Left Quadrant of Figure 5.17

half that of the original. In addition, the sides of the Pentagon as shown in Figure 5.17 and 5.18 are displayed with fewer grey levels, the transition defining the sides is more sharp and the "hole" is somewhat larger than as shown in Figure 5.3 and 5.4, as would be expected by a resolution enhancement. There is also better delineation between the sides of the Pentagon and the topographical features immediately surrounding it in the restored images of Figure 5.17 and 5.18. Also an examination of the other topographical features of Figure 5.3 and 5.4 shows that these features are displayed with greater contrast and are less amorphous in shape in the restored images of Figure 5.17 and 5.18.

One of the most significant results of the restorations shown in Figure 5.17 and 5.18 is with regard to the data truncation error. For the classical "inverse" restoration filter, with no constraint of the radius of gyration of its point-spread function, this error would have propagated throughout the corrected data set substantially reducing image quality. As shown by the restorations in these figures, this error though noticeable at the extreme edges, becomes negligible after about 25 points into the data record from each edge. In addition to reducing the data truncation error, the constraint in the radius of gyration of the point-spread function of the restoration filter also produced a function which contained less than 30 points of significant amplitude as compared to the classical "inverse" restoration

point-spread function which would have required as many points as the data record to be corrected, which for the corrections of Chapter 5 would have been 512 points. This reduction in the size of the restoration function should also increase data processing efficiency.

5.4 Problems of ERTS Data Collection System

As a consequence of this study, two significant problems were encountered that are inherent in the ERTS data collection system. The first problem is the poor signal-to-noise ratio of the ERTS data. This problem could be reduced by both reducing the quantization level increment and by increasing the dynamic range of the data prior to quantization. The second problem, the need for relatively large interpolation ratios to match the effective blurring aperture of the ERTS data system to the available restoration functions, could be minimized by increasing the data sampling rate. Since less interpolation would be required, both greater interpolation accuracy and increased processing efficiency could be achieved. By addressing both of these problems, more powerful restoration functions may be applied to the data thus producing even greater resolution improvement.

CHAPTER 6

CONCLUSIONS AND SUGGESTIONS FOR FURTHER STUDY

6.1 Conclusions

This study has demonstrated that it is possible to design a restoration filter based upon minimizing the radius of gyration of the composite system point-spread function while constraining the radius of gyration of the point-spread function of the restoration filter and the noise power in the restored image. By assuming that the blurring aperture and composite system noise process are separable,a significant reduction in solution complexity was introduced. Transformation of the defining spatial equations into the frequency domain led to a further simplification in that a system of linear differential equations results for second-order spatial weighting funcations in both the radii of gyration of the composite system and restoration filter point-spread function. Through application of well-known numerical solution techniques to this system of equations, a solution which satisfied the original constraints was obtained. Additional control over secondary oscillations in the composite system point-spread function was made possible by the introduction of an iterative technique. It was further shown that the resulting restoration filters satisfied the fundamental design criteria: reduction of the radius of gyration of the composite system point-spread function, and reduction of truncation error by constraining the radius of

gyration of the restoration filter point-spread function.

One of the most significant results of this study was the successful application of this restoration technique to data which was blurred by an unknown function. By assuming a Gaussian model for the ERTS multispectral scanner aperture and employing a interpolation technique to match the effective scanner blurring aperture to the Gaussian aperture for which the most powerful restoration functions had been computed, a significant restoration of truncated ERTS data was obtained. In addition, because of the constraint on the radius of gyration of the restoration filter point-spread function, the truncation error was almost entirely limited to a small region near the edges of the image. Thus substantial restorations having a high signal-to-noise ratio and negligible truncation error were achieved.

6.2 Suggestions for Further Study

As a consequence of this investigation, several areas of additional study may be defined. First by compressing the enhanced interpolated data to its original scale, classification studies may be performed to determine the effect of resolution enhancement in classification accuracy. Secondly, by increasing the numerical precision of the restoration function computation program, more powerful restoration functions computed for blurring functions having more points per blurring aperture width than that for the Gaussian aperture with a radius of gyration of five could be applied to

the ERTS data. Thirdly, the design of a restoration filter which would have a spatially variant constraint on the radius of gyration of the point-spread function of the restoration filter should provide greater resolution enhancement near the center of a truncated image while simultaneously controlling truncation error at the edges of the restoration than the spatially invariant constraint on the filter of this study. Fourthly, the development of a similar filter using finite difference equations rather than differential equations may reduce the numerical errors and resulting solution instabilities encountered with differential equation solution algorithms. Finally the analysis of blurring apertures for other than Gaussian functions should provide useful results, particularly for rectangular functions where linear motion blur correction is desired.

BIBLIOGRAPHY

BIBLIOGRAPHY

1. Arguello, R., H. Sellner, and J.A. Stuller, "Transfer Function Compensation of Sampled Imaging," IEEE Trans. on Computers, Vol. C-21, No. 7, pp. 812-818, July, 1972.

2. Becherer, R.S., "Optimum Shaded Apertures for Reducing Photographic Grain Noise," SPIE-Image Information Recovery Seminar Proceedings, pp. 86-96, October 24-25, 1968.

3. Bennett, W.R., "Spectra of Quantized Signals," BSTJ, Vol. 27, pp. 446-472, July, 1948.

4. Bracewell, R.N., "Correcting for Gaussian Aerial Smoothing," Australian Journal of Physics, Vol. 8, No. 1, pp. 54-60, 1955.

5. Bracewell, R.N., "Correcting for Running Means by Successive Substitutions," Journal of Physics, Vol. 8, No. 3, pp. 329-334, 1955.

6. Cattermole, K.W., Principles of Pulse Code Modulation, New York: American Elsevier Publishing Company, 1969.

7. Epstein, B., Linear Functional Analysis, New York: W.B. Saunders, Company, 1970.

8. Franks, L.E., Signal Theory, New Jersey: Prentice-Hall, 1969.

9. Harris, J.L., Sr., "Image Evaluation and Restoration," Journal of the Optical Society of America, Vol. 56, No. 5, pp. 569-574, May, 1966.

10. Horner, J.L. and M.J. Rycus, "Restoration of Linearly Smeared Transparencies," SPIE-Image Information Recovery Seminar Proceedings, pp. 121-129, October 24-25, 1968.

11. Huang, T.S., W.F. Schreiber, and Q.J. Tretiak, "Image Processing," Proc. IEEE, Vol. 59, No. 11, pp. 1586-1609, November, 1971.

12. IBM System/360 Scientific Subroutine Package Version III, Programmer's Manual, No. 360A-CM-03X, August, 1970.

13. Kinzly, R.E., R.C. Harris, and P.G. Roetling, "Designing Filters for Image Processing to Recover Detail, SPIE-Image Information Recovery Seminar Proceedings, pp. 97-104, October 24-25, 1968.

14. Luenberger, D.G., Optimization by Vector Space Methods, New York: John Wiley and Sons, Inc., 1969.

15. Pierre, D.A., Optimization Theory with Applications, New York: John Wiley and Sons, Inc., 1969.

16. Pontryagin, L.S., Ordinary Differential Equations, Reading, Mass.: Addison-Wesley, 1962.

17. Rice, R.B., "Inverse Convolution Filters," Geophysics, Vol. 57, No. 1, pp. 4-18, February, 1962.

18. Robinson, E.A., Statistical Communication and Detection; London: Charles Griffin and Company, 1967.

19. Smith, H.A., "Improvement of the Resolution of a Linear Scanning Device," SIAM Journal on Applied Math, Vol. 14, No. 1, pp. 23-40, January, 1966.

20. Sondhi, M.M., "Image Restoration: The Removal of Spatially Invariant Degradations," Proc. IEEE, Vol. 60, No. 7, pp. 842-853, July, 1972.

21. Stuller, J.A., "An Algebraic Approach to Image Restoration Filter Design," Computer Graphics and Image Processing, Vol. 1, No. 2, pp. 107-122, August, 1972.

22. Thurman, L.A., "Radar Resclution Enhancement and Target Surface Reconstruction," Ph.D. Thesis, Purdue University, Lafayette, Indiana, December, 1972.

23. Wolfe, P., "The Secant Method for Simultaneous Nonlinear Equations,: Communications of the ACM, Vol. 2, No. 12, pp. 12-13, December, 1959.

24. Yosida, K., Lectures on Differential and Integral Equations, New York: Interscience Publishers, Inc., 1960.

25. Zemanian, A.H., Distribution Theory and Transform Analysis, New York: McGraw-Hill, 1965.

General References

1. Andrews, H.C., A.G. Tescher, and R.P. Kruger, "Image Processing by Digital Computer," IEEE Spectrum, Vol. 9, No. 7, pp. 20-32, July, 1972.

2. Bergland, G.D., "A Guided Tour of the Fast Fourier Transform," IEEE Spectrum, Vol. 6, No. 7, pp. 41-52, July, 1969.

3. Billingsley, F., "Applications of Digital Image Processing," Applied Optics, Vol. 9, No. 2, pp. 289-299, February, 1970.

4. Blackman, R.B. and J.W. Tukey, The Measurement of Power Spectra, New York: Dover, 1959.

5. Bracewell, R.N., "A Method of Correcting the Broadening of X-Ray Line Profiles," Australian Journal of Physics, Vol. 8, No. 1, pp. 61-67, 1955.

6. Bracewell, R.N., The Fourier Transform and its Application, New York: McGraw-Hill, 1965.

7. Cochran, W.T., et.al., "What is the Fast Fourier Transform?," Proc. IEEE, Vol. 55, No. 10, pp. 1664-1674, October, 1967.

8. Courrant and Hilbert, Methods of Mathematical Physics, Vol. 1, New York: Interscience, 1966.

9. Dettman, J.W., Mathematical Methods in Physics and Engineering, New York: McGraw-Hill, 1969.

10. Goodman, J.W., Introduction to Fourier Optics, New York: McGraw-Hill, 1968.

11. Hamming, R.W., Numerical Methods for Scientists and Engineers, New York: McGraw-Hill, 1962.

12. Harris, J.L., "Image Restoration," Proceedings of the National Aerospace Electronics Conference, pp. 403-408, 1963.

13. Harris, J.L., "Diffraction and Resolving Power," Journal of the Optical Society of America, Vol. 54, No. 7, pp. 931-936, July, 1964.

14. McGillem, C.D., and G.R. Cooper, Continuous and Discrete Signal and System Analysis, New York: Holt, Rinehart and Winston, 1971.

15. McGillem, C.D., and T.E. Riemer, "Moiré Patterns and Two-Dimensional Aliasing in Line Scanner Data Acquisition Systems," IEEE Transactions on Geoscience Electronics, Vol. GE-12, No. 1, pp. 1-8, January, 1974.

16. McGillem, C.D., and T.E. Riemer, "A Linear Shift-Invariant Image Preprocessing Technique for Multispectral Scanner Systems," LARS Information Note: 022673, Laboratory for the Application of Remote Sensing, Purdue University, Lafayette, Indiana.

17. Nathan, R., R. Selzer, and F. Billingsley, "Image Processing," VPL Tech Report, No. 30-792, January 30, 1970.

18. Papoulis, A., The Fourier Integral and Its Applications, New York: McGraw-Hill, 1962.

19. Papoulis, A., Systems and Transforms with Applications in Optics, New York: McGraw-Hill, 1968.

20. Riemer, T.E. and C.D. McGillem, "Constrained Optimization of Image Restoration Filters," Applied Optics, Vol. 12, No. 9, pp. 2027-2029, September, 1973.

21. Robbins, G.M., and T.S. Huang, "Inverse Filtering for Linear Shift-Variant Imaging Systems," Proc. IEEE, Vol. 60, No. 7, pp. 862-872, July, 1972.

22. Silverman, H. and A. Pearson, "On Deconvolution Using the Discrete Fourier Transform," IEEE Trans. on Audio, Vol. AV-21, No. 2, pp. 112-118, April, 1973.

23. Slepian, D., "Restoration of Photographs Blurred by Image Motion," BSTJ, Vol. 46, No. 10, pp. 2353-2362, December, 1967.

24. Temes, G., V. Barcilon, and F. Marshall III, "The Optimization of Bandlimited Systems," Proc. IEEE, Vol. 61, No. 2, pp. 196-234, February, 1973.

25. Tescher, A.G. and H.C. Andrews, "Data Compression and Enhancement of Samples Images," Applied Optics, Vol. 11, No. 4, pp. 919-925, April, 1972.

C - 3

26. Van Trees, H.L., Detection Estimation, and Linear Modulation Theory, New York: Wiley, Vol. 1, 1968; Vol. 2, 1971

27. Yu, F.T.S., "Image Restoration Uncertainty, and Information," Applied Optics, Vol. 8, No. 1, pp. 53-58, January, 1969.

APPENDICES

APPENDIX A

DERIVATION OF RELATIONSHIP BETWEEN DATA RECORD TRUNCATION ERROR AND RESTORATION FILTER POINT-SPREAD FUNCTION

For clarity, the following analysis is based upon one-dimensional blurring and restoration functions. Figure A-1 defines the parameters of the basic system under consideration. The blurring system output, $y(t)$, can be expressed as

$$y(t) = \int_{-\infty}^{\infty} x(\tau) h_b(t-\tau) d\tau \qquad \text{(A-1)}$$

where $x(t)$ is the original signal and $h_b(t)$ is the blurring function. A truncated record of $y(t)$ could be defined as

$$\begin{aligned} y_T(t) &= y(t)\ u(t-t_0) \\ &= y(t) - y(t)\ u(t_0-t). \end{aligned} \qquad \text{(A-2)}$$

Define $\hat{z}(t)$ to be the restored version of $x(t)$ which is obtained from a correction of $y_T(t)$ as

$$\hat{z}(t) = \int_{-\infty}^{\infty} h_r(t-\beta) y_T(\beta) d\beta \qquad \text{(A-3)}$$

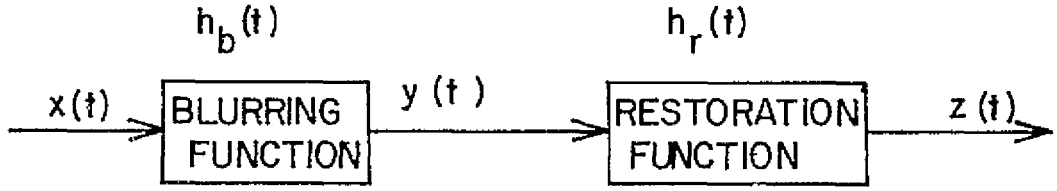

Figure A-1: One Dimensional Composite Imaging System

which after substituting Eq. A-3 into A-2 becomes

$$\hat{z}(t) = \int_{-\infty}^{\infty} h_r(t-\beta)[y(\beta)-y(\beta)u(t_0-\beta)]d\beta$$

$$= \int_{-\infty}^{\infty} h_r(t-\beta)y(\beta)d\beta - e_T(t) \qquad \text{(A-4)}$$

for

$$t_0 \leq t < \infty$$

where $e_T(t)$ represents the error resulting from a truncation of $y(t)$ and may be expressed as

$$e_T(t) = \int_{-\infty}^{t_0} h_r(t-\beta)\, y(\beta)d\beta \qquad \text{(A-5)}$$

for

$$t_0 \leq t < \infty$$

Define $h_{r1}(t-\beta)$, a duration limited form of $h_r(t-\beta)$ so that

$$h_{r1}(t-\beta) = m(t-\beta)\, h_r(t-\beta) \qquad \text{(A-6)}$$

where $m(t-\beta)$ is a monotomically decreasing weighting function such as $\exp[-(t-\beta)^2]$ so that

$$m(0) = 1 \qquad \text{(A-7)}$$

and

$$\lim_{(t-\beta)\to\infty} \quad m(t-\beta) = 0 \qquad \text{(A-8)}$$

From Eq. A5 and 6 define the truncation error resulting from a restoration with a duration limited form of $h_r(\cdot)$ as

$$e_{T1}(t) = \int_{-\infty}^{t_0} h_{r1}(t-\beta)y(\beta)d\beta$$

for

$$t_0 \leq t < \infty. \qquad \text{(A-9)}$$

From Eq. A-6 and 9,

$$E\{e_{T1}^2(t)\} = E\{\int_{-\infty}^{t_0} m(t-\beta)h_r(t-\beta)y(\beta)d\beta \int_{-\infty}^{t_0} m(t-\alpha)h_r(t-\alpha)y(\alpha)d\alpha\}$$

$$= E\{\iint_{-\infty}^{t_0} m(t-\beta)m(t-\alpha)h_r(t-\beta)h_r(t-\alpha)y(\beta)y(\alpha)d\alpha d\beta\} \qquad \text{(A-10)}$$

which because of the shape of the weighting function, Eq. A-7 and 8, may be upper bounded

$$E\{e_{T1}^2(t)\} \leq m^2(t)E\{\iint_{-\infty}^{t_0} h_r(t-\beta)h_r(t-\alpha)y(\beta)y(\alpha)d\alpha d\beta\}. \qquad \text{(A-11)}$$

Assuming that $y(\cdot)$ is a sample function from a wide-sense stationary random process, then Eq. A-11 may be rewritten as

$$E\{e_{T1}^2(t)\} \leq m^2(t)\iint_{-\infty}^{t_0} h_r(t-\beta)h_r(t-\alpha)R_{yy}(\alpha-\beta)d\alpha d\beta$$

$$\leq m^2(t)\, R_{yy}(0)\, [\int_{-\infty}^{t_0} h_r(t-\beta)d\beta]^2. \qquad \text{(A-12)}$$

Since there is a constraint on the energy of the restoration function, the right side of Eq. A-12 is finite for all t. Taking the limit with respect to t of both sides of Eq. A-12,

$$\lim_{t\to\infty} \; E\{e_{T1}{}^2(t)\} = 0 , \qquad \text{(A-13)}$$

since

$$\lim_{t\to\infty} \; m^2(t) = 0, \text{ from Eq. A-8 .}$$

Thus as the distance from the truncation point approaches infinity, the variance of the truncation error produced by a duration limited restoration function approaches zero.

APPENDIX B

DERIVATION OF EQUATION 2-21

The gradient of Eq. 2-12 may be written as

$$\nabla I = \int_{-\infty}^{\infty} [A_1(\bar{u},\bar{z}) + A_1'(\bar{u},\bar{z})]h_r(\bar{z})d\bar{z}$$

$$+ \lambda_1 \int_{-\infty}^{\infty} [A_2(\bar{u},\bar{z}) + A_2'(\bar{u},\bar{z})]h_r(\bar{z})d\bar{z}$$

$$+ \lambda_2 \int_{-\infty}^{\infty} [A_3(\bar{u},\bar{z}) + A_3'(\bar{u},\bar{z})]h_r(\bar{z})d\bar{z}$$

$$+ \lambda_3 \int_{-\infty}^{\infty} [A_4(\bar{u},\bar{z}) + A_4'(\bar{u},\bar{z})]h_r(\bar{z})d\bar{z}. \quad \text{(B-1)}$$

Substituting Eq. 2-14, 2-17 through 2-20 into Eq. B-1,

$$\int_{-\infty}^{\infty} [A_1(\bar{u},\bar{z}) + \lambda_2 A_3(\bar{u},\bar{z}) + \lambda_3 A_4(\bar{u},\bar{z})]h_r(\bar{z})d\bar{z}$$

$$+ \lambda_1 \int_{-\infty}^{\infty} s(\bar{h})\delta(\bar{u}-\bar{z})h_r(\bar{z})d\bar{z} = 0$$

or

$$\int_{-\infty}^{\infty} [A_1(\bar{u},\bar{z}) + \lambda_2 A_3(\bar{u},\bar{z}) + \lambda_3 A_4(\bar{u},\bar{z})]h_r(\bar{z})d\bar{z}$$

$$+ \lambda_1 s(\bar{u})h_r(\bar{u}) = 0. \quad \text{(B-2)}$$

APPENDIX C

DERIVATION OF EQUATIONS 2-25, 27, 29, and 31

Substituting Eq. 2-13 into 2-24,

$$B_1(\bar{f},\bar{\nu}) = \int\int\int_{-\infty}^{\infty} w(\bar{v})h_b(\bar{v}-\bar{z})h_b(\bar{v}-\bar{u})d\bar{v}$$

$$e^{-j2\pi\bar{f}\bar{u}}\, e^{j2\pi\bar{\nu}\bar{z}}\, d\bar{u}\, d\bar{z}. \qquad \text{(C-1)}$$

Introducing a change of variable into Eq. C-1 where

$$\bar{v} - \bar{u} = \bar{\alpha} \qquad \text{(C-2)}$$

$$B_1(\bar{f},\bar{\nu}) = \int\int\int_{-\infty}^{\infty} w(\bar{v})h_b(\bar{v}-\bar{z})h_b(\alpha)e^{-j2\pi f(\bar{v}-\bar{\alpha})}$$

$$e^{j2\pi\bar{\nu}\bar{z}}\, d\bar{v}\, d\bar{\alpha}\, d\bar{z}$$

$$= H_b^*(\bar{f}) \int\int_{-\infty}^{\infty} w(\bar{v})h_b(\bar{v}-\bar{z})e^{-j2\pi\bar{f}\bar{v}}\, e^{j2\pi\bar{\nu}\bar{z}} d\bar{v}\, d\bar{z} \qquad \text{(C-3)}$$

and introducing another change of variable into Eq. C-3 where

$$\bar{v} - \bar{z} = \bar{\beta} \qquad \text{(C-4)}$$

$$B_1(\bar{f},\bar{\nu}) = H_b^*(\bar{f}) \int\int_{-\infty}^{\infty} w(\bar{v})h_b(\bar{\beta})e^{-j2\pi\bar{f}\bar{v}}e^{j2\pi\bar{\nu}(\bar{v}-\bar{\beta})}d\bar{v}\, d\bar{\beta}$$

$$= H_b^*(\bar{f})H_b(\bar{\nu}) \int_{-\infty}^{\infty} w(\bar{v})e^{-j2\pi\bar{v}(\bar{f}-\bar{\nu})}d\bar{v}$$

$$= H_b^*(\bar{f})H_b(\bar{\nu})W(\bar{f}-\bar{\nu}). \qquad \text{(C-5)}$$

Following a similar development,

$$B_2(\bar{f},\bar{\nu}) = \int_{-\infty}^{\infty}\int A_2(\bar{u},\bar{z})e^{-j2\pi\bar{f}\bar{u}}e^{j2\pi\bar{\nu}\bar{z}}d\bar{u}d\bar{z} \qquad (C\text{-}6)$$

and substituting Eq. 2-14 into Eq. C-6,

$$B_2(\bar{f},\bar{\nu}) = \int_{-\infty}^{\infty}\int s(\bar{u})\delta(\bar{u}-\bar{z})e^{-j2\pi\bar{f}\bar{u}}e^{j2\pi\bar{\nu}\bar{z}}d\bar{u}d\bar{z}$$

$$= \int_{-\infty}^{\infty} s(\bar{z})e^{-j2\pi\bar{z}(\bar{f}-\bar{\nu})}d\bar{z}$$

$$= S(\bar{f}-\bar{\nu}). \qquad (C\text{-}7)$$

$$B_3(\bar{f},\bar{\nu}) = \int_{-\infty}^{\infty}\int A_3(\bar{u},\bar{z})e^{-j2\pi\bar{f}\bar{u}}e^{j2\pi\bar{\nu}\bar{z}}d\bar{u}d\bar{z} \qquad (C\text{-}8)$$

which after substituting Eq. 2-15 into Eq. C-8 becomes,

$$B_3(\bar{f},\bar{\nu}) = \int_{-\infty}^{\infty}\int R_{nn}(\bar{z}-\bar{u})e^{-j2\pi\bar{f}\bar{u}}e^{j2\pi\bar{\nu}\bar{z}}d\bar{u}d\bar{z}. \qquad (C\text{-}9)$$

Introducing the change of variable,

$$\bar{z} - \bar{u} = \bar{\alpha} \qquad (C\text{-}10)$$

into Eq. C-9,

$$B_3(\bar{f},\bar{\nu}) = \int_{-\infty}^{\infty}\int R_{nn}(\bar{\alpha})e^{-j2\pi\bar{f}\bar{u}}e^{j2\pi\bar{\nu}(\bar{u}+\bar{\alpha})}d\bar{u}d\bar{\alpha}$$

$$= \Phi^*_{nn}(\bar{\nu})\int_{-\infty}^{\infty} e^{-j2\pi\bar{u}(f-\bar{\nu})}d\bar{u}$$

$$= \Phi^*_{nn}(\bar{\nu})\delta(\bar{f}-\bar{\nu}). \qquad (C\text{-}11)$$

And finally,

$$B_4(\bar{f},\bar{\nu}) = \int_{-\infty}^{\infty}\int A_4(\bar{u},\bar{z})e^{-j2\pi\bar{f}\bar{u}}e^{j2\pi\bar{\nu}\bar{z}}d\bar{u}d\bar{z} \qquad (C\text{-}12)$$

Substituting Eq. 2-16 into Eq. C-12,

$$B_4(\bar{f},\bar{\nu}) = -\frac{1}{4\pi^2 f_H^{\,2}} \int_{-\infty}^{\infty}\int h_b'' (\bar{\nu}-\bar{z})h_b(\bar{\nu}-\bar{u})d\bar{\nu}$$

$$= e^{-j2\pi\bar{f}\bar{u}}e^{j2\pi\bar{\nu}\bar{z}}d\bar{u}d\bar{z}. \qquad (C\text{-}13)$$

By introducing a change of variable into Eq. C-13 where

$$\bar{\nu} - \bar{z} = \bar{\alpha}, \qquad (C\text{-}14)$$

$$B_4(\bar{f},\bar{\nu}) = -\frac{1}{4\pi^2 f_H^{\,2}} \int_{-\infty}^{\infty}\int \{\int_{-\infty}^{\infty} h_b'' (\bar{\alpha})e^{-j2\pi\bar{\nu}\bar{\alpha}}d\bar{\alpha}$$

$$h_b(\bar{\nu}-\bar{u})e^{-j2\pi\bar{f}\bar{u}}e^{j2\pi\bar{\nu}\bar{\nu}}d\bar{u}d\bar{\nu} \qquad (C\text{-}15)$$

and recognizing that

$$\int_{-\infty}^{\infty} h_b'' (\bar{\alpha})e^{-j2\pi\bar{\nu}\bar{\alpha}}d\bar{\alpha} = \int_{-\infty}^{\infty} \{h_b(\bar{\alpha})*\delta''(\bar{\alpha})\}e^{-j\pi\bar{\nu}\bar{\alpha}}d\bar{\alpha}, \qquad (C\text{-}16)$$

and using the convolution property of the Fourier transform,

$$\int_{-\infty}^{\infty} h_b''(\bar{\alpha})e^{-j2\pi\bar{\nu}\bar{\alpha}}d\bar{\alpha} = -4\pi^2\bar{\nu}^2 H_b(\bar{\nu}). \qquad (C\text{-}17)$$

Substituting Eq. C-17 into C-15,

$$B_4(\bar{f},\bar{\nu}) = \frac{\bar{\nu}^2}{f_H^{\,2}} H_b(\bar{\nu}) \int_{-\infty}^{\infty}\int h_b(\bar{\nu}-\bar{u})e^{-j2\pi\bar{f}\bar{u}}e^{j2\pi\bar{\nu}\bar{\nu}}d\bar{u}d\bar{\nu} \qquad (C\text{-}18)$$

and introducing another change of variable where

$$\bar{v} - \bar{u} = \bar{\beta}, \qquad \text{(C-19)}$$

Eq. C-18 becomes,

$$B_4(\bar{f},\bar{\nu}) = \frac{\bar{\nu}^2}{f_H^2} \int_{-\infty}^{\infty}\int h_b(\bar{\beta}) e^{j2\pi\bar{\nu}(\bar{u}+\bar{\beta})} e^{-j2\pi\bar{f}\bar{u}} d\bar{u}d\bar{\beta}$$

$$= \frac{\bar{\nu}^2}{f_H^2} |H_b(\bar{\nu})|^2 \int_{-\infty}^{\infty} e^{-j2\pi u(\bar{f}-\bar{\nu})} d\bar{u}$$

$$= \frac{\bar{\nu}^2}{f_H^2} |H_b(\bar{\nu})|^2 \delta(\bar{f}-\bar{\nu}). \qquad \text{(C-20)}$$

APPENDIX D

DERIVATION OF EQUATION 2-92

Substituting Eq. 2-47 and 50 into 2-91,

$$\nabla I_x = \int_{-\infty}^{\infty} [H^*_{bx}(f_x)H_{bx}(\nu_x)\{-\frac{1}{4\pi^2 x_w^2}\delta''(f_x-\nu_x)$$

$$+ c_x\delta(f_x-\nu_x) - \frac{1}{4\pi^2 x_w^2}\delta''(\nu_x-f_x) + c_x\delta(\nu_x-\delta_x)\}$$

$$+ \lambda_{1x}\{-\frac{1}{4\pi^2 x_s^2}\delta''(f_x-\nu_x) + d_x\delta(f_x-\nu_x) - \frac{1}{4\pi^2 x_s^2}\delta''(\nu_x-f_x)$$

$$+ d_x\delta(\nu_x-f_x)\}]H_{rx}(\nu_x)d\nu_x + 2[\lambda_{2x}\Phi_{nnx}(f_x)$$

$$+ \lambda_{3x}(\frac{f_x}{f_{Hx}})^2 |H_{bx}(f_x)|^2]H_{rx}(f_x) = 0, \qquad \text{(D-1)}$$

or

$$\nabla I_x = -\frac{H^*_{bx}(f_x)}{2\pi^2 x_w^2}\frac{d^2}{df_x^2}[H_{bx}(f_x)H_{rx}(f_x)]$$

$$+ 2c_x|H_{bx}(f_x)|^2H_{rx}(f_x) - \frac{\lambda_{1x}}{2\pi^2 x_s^2}\frac{d^2}{df_x^2}H_{rx}(f_x)$$

$$+ 2d_x H_{rx}(f_x) + 2[\lambda_{2x}\Phi_{nnx}(f_x) + \lambda_{3x}(\frac{f_x}{f_{Hx}})^2$$

$$|H_{bx}(f_x)|^2]H_{rx}(f_x) = 0, \qquad \text{(D-2)}$$

or

$$VI_x = -\frac{H^*_{bx}(f_x)}{2\pi^2 x_w^2}\left[H''_{bx}(f_x)H_{rx}(f_x) + 2H'_{bx}(f_x)H'_{rx}(f_x)\right.$$

$$+ H_{bx}(f_x)H''_{rx}(f_x)] - \frac{\lambda_{1x}}{2\pi^2 x_s^2} H''_{rx}(f_x)$$

$$+ 2[(c_x+\lambda_{3x}[\frac{f_x}{f_{Hx}}]^2)|H_{bx}(f_x)|^2 + \lambda_{2x}\Phi_{nnx}(f_x)$$

$$+ d_x]H_{rx}(f_x) = 0, \qquad (D-3)$$

or

$$VI_x = -[\frac{|H_{bx}(f_x)|^2}{2\pi^2 x_w^2} + \frac{\lambda_{1x}}{2\pi^2 x_s^2}]H''_{rx}(f_x)$$

$$- \frac{H^*_{bx}(f_x)H'_{bx}(f_x)}{\pi^2 x_w^2} H'_{rx}(f_x) - [\frac{H^*_{bx}(f_x)H''_{bx}(f_x)}{2\pi^2 x_w^2}$$

$$- 2(\{c_x+\lambda_{3x}(\frac{f_x}{f_{Hx}})^2\}|H_{bx}(f_x)|^2 + \lambda_{2x}\Phi_{nnx}(f_x) + d_x)]$$

$$\cdot H_{rx}(f_x) = 0, \qquad (D-4)$$

or

$$\nabla I_x = -\left[\frac{|H_{bx}(f_x)|^2 x_s^2 + \lambda_{1x} x_w^2}{2\pi^2 x_w^2 x_s^2}\right] H''_{rx}(f_x)$$

$$- \frac{H^*_{bx}(f_x) H'_{bx}(f_x)}{\pi^2 x_w^2} H'_{rx}(f_x)$$

$$- \frac{1}{2\pi^2 x_w^2}\left[H^*_{bx}(f_x) H''_{bx}(f_x) - 4\pi^2 x_w^2 \{[c_x + \lambda_{3x}(f_x/f_{Hx})^2]\right.$$

$$\left. |H_{bx}(f_x)|^2 + \lambda_{2x}\Phi_{nnx}(f_x) + d_x\}\right] H_{rx}(f_x)$$

$$= 0, \qquad \text{(D-5)}$$

which may be written in normalized form as

$$\nabla I_x = H''_{rx}(f_x) + 2H^*_{bx}(f_x) H'_{bx}(f_x) x_s^2 H'_{rx}(f_x)$$

$$/ \left[|H_{bx}(f_x)|^2 x_s^2 + \lambda_{1x} x_w^2\right] + x_s^2 [H^*_{bx}(f_x) H''_{bx}(f_x)$$

$$- 4\pi^2 x_w^2 \{[c_x + \lambda_{3x}(f_x/f_{Hx})^2] |H_{bx}(f_x)|^2$$

$$+ \lambda_{2x}\Phi_{nnx}(f_x) + d_x\}] H_{rx}(f_x) / [|H_{bx}(f_x)|^2 x_s^2$$

$$+ \lambda_{1x} x_w^2] = 0. \qquad \text{(D-6)}$$

APPENDIX E

DERIVATION OF EQUATION 2-93

From Eq. 2-37, 2-50, and 2-75,

$$K_{lx} = -\frac{1}{4\pi^2 x_s^2}\int_{-\infty}^{\infty}\int \delta''(f_x-\nu_x)H_{rx}^*(f_x)H_{rx}(\nu_x)d\nu_x df_x$$

$$+ d_x \int_{-\infty}^{\infty}\int \delta(f_x-\nu_x)H_{rx}^*(f_x)H_{rx}(\nu_x)d\nu_x df_x$$

$$- \frac{1}{4\pi^2 x_s^2}\int_{-\infty}^{\infty} H_{rx}^*(f_x)H_{rx}''(f_x)df_x$$

$$+ d_x \int_{-\infty}^{\infty} |H_{rx}(f_x)|^2 df_x . \qquad \text{(E-1)}$$

From Eq. 2-94,

$$H_{rx}''(f_x) = H_{rrx}''(f_x) + j\, H_{rix}''(f_x) \qquad \text{(E-2)}$$

and

$$H_{rx}^*(f_x) = H_{rrx}(f_x) - j\, H_{rix}(f_x) \qquad \text{(E-3)}$$

Multiplying Eq. E-2 and E-3,

$$H_{rx}''(f_x)H_{rx}^*(f_x) = H_{rrx}''(f_x)H_{rrx}(f_x)$$

$$+ H_{rix}''(f_x)H_{rix}(f_x) + j\,[H_{rix}''(f_x)H_{rrx}(f_x)$$

$$- H_{rrx}''(f_x)H_{rix}(f_x)]. \qquad \text{(E-4)}$$

Substituting Eq. E-4 into E-1,

$$K_{lx} = -\frac{1}{4\pi^2 x_s^2}\Big[\int_{-\infty}^{\infty}\{H''_{rrx}(f_x)H_{rrx}(f_x) + H''_{rix}(f_x)H_{rix}(f_x)\}df_x + j\int_{-\infty}^{\infty}\{H'_{rix}(f_x)H_{rrx}(f_x) - H'_{rrx}(f_x)H_{rix}(f_x)\}df_x\Big] + d_x\int_{-\infty}^{\infty}|H_{rx}(f_x)|^2 df_x. \quad \text{(E-5)}$$

Since $h_{rx}(x)$ is assumed to be a real function, then

$H''_{rrx}(f_x)$ is an even function

and

$H''_{rix}(f_x)$ is an odd function.

Thus the second integral in Eq. E-5 is zero, and

$$K_{lx} = -\frac{1}{4\pi^2 x_s^2}\int_{-\infty}^{\infty}[H''_{rrx}(f_x)H_{rrx}(f_x)+H''_{rix}(f_x)H_{rix}(f_x)]df_x + d_x\int_{-\infty}^{\infty}|H_{rx}(f_x)|^2 df_x. \quad \text{(E-6)}$$

APPENDIX F

DERIVATION OF EQUATION 2-119

Substituting

$$h_{rx}(\tau) = \mathcal{F}^{-1}\{H_{rx}(f_x)\} = \int_{-\infty}^{\infty} H_{rx}(f_x)e^{j2\pi f_x \tau}df_x \qquad \text{(F-1)}$$

into Eq. 2-116,

$$I_m = -2\int_{-\infty}^{\infty}\int w_x(x)m_x(x)h_{bx}(x-\tau)\int_{-\infty}^{\infty} H_{rx}(f_x)e^{j2\pi f_x \tau}df_x d\tau dx. \qquad \text{(F-2)}$$

Introducing the change of variables into Eq. F-2,

$$x - \tau = \alpha, \qquad \text{(F-3)}$$

ther

$$I_m = -2\int_{-\infty}^{\infty} H_{rx}(f_x)\int_{-\infty}^{\infty}\int w_x(x)m_x(x)h_{bx}(\alpha)e^{j2\pi f_x(x-\alpha)}dxd\alpha df_x$$

$$= -2\int_{-\infty}^{\infty} H_{rx}(f_x)H_{bx}(f_x)\int_{-\infty}^{\infty} w_x(x)m_x(x)e^{j2\pi f_x x}dxdf_x. \qquad \text{(F-4)}$$

By making the substitution,

$$w_x(x) = \mathcal{F}^{-1}\{W_x(\nu_x)\} = \int_{-\infty}^{\infty} W_x(\nu_x)e^{j2\pi\nu_x x}\,d\nu_x \qquad \text{(F-5)}$$

into Eq. F-4,

$$I_m = -2\int_{-\infty}^{\infty} H_{rx}(f_x)H_{bx}(f_x)\iint_{-\infty}^{\infty} W_x(\nu_x)m_x(x)e^{j2\pi x(f_x+\nu_x)}$$

$$dx d\nu_x df_x$$

$$= -2\int_{-\infty}^{\infty} H_{rx}(f_x)H_{bx}(f_x)\int_{-\infty}^{\infty} W_x(\nu_x)M_x^*(f_x+\nu_x)d\nu_x df_x. \quad \text{(F-6)}$$

Finally Eq. F-6 may be written in the form of Eq. 2-118,

$$I_m = \int_{-\infty}^{\infty} B_{5x}(f_x)H_{rx}(f_x)df_x \quad \text{(F-7)}$$

where

$$B_{5x}(f_x) = -2H_{bx}(f_x)\int_{-\infty}^{\infty} W_x(\nu_x)M_x^*(f_x+\nu_x)d\nu_x. \quad \text{(F-8)}$$

APPENDIX G

TABULATION OF RESTORATION POINT-SPREAD FUNCTIONS OF FIGURES 4.67, 4.70, 4.73, 4.76, 4.79, 4.83, 4.87, and 4.91

Figure 4.67

I	RESTORATION PSF
1	6.4630317E-02
2	3.8608855E-01
3	3.3394415E-02
4	6.0310544E-01
5	-1.0000000E 00
6	-3.8361359E-01
7	1.9061363E-01
8	-2.6974414E-02
9	1.1436188E-01
10	5.6722388E-03
11	7.1597045E-02
12	1.4894494E-03
13	3.9733175E-02
14	-9.2360674E-03
15	1.0952328E-02
16	-1.7076654E-02
17	4.8257224E-03
18	-1.9841274E-02
19	7.2562565E-04
20	-1.5807956E-02
21	2.1319313E-03
22	-1.0072824E-02
23	5.4409616E-03
24	-4.8109576E-03
25	7.7762492E-03
26	-1.9022306E-03
27	7.8737251E-03
28	-1.5441642E-03
29	6.1113444E-03
30	-2.6021832E-03
31	3.7229421E-03
32	-4.1215494E-03
33	2.0857342E-03
34	-4.5727300E-03
35	1.5743365E-03
36	-4.0100830E-03
37	1.9877495E-03
38	-2.9270358E-03
39	2.6511106E-03
40	-1.3842172E-03
41	2.0194365E-03
42	-1.5756321E-03
43	2.6543578E-03
44	-1.6854556E-03
45	2.3427947E-03
46	-2.0232131E-03
47	1.8191664E-03
48	-2.2581036E-03
49	1.5347633E-03
50	-2.2446771E-03
51	1.5378592E-03
52	-1.9786935E-03
53	1.7365541E-03
54	-1.7047375E-03
55	1.8678344E-03
56	-1.5598995E-03
57	1.9080005E-03
58	-1.4744654E-03
59	1.8138506E-03
60	-1.5654501E-03
61	1.6498019E-03
62	-1.6985284E-03
63	1.5048536E-03
64	-1.7895324E-03
65	1.4482363E-03

Figure 4.70

I	RESTORATION PSF
1	1.0000000E 00
2	3.4043962E-01
3	-7.9094410E-01
4	8.9706576E-04
5	-9.0277874E-02
6	2.2345465E-02
7	-2.1264467E-02
8	2.3119371E-02
9	-3.2533004E-03
10	1.9369283E-02
11	1.0266155E-03
12	1.4154073E-02
13	4.1795615E-04
14	8.8619186E-03
15	-1.6308299E-03
16	4.5028254E-03
17	-3.4373365E-03
18	1.6506102E-03
19	-4.2122751E-03
20	3.8696639E-04
21	-3.8958665E-03
22	3.5212189E-04
23	-2.8747749E-03
24	9.4138482E-04
25	-1.7031878E-03
26	1.5625922E-03
27	-8.3502848E-04
28	1.2427109E-03
29	-4.6472707E-04
30	1.7029284E-03
31	-5.2002442E-04
32	1.2930779E-03
33	-7.7561127E-04
34	8.4853758E-04
35	-9.9834241E-04
36	5.5260118E-04
37	-1.0532134E-03
38	4.6408247E-04
39	-9.3875968E-04
40	5.3251417E-04
41	-7.4116599E-04
42	6.4200223E-04
43	-5.6359661E-04
44	7.0844311E-04
45	-4.8914612E-04
46	6.9446675E-04
47	-4.6159467E-04
48	6.1951182E-04
49	-5.0200662E-04
50	5.2988119E-04
51	-5.4265209E-04
52	4.6548001E-04
53	-5.5401144E-04
54	4.4117961E-04
55	-5.3385926E-04
56	4.4474435E-04
57	-4.9871160E-04
58	4.6375189E-04
59	-4.6774535E-04
60	4.7455961E-04
61	-4.5055152E-04
62	4.7599059E-04
63	-4.4529303E-04
64	4.7360151E-04
65	-4.4477032E-04

Figure 4.73

I	RESTORATION PSF
1	5.9836630E-02
2	4.9497211E-01
3	3.6912590E-02
4	8.5985929E-01
5	-1.0000000E 00
6	-6.3350022E-01
7	1.6410816E-01
8	-9.0481400E-02
9	1.1172670E-01
10	-1.6274631E-02
11	8.1338823E-02
12	-1.3010993E-03
13	5.5773973E-02
14	-3.5637289E-03
15	3.4136888E-02
16	-1.0243732E-02
17	1.7737661E-02
18	-1.5619422E-02
19	7.5077079E-03
20	-1.7375469E-02
21	3.1163509E-03
22	-1.5518233E-02
23	2.9871317E-03
24	-1.1488989E-02
25	4.9101748E-03
26	-7.1786679E-03
27	6.8994664E-03
28	-4.0979252E-03
29	7.6201484E-03
30	-2.7023044E-03
31	6.9756173E-03
32	-2.8137926E-03
33	5.4544508E-03
34	-3.6072808E-03
35	3.8454634E-03
36	-4.2969994E-03
37	2.7530365E-03
38	-4.4396706E-03
39	2.3731329E-03
40	-4.0201172E-03
41	2.5278632E-03
42	-3.3142452E-03
43	2.8654810E-03
44	-2.6613511E-03
45	3.0794490E-03
46	-2.2780360E-03
47	3.0370967E-03
48	-2.1933003E-03
49	2.7834594E-03
50	-2.2951155E-03
51	2.4569579E-03
52	-2.4295966E-03
53	2.1979965E-03
54	-2.4879316E-03
55	2.0667841E-03
56	-2.4409706E-03
57	2.0561444E-03
58	-2.3222759E-03
59	2.1137928E-03
60	-2.1876302E-03
61	2.1851116E-03
62	-2.0815376E-03
63	2.2361232E-03
64	-2.0256396E-03
65	2.2539189E-03

Figure 4.76

I	RESTORATION PSF
1	5.0303914E-02
2	5.3378749E-01
3	3.8170591E-02
4	1.0000000E 00
5	-8.1527655E-01
6	-7.6431632E-01
7	1.1140245E-01
8	-1.4241391E-01
9	8.5701942E-02
10	-4.2731401E-02
11	7.0096731E-02
12	-1.2188725E-02
13	5.5111080E-02
14	-4.1541718E-03
15	4.0191080E-02
16	-5.1627643E-03
17	2.6511304E-02
18	-9.0587549E-03
19	1.5500500E-02
20	-1.2464306E-02
21	8.0819391E-03
22	-1.3858155E-02
23	4.3179765E-03
24	-1.2962949E-02
25	3.4509546E-03
26	-1.0497965E-02
27	4.2482242E-03
28	-7.5393654E-03
29	5.4647475E-03
30	-5.0412752E-03
31	6.2224455E-03
32	-3.5242976E-03
33	6.1750114E-03
34	-3.0137073E-03
35	5.4434171E-03
36	-3.1816429E-03
37	4.4052452E-03
38	-3.5795602E-03
39	3.4552377E-03
40	-3.8473208E-03
41	2.8389796E-03
42	-3.8212055E-03
43	2.6003257E-03
44	-3.5322652E-03
45	2.6286458E-03
46	-3.1164372E-03
47	2.7516382E-03
48	-2.7356432E-03
49	2.8301959E-03
50	-2.4851945E-03
51	2.8336629E-03
52	-2.3822566E-03
53	2.6759361E-03
54	-2.3811135E-03
55	2.5143678E-03
56	-2.4143152E-03
57	2.3778055E-03
58	-2.4297636E-03
59	2.2979705E-03
60	-2.4102185E-03
61	2.2734611E-03
62	-2.3705554E-03
63	2.2702609E-03
64	-2.3398781E-03
65	2.2838595E-03

Figure 4.79

I	RESTORATION PSF
1	1.55853038-02
2	4.71321948-01
3	1.66040868-02
4	1.00000008 00
5	-1.64271448-01
6	-7.37004768-01
7	2.34399978-02
8	-1.85731178-01
9	2.37161148-02
10	-8.13432348-02
11	2.59315338-02
12	-3.68935978-02
13	2.66C76918-02
14	-1.97296798-02
15	2.55020718-02
16	-9.75342098-03
17	2.27691128-02
18	-5.48504298-03
19	1.89105128-02
20	-4.66618248-03
21	1.46192728-02
22	-4.97910018-03
23	1.05012558-02
24	-5.54468798-03
25	7.30644548-03
26	-6.54935268-03
27	5.03808268-03
28	-6.79325068-03
29	3.75383678-03
30	-6.37585398-03
31	3.21922078-03
32	-5.55396678-03
33	5.11453998-03
34	-4.67886408-03
35	3.33445788-03
36	-3.84281238-03
37	3.45335168-03
38	-3.20924908-03
39	3.44805688-03
40	-2.01C46378-03
41	3.30448178-03
42	-2.60995918-03
43	3.06517108-03
44	-2.53773278-03
45	2.79284018-03
46	-2.52171688-03
47	2.54265718-03
48	-2.50884948-03
49	2.34771198-03
50	-2.47210598-03
51	2.21711C98-03
52	-2.40744168-03
53	2.14202318-03
54	-2.32508808-03
55	2.10543758-03
56	-2.24014268-03
57	2.08989208-03
58	-2.16544918-03
59	2.08315518-03
60	-2.10842548-03
61	2.07693578-03
62	-2.07136168-03
63	2.07583498-03
64	-2.05347998-03
65	2.07470898-03

Figure 4.83

I	RESTORATION PSF
1	9.10556828-01
2	1.00000008 00
3	2.79912718-01
4	-4.38752838-01
5	-1.18663078-01
6	4.17992008-01
7	1.70618598-01
8	-3.76432188-01
9	2.71836528-01
10	-1.99349708-01
11	1.31808288-01
12	-9.34840448-02
13	7.43339908-02
14	-5.20536128-02
15	4.92520038-02
16	-3.36355648-02
17	3.54679348-02
18	-2.43277258-02
19	2.66402568-02
20	-1.91474228-02
21	2.04767458-02
22	-1.60228468-02
23	1.63357218-02
24	-1.39563758-02
25	1.27827048-02
26	-1.23808538-02
27	1.04997C18-02
28	-1.09772058-02
29	8.99584598-03
30	-9.63692748-03
31	8.04239408-03
32	-8.39909178-03
33	7.39945478-03
34	-7.34769558-03
35	6.80172608-03
36	-6.52992358-03
37	6.39471418-03
38	-5.93043868-03
39	5.92197058-03
40	-5.49235198-03
41	5.48581788-03
42	-5.15292218-03
43	5.10974608-03
44	-4.86924568-03
45	4.88038308-03
46	-4.62341688-03
47	4.54749918-03
48	-4.41382458-03
49	4.33560098-03
50	-4.24193598-03
51	4.15462638-03
52	-4.10346748-03
53	4.00370738-03
54	-3.98836208-03
55	3.88685548-03
56	-3.68733138-03
57	3.80502188-03
58	-3.79871308-03
59	3.75116298-03
60	-3.72904598-03
61	3.71484928-03
62	-3.68481468-03
63	3.69074738-03
64	-3.66513348-03
65	3.68168148-03

Figure 4.87

I	RESTORATION PSF
1	3.46167398-01
2	5.52535128-01
3	2.11327858-01
4	7.19748148-02
5	-1.00000008 00
6	1.52659458-02
7	2.27924888-01
8	-1.82224938-01
9	1.25C85838-01
10	-7.03842648-02
11	6.91181428-02
12	-3.42284558-02
13	4.49033128-02
14	-2.14595358-02
15	3.04281648-02
16	-1.66822308-02
17	2.06726278-02
18	-1.46606088-02
19	1.41150008-02
20	-1.33090588-02
21	9.99171668-03
22	-1.18503168-02
23	7.68855968-03
24	-1.01280218-02
25	6.62013148-03
26	-8.29348348-03
27	6.22387238-03
28	-6.61926728-03
29	6.02353748-03
30	-5.33799838-03
31	5.72083098-03
32	-4.53029578-03
33	5.23198778-03
34	-4.11408778-03
35	4.63229058-03
36	-3.92070048-03
37	4.05145068-03
38	-3.79124038-03
39	3.58592008-03
40	-3.63390208-03
41	3.26532508-03
42	-3.42844758-03
43	3.06628718-03
44	-3.19670758-03
45	2.94397598-03
46	-2.97197448-03
47	2.85645708-03
48	-2.78107568-03
49	2.77410028-03
50	-2.63899528-03
51	2.68181028-03
52	-2.54768118-03
53	2.57225558-03
54	-2.49567168-03
55	2.47954958-03
56	-2.46203138-03
57	2.40169748-03
58	-2.42660468-03
59	2.35817028-03
60	-2.38228758-03
61	2.34566218-03
62	-2.33835478-03
63	2.34854508-03
64	-2.31100698-03
65	2.35142798-03

Figure 4.91

I	RESTORATION PSF
1	1.00000008 00
2	8.56250768-01
3	6.79676718-01
4	-8.41940648-02
5	-7.40876388-01
6	-4.73417048-01
7	6.68324418-01
8	-4.37143058-01
9	9.58742508-02
10	-1.83071728-02
11	-5.44416498-02
12	2.96916708-02
13	-4.72645358-02
14	2.44021238-02
15	-3.20186028-02
16	1.87855338-02
17	-2.17541018-02
18	1.53334708-02
19	-1.52368818-02
20	1.30158598-02
21	-1.11102288-02
22	1.11977098-02
23	-8.52945658-03
24	9.61569708-03
25	-6.94652658-03
26	8.19646948-03
27	-5.98380348-03
28	6.94470858-03
29	-5.57664868-03
30	5.88327278-03
31	-4.95737758-03
32	5.02494578-03
33	-4.61584338-03
34	4.35888188-03
35	-4.30195038-03
36	3.86247858-03
37	-3.99811198-03
38	3.50038228-03
39	-3.70559578-03
40	3.23630718-03
41	-3.43304698-03
42	3.03856948-03
43	-3.18937338-03
44	2.89328418-03
45	-2.99011428-03
46	2.75418[illegible]-03
47	-2.[illegible]-03
48	2.64220[illegible]-03
49	-2.66617338-03
50	2.54202068-03
51	-2.55532C3E-03
52	2.45508698-03
53	-2.46900538-03
54	2.37991438-03
55	-2.40235478-03
56	2.31536458-03
57	-2.33171038-03
58	2.26431578-03
59	-2.31461098-03
60	2.22631548-03
61	-2.28912768-03
62	2.20122758-03
63	-2.27412568-03
64	2.18866168-03
65	-2.26913168-03